Study on Bridge Health Diagnosis using Time-series Modeling and Standing-wave based NDT

Haitao XIAO

January 2016

Waseda University Doctoral Dissertation

Study on Bridge Health Diagnosis using Time-series Modeling and Standing-wave based NDT

Haitao XIAO

Graduate School of Information, Production, and Systems

Waseda University

January 2016

Contents

Chapter 1

Introduction

1.1 Background

1.1.1 Research Background

Civil infrastructures include various units and systems such as buildings, transportation systems, and communication systems. However, much of civil infrastructure like buildings, bridges, offshore oil platforms and other lifeline systems deteriorate with time because of variety of cause, such as fatigue failure caused by environmental factors and natural calamities. Especially in Japan, construction of modern infrastructures started in Meiji Era (1868) [1]. Rapid growth of the Japanese economy started in 1960's and intensive investment in infrastructures construction followed to meet expansion of industrial activities. Thus, many of bridges are in serious aging condition or currently closing to the original lifetime. This situation has become an issue concerned by government, since Japan is a mountainous and rugged country. According to the investigation report of road installations (2005), the Japan Ministry of Land, Infrastructure, Transport and Tourism (JMLITT) calculates that almost 40% of nation's bridges are senile structures in 2011, and 70% will be senile structures in 2020 (shown in Figure 1.1) [2]. Regarding road bridges, the traffic in major highways is as large as 15,000 vehicles per line and the ratio of heavy trucks in the traffic is also high (as high as 30%). On some of bullet train routes, trains run quite frequently. Many problems of bridges are because of the high loading. Therefore, how to continuously evaluate the structural condition, detect existing damage in bridge structures at the earliest possible time, and timely maintain the aging bridges is critical so that the bridges can continue to be safely used, and further improve the public safety.

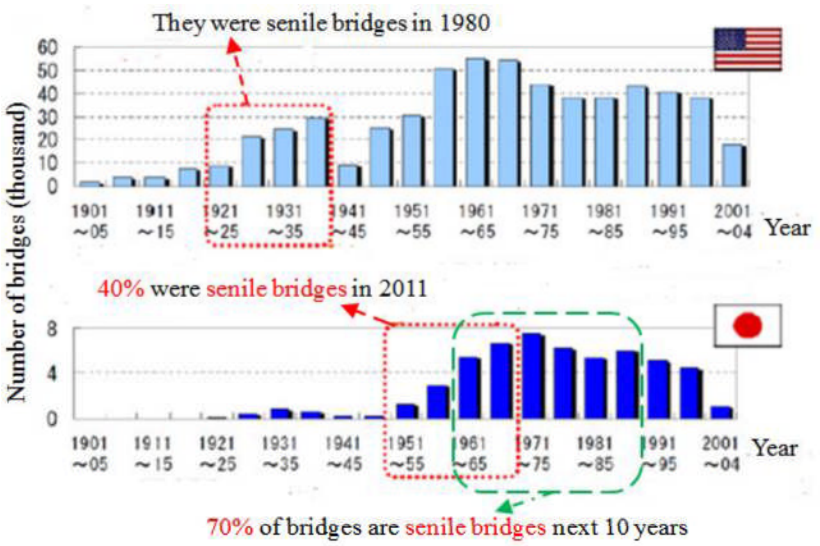

Figure 1.1 Construction year of bridges in America and Japan [2]

In order to maintain the safety of bridges, government periodically, usually once every several years, inspect bridges. To date, the primary way used to perform these inspections is schedule driven and relies on visual inspection. However, such visual inspections have limited efficiency and reliability. The variation of inspector's experience and invisibility of serious damage can make the damage be overlooked, whereas the propagation of the damage between two inspections can potentially put the bridge at risk. Therefore, a much more effective and reliable way to monitor and assess the integrity and functionality of nation's bridges is needed.

Structural health monitoring (SHM) provides a way to continuously capture structural response and assess structural condition in real-time. SHM is able to describe the characteristic of loads in situ, thereby useful to predict the structural response due to extreme loading condition. SHM can also be used to access post-extreme event condition due to natural hazards or man make disasters. This can potentially allow the authority to access the affected area faster and eventually reduce economic and social impact of damage. The essential purpose of SHM for bridge structures is to detect the existing damage in the systems. The damage is defined as the changes of material attribute and geometry such as boundary conditions and system connectivity. Vibration-based SHM methods for bridge structures have evolved in 1980s. The vibration-based SHM method is based on detecting the changes of the characteristics structural, such as damping, stiffness and mass. The procedure of vibration-based SHM methods for bridge consists of two parts: measurement of structural dynamic responses and evaluation of current bridge condition based on damage identification algorithm, where by studying and comparing the changes in monitored vibration response between initial and current structural condition, the structural unknown damages can be identified in [3]. Figure 1.2 shows the envisaged

benefits of structures with SHM systems. This Figure fully reflects the advantages of SHM to bridge maintenance, comparing with the traditional method without SHM. In summary, SHM in bridge has great advantage in terms of real-time monitoring and assessment, timely maintenance practices, and rapid response after extreme event.

Therefore, to make overall road operate in safety with economic limitations, developing a low cost, automatic and long-term Bridge Structural Health Monitoring (BSHM) systems is required urgently and highly.

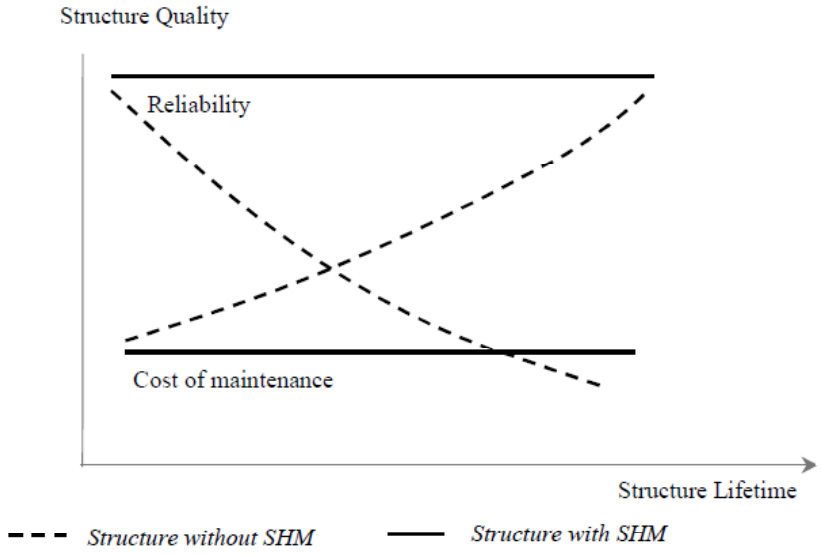

Figure 1.2 Benefit of SHM [3]

1.1.2 Current Problems

The rapid development of BSHM favored the transportation system, improved overall road operational safety and reduced the cost of maintenance. The merits of a BSHM system is mainly decided by two factors: (1) sensors' sensitivity and precision and the performance of data acquiring devices, and (2) measured-data analysis. From the point of the current development, hardware facilities used for structural health monitoring are more and more advanced, and the current sensor technology has reached a higher level. Therefore, sensor signal acquisition is not a critical problem.

In BSHM system, data analysis needs to complete damage identification and bridge health status evaluation. Therefore, it can be seen as the most critical stage in BSHM. However, data analysis still have many problems, such as impact of noises on the precision of damage diagnosis, influence of varying operation and environment on damage detection, damage identification sensitivity and precision problem, damage locating problem, damage details detecting, and etc.

Impact of Noises on the Precision of Damage Identification

In BSHM, measurement noises widely exist in acquired vibration-data, and are derived from thermal, magnetic and electric effect of data acquiring devices and observation error. These noises can bring difficulties to damage identification while the noise pollution of vibration-data is large. Therefore, the data needs to be de-noised before further data analysis for damage detection. The performance of de-noising can affect the precision of damage diagnosis significantly, because noises can cover characteristic changes caused by damages. Wavelet Transform (WT) is a common method for data processing in BSHM. In order to determine appropriate threshold to reduce noise in the appropriate range, usually WT needs to estimate the range of characteristic frequency about true signal and noise firstly. If there is no prior knowledge about the range of characteristic frequency, it is difficult to get satisfied noise reduction. Fast Independent Component Analysis (ICA) is another application on data processing. As we known, Fast ICA is a linear ICA algorithm, which is suitable to the processing of signal in linear mixing environments. Thus, there are some obvious disadvantages in the de-noising of non-linear system, such as the vibration signals of bridge.

Influence of Varying Operational and Environmental conditions on Damage Identification

When a BSHM system is deployed on a field bridge which is exposed to outside environment, damage detection process will have to deal with uncertainties from operational and environmental influence. The uncertainties from operational condition include live traffic, while environmental condition includes temperature and moisture. These changes in the data caused by the variation in operating condition and environment maybe regard as an effect of damage mistakenly, because the existing vibration-based damage diagnosis algorithms are based on studying and comparing the changes in monitored vibration response between benchmark and current structural condition. Therefore, when operational and environmental variability is an issue, how to separate changes caused by the variability from changes caused by real damage is also a challenge to the field implementation of a robust SHM system.

Damage Identification Sensitivity and Precision Problem

In recent years, many algorithms have been proposed by different researchers to identify structural damage, such as model-based algorithms and feature-based algorithms, for BSHM. Fundamental difficulty with model based methods is that physical-parameters which are acquired from the model updating is likely to unrelated to the information of real damage (location and severity). Deferent to model-based

algorithms, the algorithms based on feature detect the changings of structure based on some damage features without a detailed structural-model, such as FFT, Transform Function (TF). Although, in most the cases, existing feature based algorithms can identify whither structure is damage in most cases, they are difficult to detect the damage severity or location(s) of damages. Furthermore, in these algorithms the sensitivity of features to kinds of damage levels shows that these features were not good indicators of damage. Thus, how to identify the severity and location of damages, and how to extract sensitive damage features are urgently to be solved.

Damage Details Detection

As mentioned above, most of the vibration data-based damage identification algorithms are difficult to detect the severity or location(s) of damages. Even if some of these algorithms can detect the location and severity of damages successfully, they can only locate the approximate areas and severity of damages. In other words, specific location and severity of damages, such as subsurface voids and cracks, are nearly impossible to be determined by these algorithms. However, the specific location and severity of damages are very important for government to maintain bridges. Although many complicated and expensive equipment-based nondestructive damage detecting systems can obtain the specific information of damages, heavy economic and time burden is a serious problem for government. Therefore, an economic and efficient method for detecting the specific information of damages is needs to be developed.

1.2 Motivation and Objective

1.2.1 Motivation

During last ten years, although development of advanced hardware facilities and high level sensing technology indicates the possibility of employing long term SHM systems in bridge daily monitoring, BSHM has been confronted by several problems in crucial data analysis such as noise impact problem, varying environment influence problem, damage identification sensitivity and precision problem, damage details (specific location and size) detecting, etc. Also, due to the tight budget of government, expenditures for maintenance-related activities cannot be expected to increase in proportion to the need. Against such issues and backgrounds, many attempts have been made to develop a BSHM system with efficient, economy, and high accuracy.

Attribute to use more and more advanced hardware facilities for BSHM system, the measurement errors is reduced significantly. However, these devices cannot make the acquired vibration-data avoid the measurement noises, which can affect the precision of damage diagnosis significantly by covering the characteristic changes caused by

damages. Otherwise, during deploying a SBHM system on a field bridge which is exposed to outside varying operation condition and environment, the changes in the data caused by the variability of operation condition and environment maybe regard as an effect of damage mistakenly. Therefore, design of a data processing method to de-noise and eliminate the impacts of varying operation condition and environment is an indispensable mean for detecting damages accurately.

Also, the problem of damage identification sensitivity and precision cannot be avoided by only de-noising and eliminating the influences of varying operational and environmental condition. Thereby, it is very important to design an advanced and sensitive damage diagnosis algorithm, including damage identification, damage severity detection, and damage locating.

When the damages of bridge have been detected and needs to be repaired, the specific location and size of damages, such as voids and cracks under the subsurface, is very important for maintainer. And in general, since the vibration data-based damage identification algorithm can only obtain the approximate areas of damages, BSHM would be confronted with a new problem that how to detect the specific information of damages, in an economical and efficient way.

1.2.2 Objective

Faced by problems mentioned above, bridge structure health monitoring (BSHM) system with characteristics of high efficient, accuracy and sensitivity is preferable in the future. Measurement noises and varying operation condition and environment directly affect the precision of damage identification. Design of high performance data processing method with an improved de-noising algorithm and new data normalizing scheme is an effective measure for better data analysis, is treated as one research field in the dissertation. Besides, a good damage identification algorithm can also increase the sensitivity of damage feature, improve the accuracy of damage identification and damage severity detection, and locate damages. Therefore, in order to improve the damage identification performances of BSHM system, design of an advanced vibration data based damage diagnosis algorithm is other promising way. Specific location and size of subsurface damages (such as voids and cracks) is difficult to detect and very important for maintainer. Hence, to detect specific information of subsurface damages economically and efficiently, is an indispensable but challenging task. In this research, standing-wave based nondestructive damage detecting system is being designed. The organization of the research is illustrated as Fig. 1.3.

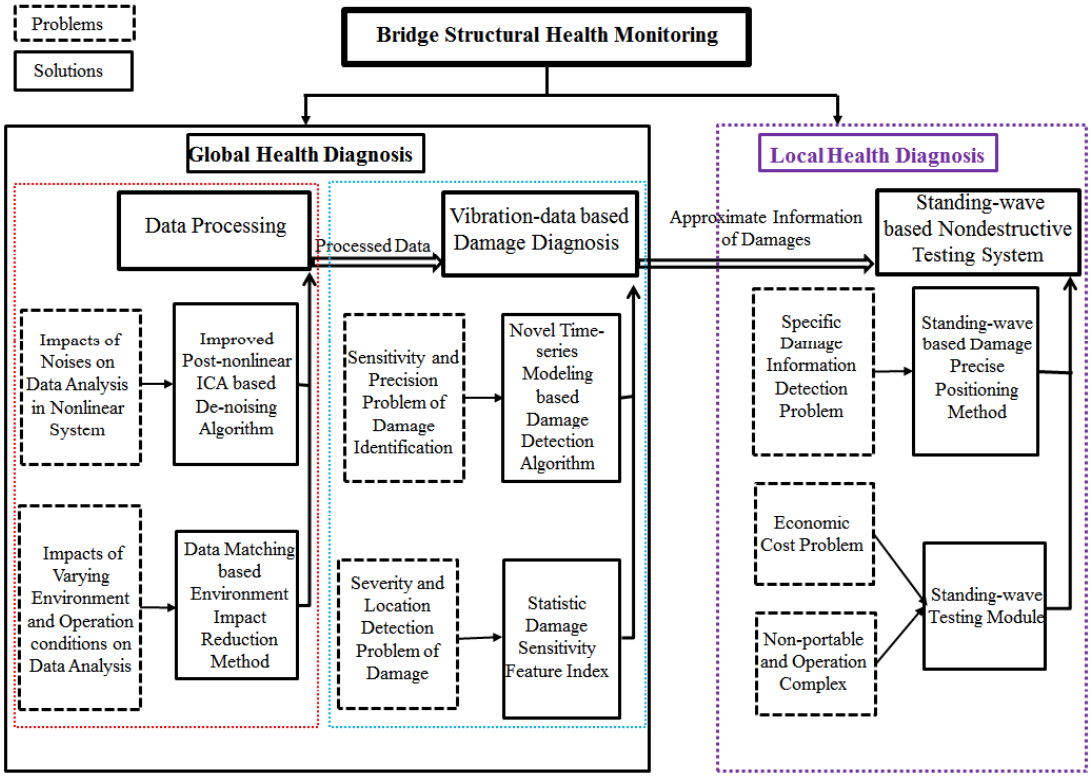

Figure 1.3 Organization of the research

The research is summarized as three fields:

☐ Design of High-performance Data Processing Method

In order to reduce the impacts of noise on data analysis and give de-noised data samples with good signal-to-noise ratio for damage detection algorithm to improve precision and sensitively, one of possible approach is employing a data processing method to de-noise acquired vibration data samples. Most of the existing de-noising methods are efficient only in linear systems. However, bridge systems belong to non-linear systems. Otherwise, most of the existing BSHM systems ignore the impacts of varying operation condition and environment on the precision and sensitively of damage detection. Actually, since these changes in the data caused by the variability of operation condition and environment maybe regard as an effect of damage mistakenly, how to eliminate impacts of the operational and environmental variability is a big challenge. In this research, a new data processing method is proposed for BSHM. In this method, a de-noising algorithm based on post-nonlinear geometric-linearization ICA is proposed for the purpose of de-noising efficiently in nonlinear system. In this de-noising algorithm, a compensation scheme is designed to reduce the error of geometric-linearization to improve the de-noising performance. To eliminate the impacts of varying operation condition and environment, a novel environment impact reduction method based on AR model and data matching is proposed. In the environment impact reduction method, acquired vibration data

samples are divided into two set, undamaged condition data set and unknown condition data set. AR model is used to extract the features of each data samples in the two sets. Based on these features, a data matching scheme based on Euclidean distance is designed to obtain the data sample pair, one sample of undamaged condition data set and one of unknown condition data set, which are sampled in a similar operation and environment condition.

☐ Design of Damage Diagnosis Algorithm

As above-mentioned, data processing method can improve the performances of damage detection by de-noising and data normalizing. Improvement of damage diagnosis algorithm performances is another promising method for improving the performances of damage detection. With a view to the accuracy of damage identification and the sensitivity of damage features, a two-stage damage diagnosis algorithm is proposed based on time-series modeling. After, data processing, in first stage after data processing, FFT is used to obtain the characteristic frequency of bridge to detect the structural novelty (detecting damages) by comparing the frequency in a healthy state with an unknown state. Based on the result of first stage, a statistical pattern recognition damage identification algorithm is proposed for second stage to determine the severity and location(s) of damages. In order to reduce the influence of external factors, ARMA model is employed to extract the damage features. During feature extraction, principal component analysis (PCA) is used to carry out the effective curtailment of the multi-feature. Then based these features, Mahalanobis distance is utilized to calculate the damage sensitive features (DSF) of each data samples. Otherwise, a statistic-based damage sensitive feature index D_{index} is proposed to obtain a diagnosis of structure condition and locations of damages when D_{index} has changed significantly from before to after damage. In this way, a judgment on status of the structure can be made accurately and swiftly.

☐ Design of Standing-Wave based Structure Non-destructive Damage Detecting System

With requirements of specific location and size of subsurface damages (such as voids and cracks) for bridge maintenance, a standing-wave based structure non-destructive Damage detecting system is developed as an assistance system to obtain the specific information of damages based on the result of the two-stage damage diagnosis algorithm. Firstly, this system sends high-frequency sweeping waves (3.8–5.8 GHz) to an object. The incident and reflection waves from the object form a standing wave whose amplitude $A(f, x)$ is related to the input wave frequency f and object distance x. The amplitude signal is detected and converted to volts with a zero-biased detector. Finally, the amplitude–frequency response $A(f, x)$ is processed

by empirical mode decomposition (EMD) to denoise and analyzed by the ICA method. Hence the object state including the existence, location and size of subsurface voids is identified. In comparison with other structure non-destructive damage detecting systems, the proposed system is compact and less expensive, and offers higher sensitivity, resolution, and accuracy.

1.3 Outline of This Dissertation

The dissertation consists of six chapters which are organized as follows.

In Chapter 1, the background of bridge structure health diagnosis (BSHM) is being discussed. Then, the current problems of BSHM and the problems which we focus on are discussed. Next motivation and objective of this research is presented.

In chapter 2, concept of SHM is intruded at first. Then current existing vibration based BSHM systems are discarded. Also the data processing methods and damage diagnosis algorithms of BSHM systems are described and discussed in detail. Then current existing Nondestructive testing methods are described. Finally, based on the discussion of the algorithms in current existing BSHM system, the problems and solution are presented.

In Chapter 3, a new data processing method focused on de-noising and eliminating the impacts of varying operation and environment condition is proposed for data analysis. To solve the problem of efficiently de-noising in bridge systems (nonlinear systems), a de-noising algorithm based on post-nonlinear geometric-linearization ICA is designed. In this algorithm, to improve the performance of de-noising, a compensation scheme is designed to reduce the linearization error of this nonlinear ICA. To eliminate impacts of operational and environmental variability, a novel environment impact reduction method based on AR model and data matching is proposed. In the environment impact reduction method, firstly, acquired vibration data samples are divided into two set, including undamaged condition data set and unknown condition data set. Then AR model is used to extract features of each data samples in the two sets. Finally, based on these features, a data matching scheme based on Euclidean distance is designed to obtain data sample pair, one sample of undamaged condition data set and one of unknown condition data set, which are sampled in a similar operation and environment condition. To verify performance of this new data processing method, performance evaluation, simulation and experiment are given.

In chapter 4, another research concerning vibration data based bridge structure damage identification algorithm is presented. Section 4.2 describes overview of the proposed two-stage output-only damage diagnosis algorithm. In section 4.3, first stage is described. In section 4.4, a novel time-series modeling based Damage Diagnosis

Algorithm is proposed to sensitively detect severity and location of damage (second stage). In this algorithm, ARMA model is selected for extracting features, PCA is used to carry out the effective curtailment of the multi-feature. Beside, based on the extracted features a new sensitive damage-sensitive feature index D_{index} is proposed to obtain a diagnosis of structure condition, and identify severity and location of damages. To verify the performance of proposed algorithm, numerical simulation is shown in section 4.5. The field bridge experiments included measurement at the Kando Bridge in Japan and analysis results are presented in section 4.5. Section 4.6 summarizes the chapter.

In chapter 5, to pinpoint exact location and severity of the damage in economy and efficiency, a standing-wave based structure DNT system was successfully built. Section 5.2 describes the overview of this standing-wave based structure DNT system. In section 5.3, at first we introduce the basic standing-wave teste algorithm. Then improvement of this test algorithm and system is proposed. At last, a new data analysis method based on modified EMD and ICA is proposed to improve accuracy of damage detection. To verify the performance, numerical simulation is shown in section 5.4, and results of experiments including 3 cases are presented and discussed in section 5.5. To show the advantages of this system, comparison of my system and other systems is shown in section 5.5. Finally section 5.6 concludes the summary.

In Chapter 6, the conclusion and future research are given.

References

[1] Structural health monitoring in civil infrastructures-research activities at the Bridge and structure Laboratory of the University of Tokyo-Y.Fujino & M.Abe Dept. of civil Engineering, University of Tokyo,Tokyo Japan

[2] "Highway Statistics Annual Report," Status investigation on road facilities, Japan Ministry of Land, Infrastructure, Transport and Tourism (2005)

[3] Farrar, C.R., and Worden, K., "Structural Health Monitoring: A Machine Learning (2013)

[4] K, Wong, "Monitoring Hong Kong's Bridges Real-Time Kinematic Spans the Gap." GPS world, Vol. 12, No. 7, pp10-18. (2001)

[5] S. Jang, "Structural Health Monitoring for Bridge Structures Using Wireless Smart sensor", Smart Structures and Systems, Vol.6, No.5-6, pp.439-459. (2010)

[6] S.N. Pakezad, "Design and Implementation of Scalable Wireless SensorNetwork for Structural Monitoring", Journal of Infrastructure Systms, Vol.4, No.1, pp.89-101. (2008)

[7] Wu ZS, "Structural health monitoring and intelligent infrastructures in Japan," Structural health monitoring and intelligent infrastructure, Lisse: Balkema, pp. 153–167 (2003)

Chapter 2

Overview of Current Research

2.1 Introduction

This chapter provides a review of some important background related to this research. First, an introduction of structural health monitoring (SHM) is given, with followings of previous applications in the field of Bridge SHM (BSHM). Second, the background of data processing is presented. It includes an overview of data de-noising techniques in existing bridge SHM systems. Furthermore, an introduction of existing vibration-based damage diagnosis algorithms are shown followed. Finally, non-destructive testing (NDT) based Local Damage detecting techniques are provided for obtaining the detailed information of damages (such as detailed location and size of damages) to satisfy the requirements of bridge health diagnosis and maintenance.

2.2 Bridge Structural Health Monitoring

2.2.1 Concept of Structural Health Monitoring

Structural health monitoring (SHM) is a method which implements damage identification strategy that aimed at assessing the existing performance of a structure. It is mainly motivated to safeguard the people`s life-safety, and by the economic impact to the public society. It can be also motivated to understand the complex relationships between loading objects with bridge, assess novel techniques in construction or designing, evaluate the condition when an extreme loading event occurs, monitor construction procedure, evaluate retrofit measures and monitor structural deterioration and degradation. SHM includes the integration of various kinds of sensors, data delivering, computing capacity, and processing capacity. By using this technology, it`s possible for people to consider: the structure design; the

structure management; and considering this management as a portion of further and wider systems. SHM systems, shown as Figure 2.1, could be organized like the following in different levels:

- Sensor monitors the type of physical phenomenon which is related to the damage, and produces a data to send to the data acquiring and storing system. A network consists of several type sensors, the data of different type sensors can be multi used and combined. The sensors used for monitoring the environment conditions can be used to implement the functions of the usage monitoring. The data obtained by the monitoring sub-system is employed by the user to establish a diagnosis.
- Using the information from the integrity monitoring system, the usage condition of the monitoring system, and the mechanics knowledge, and behavior laws to decide the prognosis and the structure health management such as repair, maintenance, and etc.

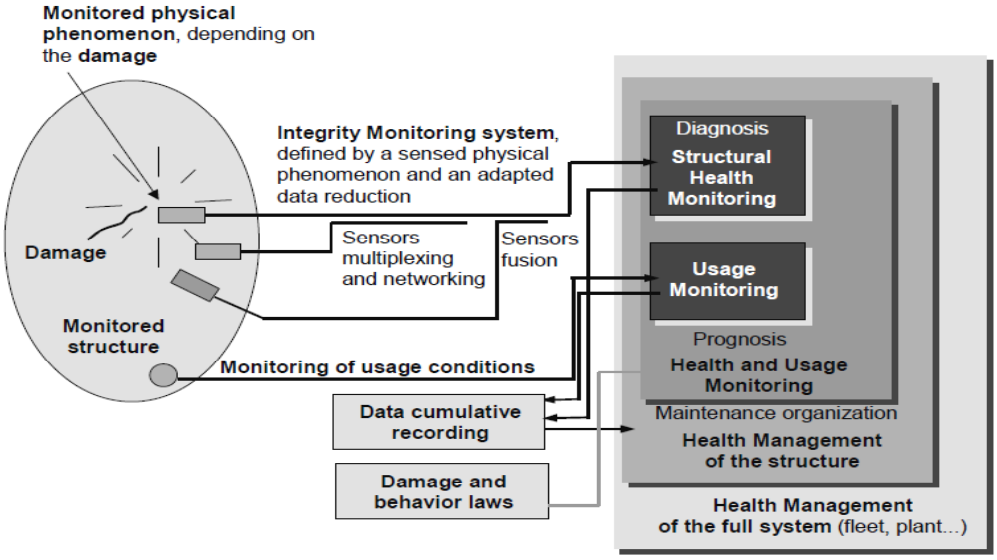

Figure 2.1 Theory of a SHM system [1]

At any level described above, the feasible systems can be established. The system's diagnosis capacity can be further enhanced obviously as the SHM system organization presented in Figure 2.1 can be enhanced by combining the data of usage condition with the function of integrity monitoring function.

2.2.2 Existing Structural Health Monitoring on Bridge

With the rapidly ageing of the worldwide civil infrastructure, much attention had been focused on Bridge SHM (BSHM) recently. The vibration-based BSHM method is based on detect changes in the characteristics of structural, such as damping, stiffness, and mass, etc. By studying and comparing the changes in monitored vibration response between initial and current structural condition, the unknown

damages of structural properties can be identified. The procedure of Vibration-based BSHM system consists of Data Acquiring and Data Analysis, including Data processing and Damage Detection. While the most damage detection algorithms of Data Analysis in vibration-based SHM require input excitation and output, measuring the input excitation from a bridge is quite difficult due to the varying bridge loading. Thus, in vibration-based BSHM, research on damage diagnosis algorithms is focused on only use vibration data excited by ambient.

In last few decades, many of modern SHM systems were developed and real deployed on many bridge projects in Europe, the United States, Japan, and China. The Hong Kong Bridge Structural Health Monitoring System (HBSHM) based on traditional wire-network is installed on Ting Kau Bridge, Kap Shui Mun Bridge, and Tsing Ma Bridge [2]. Similar study can be found in Bill Emerson Memorial Bridge, Missouri [3]. Other examples of BSHM are the Tamar Bridge (UK) [4], the Zhanjiang Bay Bridge (China) [5], SHM system on Golden Gate Bridge [6], long term SHM system on Jindo Bridge [7], and SHM on Railway Bridge [8], etc.

2.2.2.1 Hong Kong Bridge Structural Health Monitoring System

Figure 2.2 shows a long-term BSHM system, named Hong Kong Wind and Bridge Structural Health Monitoring System (HBSHM), using a total number of 350 sensors with seven different types on the Kap Shui Mun Bridge (KSMB) [2]. Large amount various kinds of sensors were installed on the bridges, including temperature sensor, anemometer sensor, displacement sensor, accelerometer sensor, weight in motion sensor, GPS, and Fiber Bragg Grating sensors. Figure 2.3 shows the architecture of WBSHM. Many kinds of data analysis algorithms are used in this system to identify damages, as shown in the data analysis part, such as FFT, FDD, etc.

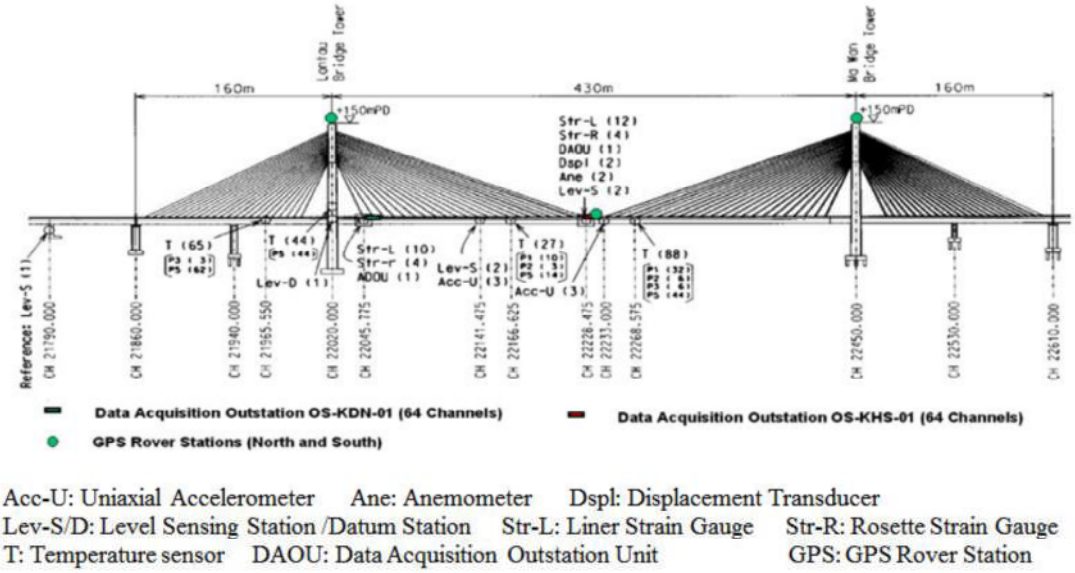

Acc-U: Uniaxial Accelerometer Ane: Anemometer Dspl: Displacement Transducer
Lev-S/D: Level Sensing Station /Datum Station Str-L: Liner Strain Gauge Str-R: Rosette Strain Gauge
T: Temperature sensor DAOU: Data Acquisition Outstation Unit GPS: GPS Rover Station

Figure 2.2 Deployment of HBSHM on Tsing Ma Bridge [2]

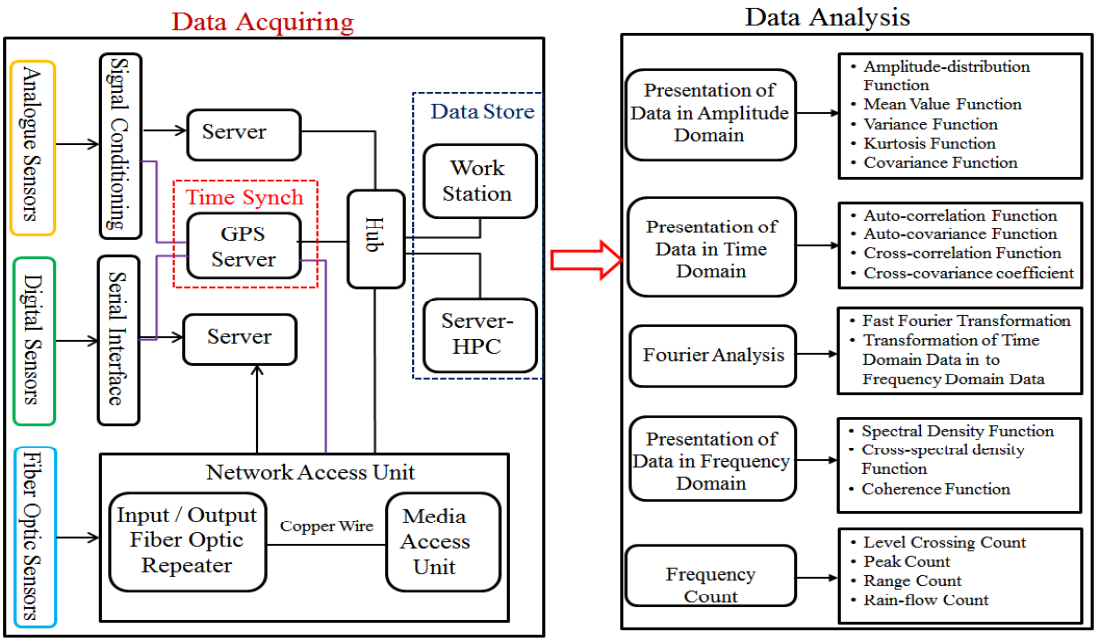

Figure 2.3 Data processing and analysis of HBSHM

2.2.2.2 BSHM System on Golden Get Bridge

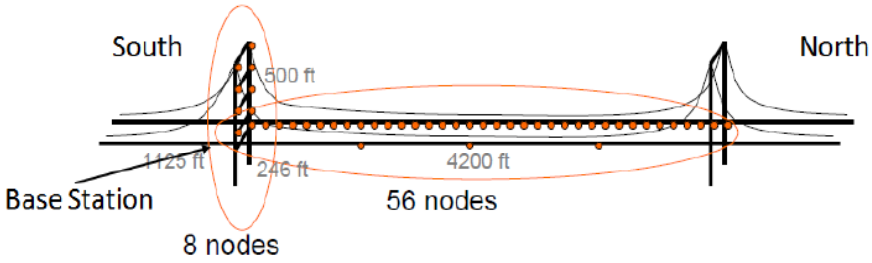

Figure 2.4 Deployment of sensor nodes on Golden Gate Bridge [6]

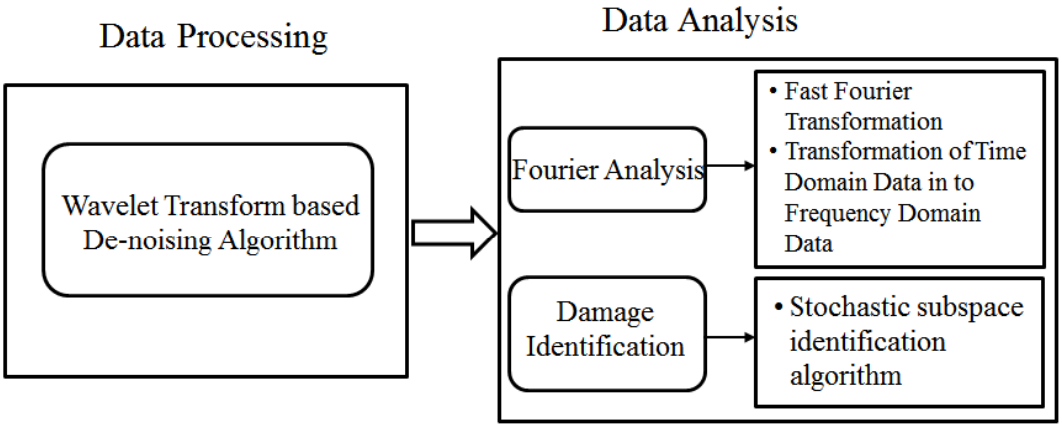

Figure 2.5 Data analysis of BSHM system on Golden Get Bridge

Many researchers have deployed WSN in full-scale bridge health monitoring. Pakzad et al. [6] designed and deployed 64 wireless nodes on the Golden Gate Bridge in San Francisco for bridge structural health monitoring. Each node has 4 channels.

The sketch of this research is shown in Figure 2.4. In this research, the system is able to make sources of distortion such as the system error, temperature variation and system noise floor including noise from amplifier, A/D converter and the accelerometer in minimum. The sampling rate of this system is set to 200 H_Z and 1 kHz as the sampling rate. In this research, Wavelet Transform (WT) [9] is applied to de-noise in data processing procedure and many data analysis algorithms are applied to detect the damage of bridge, such as FFT and Stochastic subspace identification (SSI) algorithm [11].

2.2.2.3 Bridge Structural Health Monitoring System on Jindo Bridge

The largest WSN implementation for BSHM was conducted on the Jindo Bridge [7], including a 344m central main span and two 70m side spans, in South Korea. On this bridge, a total number of 70 wireless sensor nodes with 427 sensor channels were installed. Figure 2.7 shows the process of this BSHM system. Empirical model decomposition (EMD) [10] is employed as data processing to de-noise in this BSHM system. Two output-only modal identification methods, i.e., FDD (frequency domain decomposition) and SSI [11] are used in this system to extract the modal characteristic of the bridge from the acceleration data. The extracted modal characteristic from both modal identification methods are validated by comparing with each other and with those from the finite element (FE) model analysis, which is constructed based on delving into the detailed drawings and design documents, and validated utilizing the acceleration data from the existing wired SHM system on the bridge.

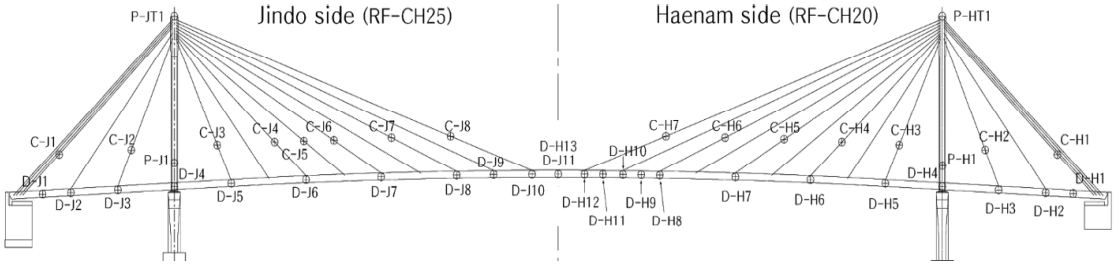

Figure 2.6 Deployment of sensors on Jindo Bridge [7]

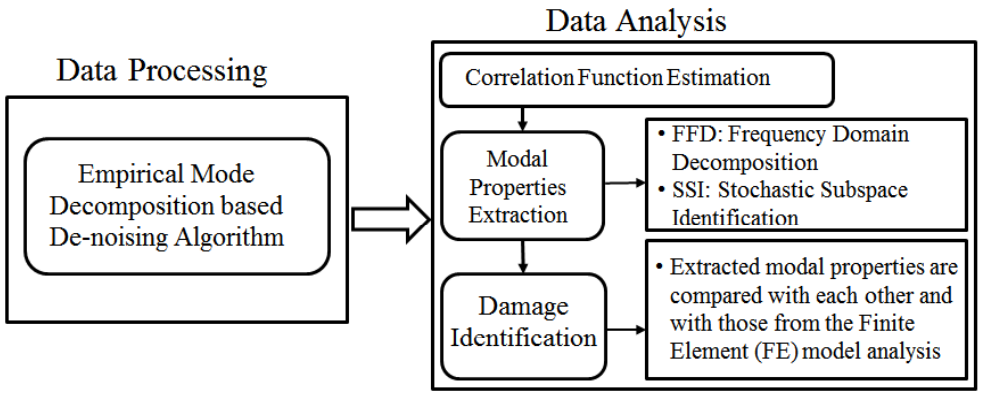

Figure 2.7 Overview of BSHM system on Jindo Bridge

2.2.2.4 Bridge Structural Health Monitoring System on Seiran Bridge

In the BSHM system of Seiran Bridge, a low-power WSN is developed and deployed to monitor and acquire vibration data of Seiran Bridge [16], in Japan. On this bridge, a total number of 22 wireless sensor nodes with 66 sensor channels were installed. This data acquiring system is shown as the Figure 2.8. Figure 2.9 shows the data analysis processes of this BSHM system. A famous independent component analysis (ICA) Fast-ICA [16] is employed as data processing to de-noise in this BSHM system. FFT (Fast Fourier Transformation) is applied to extract the characteristic frequency of the bridge from the acceleration data measured in health condition and unknown condition. By comparing frequencies of these two condition, the global damages of bridge were detected. In order to detect local damages and location of damages, transform function (TF) based method [32] is developed. This method use one sensor's sampling data as input and anther sensor's data as output. Then the TF of the two sensors are obtained. By comparing the TF of two bridge conditions to detect whither damage exists in the area between two sensors. In this way, the damage can be detected and located. Based on these results of data analysis, maintenance decision can be made for this bridge.

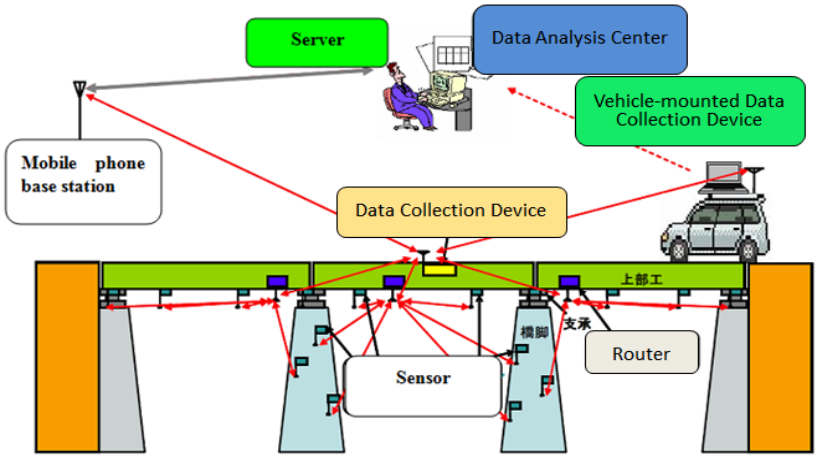

Figure 2.8 Data acquiring system of Seiran Bridge system [16]

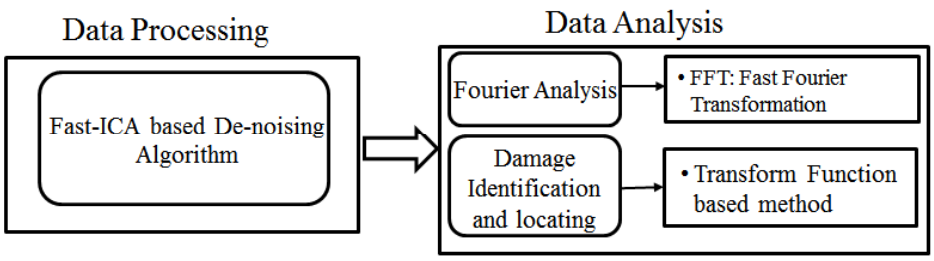

Figure 2.9 Overview of data analysis on Seiran Bridge system [16]

2.3 Data Processing Method in BSHM

2.3.1 ICA based Data Processing Method

In BSHM system on Seiran Bridge [16], ICA (independent component analysis) based de-noising method is used to de-noise for data processing. ICA is a famous blind source signals separation technology. Figure 2.10 shows how ICA separates blind sources and reconstructs signal. Assuming that the linear mixtures of $x(t)$show as $x(t) = [x_1(t), \cdots, x_n(t)]^T$, $s(t) = [s_1(t), \cdots, s\ \ )]^T$ is the n independent components of $s_1(t)$, and $E\{s(t)\} = 0$ in every time-period *t*, like equation (2.1), in this equation *A* as a full rank scalar matrix. ICA aims to search a linear matrix W to get the recovered signals *u*, shown as equation (2.2), which are the max statistically independent. Because the variances of $s_i - s$ is unsureness in theory, we suppose the variance of each s_i as $E\{s_i^2\} = 1$. In this way, the components are independent.

$$x(t) = As(t) \tag{2.1}$$

$$u(t) = Wx(t) = WAs(t) \tag{2.2}$$

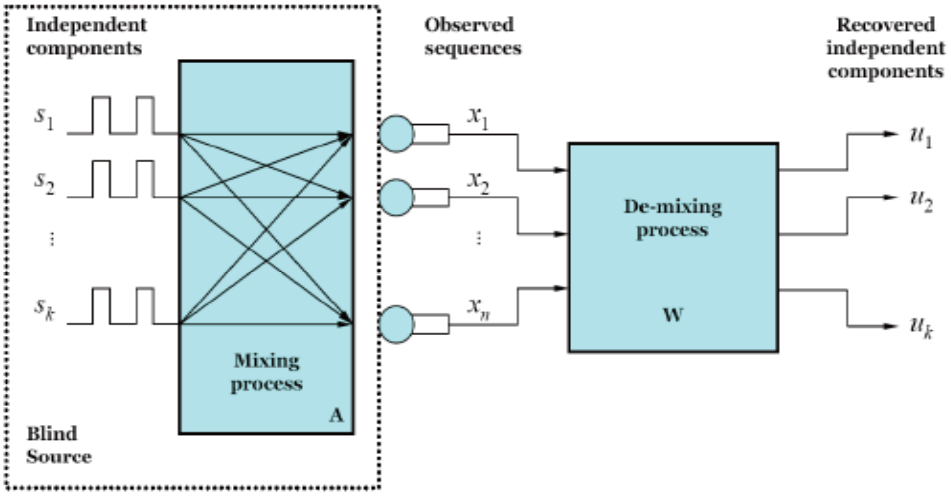

Figure 2.10 schematic diagram of ICA [16]

This algorithm is consists of two steps as follows.

- Step 1: Use ICA to separate the signals of the bridge from others (such as noise, car, and etc.). Herein, FastICA is chosen for the singles separation, since it is well known, fast, and representative.
- Step 2: FastICA calculates the power value to check which signal is the most powerful and can represent the bridge's vibration. Power value calculation is important for linear ICA and is useful for choosing the signal that represents the bridge's vibration. The most powerful signal is considered to be the bridge's signal, because our sensors are set directly on the bridge. in this way, the acquired vibration data is de-noised and used for damage diagnosis.

2.3.2 Wavelet Transform based Data Processing Method

Contraction threshold based Wavelet Transform (WT) is a common method for data processing in BSHM such as the BSHM system on Golden Gate Bridge [6]. Wavelet transform is a kind of time - frequency signal analysis method, which has the characteristics of multi-resolution analysis, and has the ability of denoting local signal characteristics in both time and frequency domain. It is a kind of time and frequency localization of analysis method which can change time window and frequency window. This method is very suitable for analyzing the change of the signal process.

For an arbitrary energy limited function $f(t) \in L^2(R)$, the wavelet transform of $f(t)$ is show as equation (2.3), where a and b are the scale factor and shift factor respectively, $a, b \in R$ and $a \neq 0$. $\varphi_{a,b}$ is the wavelet base, which is the wavelet function cluster of the mother wavelet $\varphi(t)$. Also, the $\varphi_{a,b}(t)$ satisfies the equation (2.5), where $F_\varphi(\omega)$ is the Fourier transform of $\varphi(t)$. The function $f(t)$ can be refactored as equation (2.6) by the wavelet coefficients $W_f(a,b)$.

$$W_f(a,b) = \langle f(t)\varphi_{a,b}(t)\rangle = \frac{1}{\sqrt{|a|}}\int_{-\infty}^{\infty} f(t)\overline{\varphi(\frac{t-b}{a})}dt \tag{2.3}$$

$$\varphi_{a,b}(t) = \frac{1}{\sqrt{|a|}}\,\varphi(\frac{t-b}{a}) \tag{2.4}$$

$$C_\varphi = \int_{-\infty}^{\infty} \frac{|F_\varphi(\omega)|^2}{|\omega|} d\omega < \omega \tag{2.5}$$

$$f(t) = \frac{1}{C_\varphi}\iint_{-\infty}^{\infty} W_f(a,b)\,\varphi(\frac{t-b}{a})\frac{1}{a^2}dadb \tag{2.6}$$

The main theoretical basis Wavelet threshold de-noising method is: in wavelet domain, the energy of the signal belonged to Besov space is concentrated in a limited number of coefficients, but the noise energy is distributed in the wavelet domain. After wavelet decomposition, the wavelet transform coefficients of signal are bigger than the wavelet transform coefficients of noise. So a suitable number lambda can be found as threshold, when the $W_{i,k}$ is less than the threshold, the $W_{i,k}$ at this moment is mainly caused by noise; conversely, when the $W_{i,k}$ is greater than the threshold, it is mainly caused by the signal. The steps of wavelet threshold de-noising method show as follows:

1) One-dimensional wavelet decomposition of signals: Select and determine the level of decomposition, and then do decomposition calculation.

2) Quantize the threshold of high frequency coefficient: Choose a threshold to do quantization threshold processing for high frequency coefficients.

3) One-dimensional wavelet reconstruction: the one-dimensional wavelet reconstruction is performed according to the bottom low frequency coefficients of wavelet decomposition and the high frequency coefficient of each layer.

2.3.3 Empirical Mode Decomposition based Data Processing Method

Empirical mode decomposition (EMD) [10] is a kind of nonlinear and non-stationary data processing method. Empirical model decomposition (EMD) is employed as data processing to de-noise in many BSHM systems such as the BSHM on Jindo Bridge. The outstanding advantage of EMD is that the data has a good adaptability. The EMD decompose the signal into more orderly Intrinsic Mode Functions (IMFs) arranged from high frequency to low frequency, each IMF represents a vibrational mode.

Definition2.1: an IMF must satisfy the two conditions shown as follow.

- In the whole IMFs, the quantity of zero-crossings has to equal to that of extrema or differ at most 1.
- At any point, the average values of the two envelopes composed of local maximum points and minimum points are equal to 0.

Decomposition steps of EMD are shown as:

(1). Confirm all the local maximum and minimum of the signal, and then insert between each set of the extrema using cubic curves to develop an upper envelope and a lower envelope.

(2). Give the two envelopes' mean m_1 based on the two envelopes.

(3). The signal x and m_1 should be defined the difference to be the first component: $h_1 = x(t) - m_1$.

(4). Use h_1 replace $x(t)$, and repeat above 3 steps until h_{1k} satisfies definition 2.1 or the given stopping criteria. Let $c_1 = h_{1k}$, and separate c_1 from x(t): $r_1 = x(t) - c_1$, $x(t) = r_1(t)$. The stopping criteria is shown as equation (2.7), where S_d is a typical value from 0.2 to 0.3.

$$S_d = \sum_{i=1}^{n} c_i(t) + r_n(t) \tag{2.7}$$

(5). Repeat above 4 steps until r_n is monotonic or has a sole extremum from which none IMF can be extracted, the decomposition process is finished and shown as equation (2.8)

$$x(t) = \sum_{i=1}^{n} c_i(t) + r_n(t) \tag{2.8}$$

The steps of EMD based de-noising method:

- Step 1, use above described EMD to decompose signal into IMFs.
- Step2, remove the IMF caused by high frequency noise from the decomposition IMFs. Since the IMF components are arranged from high to low frequency, the first IMF is caused by high frequency random noise. After removal of the First IMF, the rest of the IMFs is used to reconstruct signal to achieve de-noising.

2.4 Data Analysis Method for Damage Detection

Accuracy and sensitivity of damage diagnosis algorithm directly determines the performance of BSHM system. How to identify damages sensitively and how to precisely detect the damage severity and location become major problems in vibration data based BSHM system. Currently, many methods have been proposed by different researchers to identify structural damage, such as model-based algorithms and feature-based algorithms, for BSHM. A fundamental difficulty with model based methods is that physical-parameters acquired from the model updating is likely to unrelated to the information of real damage (location and severity). Deferent to model-based algorithms, the feature-based algorithms detect the changes of structure based on some damage features without a particular structural-model. The Features used for damage identification are typically based on mode-shape derivative, natural frequency, and stiffness-matrix etc.

2.4.1 Frequency Domain Decomposition based Damage Diagnosis Method

Frequency Domain Decomposition (FDD) method is proposed by Brinker et al. [26] and applied in the BSHM system of Jindo Bridge [7]. FDD starts by constructing and decomposing the PSD matrix for the measured data via the singular value decomposition (SVD) shown as equation (2.9), where y is the measurement vector; $S_{yy}(\omega)$ is the PSD matrix; Σ is the diagonal matrix, which contains the singular values ($\sigma_i(\omega)$) in descending order; $\boldsymbol{U}$ is the unitary matrices with left singular vector, and $\boldsymbol{V}$ is unitary matrices with right singular vector. Due to the symmetry of $S_{yy}(\omega)$, $\boldsymbol{U}$ is equal to $\boldsymbol{V}$. The magnitudes of the singular values indicate the relative level of vibration at the corresponding frequencies. The peaks in the plot of the 1st singular value versus frequency can be interpreted as natural frequencies of the structure, while the corresponding 1st singular vectors at these frequencies can be interpreted as the associated mode shapes. Thus, based on the 1st singular value function, the conventional peak picking method is used to obtain the natural frequency.

$$S_{yy}(\omega) = \boldsymbol{U}(\omega)V^T(\omega)\sum(\omega) \tag{2.9}$$

The steps of the FDD based damage diagnosis algorithm are shown as:

- Step 1: Use FDD to obtain the natural frequency of bridge in health condition and unknown condition based on the acquired vibration data.
- Step 2: Compare the natural frequency of the undamaged condition and unknown conditions to determine the structure health condition of bridge. Change in frequencies means there are damages on the bridge.

2.4.2 ICA based FFT Method

Cheng et al. proposed a feature based algorithm in [16]. ICA (independent component analysis) is used to de-noise. And then FFT is employed to obtain the structural health status of Seiran Bridge in Japan. Data processing is described in section 2.3.1, and the processes of this Method are shown in Figure 2.11.

This algorithm is consists of three steps as follows.

- Step 1: Use ICA to separate the signals of the bridge from others (e.g., noise, car, and wind signals). Herein, FastICA is chosen for the singles separation to obtain the bridge' signal, since it is well known, fast, and representative.
- Step 2: Use FFT to obtain the characteristic frequency of bridge from the signal separated by ICA in the undamaged condition (or known condition) and unknown conditions.
- Step 3: Compare the extracted frequency of the undamaged condition and unknown conditions to determine the structure health condition of bridge. Change in characteristic frequencies means there are damages on the bridge.

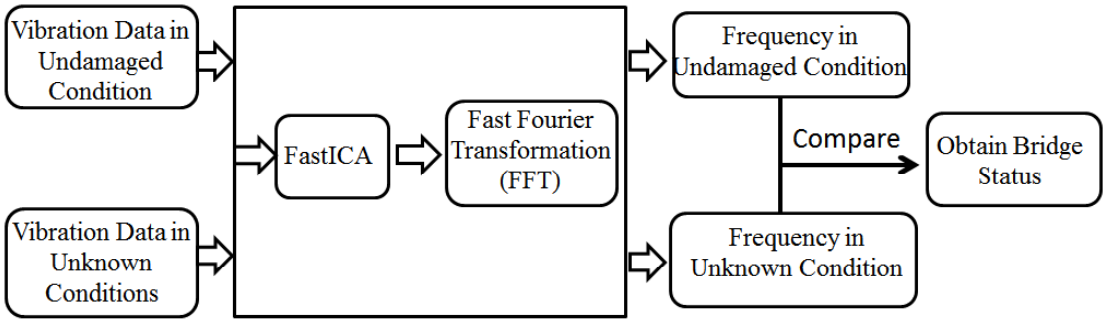

Figure 2.11 Processes of ICA based FFT Method

2.4.3 Statistical Pattern Recognition based Damage Diagnosis Method

Lately, statistical pattern recognition techniques (SPR) have made a survey about expectation of seeking a more high-performance method for distributed damage detecting. A SPR based damage diagnosis algorithm is proposed and applied in [17], on which residual error is used to extract the damage sensitive feature (DSF), it helps to determine the severity besides location of damage. For a signal $x(t)$, auto-regressive model of p order can be written as equation (2.10), where $e_{(x)}(t)$ is the residual error, $\phi_i^{(x)}$ is AR coefficients to be determined by Yule-Walker or Burg method.

$$x(t) = \sum_{i=1}^{p} \phi_{ix} x(t-i) + e_{(x)}(t) = \Phi_X^T X + e_{(x)}(t) \qquad (2.10)$$

Let $y(t)$ be the response of unknown structural condition, so following the same model in equation (2.10) it can be written as equation (2.11), where the notations carry their usual meaning as earlier.

$$y(t) = \sum_{i=1}^{p} \phi_{iy} y(t-i) + e_{(y)}(t) = \Phi_Y^T Y + e_{(y)}(t) \quad (2.11)$$

Now, to judge whether two cases (reference and unknown) are comparable to an extent, based on residual errors, the damage sensitive feature is found out as equation (2.12), reflecting the difference between those two signals. If the DSF is close to 1, the anonymous signal is close to the reference model; hence a way to detect as well as quantify damage. These processes are shown in the Figure 2.12.

$$DSF = e_{(y)}(t)/e_{(x)}(t) \quad (2.12)$$

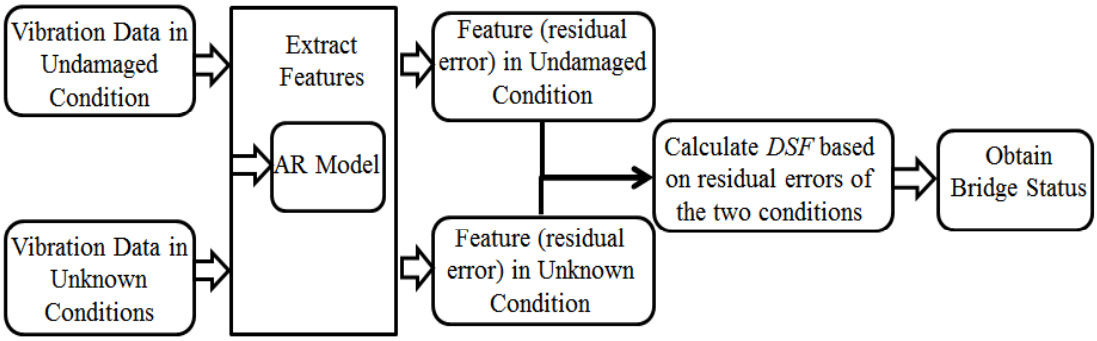

Figure 2.12 Processes of SPR based damage diagnosis method

2.4.4 Other Algorithms

Farrar et al. [18, 20] evaluated the sensitivity of some features to all kinds of damages based on data sampled on the real bridge. It was proved that the features based on modal property were not good at damage identification. R. Koushik et al. [21] developed an attractive damage diagnosis for mechanical systems. A damage identification method based on time-series analysis with AR (autoregressive) model is designed to extract damage feature in [21]. A detection scheme is proposed to detect structural novelty and locate damage by using the damage features obtained from data. Peter et al. [22] further presented a feature extraction method based on ARMA (autoregressive with moving average [22]) modeling. It explored the effectiveness of AR damage indicators and classification algorithms, and applied statistical methods to different types of structures.

2.5 Nondestructive Testing Method for Local Damage Detection

Most of vibration data-based BSHM systems can only locate the approximate areas and severity of damages. In other words, the specific location and severity of damages, such as subsurface voids and cracks, are nearly impossible to be determined by these algorithms. However, the specific location and severity of damages are very important for government to maintain bridges. Therefore, when the BSHM system detects a

severe damage, nondestructive testing (NDT) [23] is required to detect the precise location and size of the damage. In last few decades, many nondestructive testing techniques and systems are developed to obtain the specific information of damages, such as Ultrasonic inspection based system, X-ray based system, Ground-penetrating radar based system, and etc.

2.5.1 Stress Waves

Figure 2.13 shows the principle of stress wave testing method. Impacting the material surface is used to generate stress waves to propagate through the material at the sound speed and reflect from outside surfaces, internal crack, and boundaries surfaces between adjacent different materials. The time used for stress wave to propagate a required distance can be utilized to detect the location of decay in bridge structure. When stress waves through decay part, its propagation speed is smaller than healthy part. Thus, based on the size of material and propagation time, location of decay can be obtained.

Usually, attenuation of stress wave in decay part is quicker than that in sound elements. Therefore, the location of decay can be detect by observing the frequency of propagating stress wave, due to the higher frequency propagating in health part and low frequency propagating in decayed part.

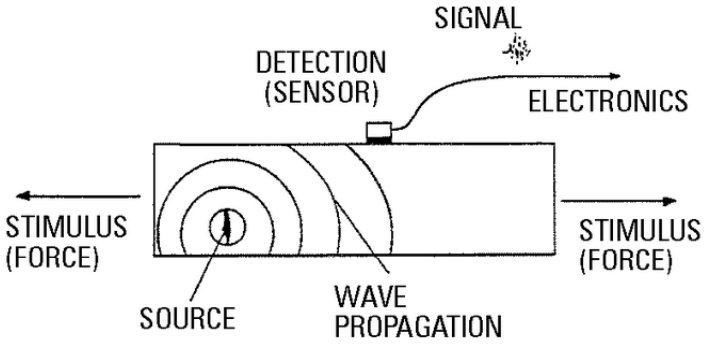

Figure 2.13 Stress Wave Probing

2.5.2 Ultrasonic Inspection

Figure 2.14 shows the principle of NDT method by using ultrasonic inspection techniques. The ultrasonic inspection techniques contain the characteristics of the stress wave with high frequency (usually bigger than 20 KHz) transmitting through material. Ultrasonic inspection techniques have been widely used to detect strength-reducing defects in bridge structural members.

In [24], ultrasonic-wave is used to detect the rebar corrosion progression. A nonlinear ultrasonic based NDT method is presented by Shah in [25] to detect the concrete. The main lack of using ultrasonic inspection for bridge structural detection is it is difficultly to effectively obtain ultrasonic coupling between the surface of

bridge and transducer. Another defect of ultrasonic inspection in bridge structural NDT is it needs to touch the bottom surface of bridge deck to transmit and receive ultrasonic wave. Due to the significant attenuation of stress waves with high-frequency, the propagating distance of stress wave is short. Thus, the ultrasonic wave based DNT method can effectively detect decay and other defects in very limited area only, which limits ultrasonic waves to be applied in bridge structures with large, heavy cross sections.

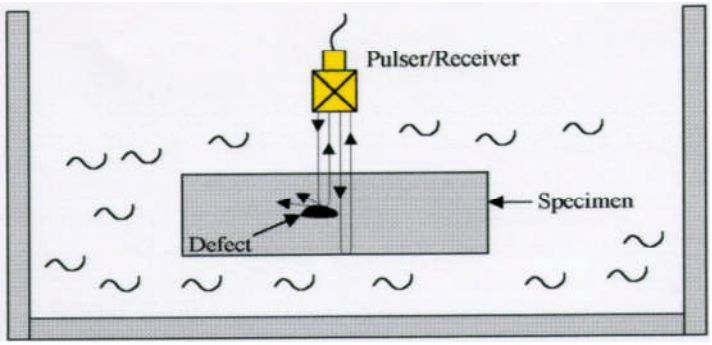

Figure 2.14 Ultrasonic Testing [24]

2.5.3 Radiography

Radiography technique uses a radiographic source placed on one side of an object to send radial and a recorder, for example a film, on the other side to record the received radial. The condition of bridge structural has been investigated by radiographic techniques based NDT methods are applied to detect the bridge structural heath condition in laboratory and field. However, portability of equipment is the main problem in field bridges. Another lack of radiographic techniques based NDT methods is it is difficult to access the bottom surface of bridge deck to place the recorder. In [26], X-ray mapping is used to evaluate the penetration of alkalis. Also we must note the hazard of radial in radiographic techniques to humans. A NDT method based on analyzing the surface waves in multichannel is proposed in [27]. However, it is expensive and time consuming.

2.5.4 Microwave / Ground Penetrating Radar

Microwave inspection techniques are based on the propagation characteristic of electromagnetic-waves (shown in Figure 2.15). Ground penetrating radar is travel microwave inspection technique. It uses an antenna intergrade transmitter and receiver to send wave and receive the reflected wave. Then based on the reflected wave techniques can obtain the time difference of two or three difference surfaces. The time difference can be used to detect the location and size of damages or defects. Chen and Wimsatt [28] used a 400 MHz antenna to detect the subsurface health conditions in pavements. Yehia et al. [29] studied many different type NDT techniques, such as

ground penetrating radar technique and impact echo technique, designed to detect the health conditions of concrete deck in bridges. Field data complexities and difficulties in data interpretation limit the application of the abovementioned techniques.

Figure 2.15 Ground penetrating radar [28]

2.6 Problem Definition

As described in above sections, with the developments of technologies in BSHM, many type vibration-based BSHM systems had been developed and applied in field bridges, such as BSHM system in Golden Gate Bridge, system in Jindo Bridge, etc. However there are still many problems in researches of BSHM. Especially in data analysis, current researches employ many de-noising algorithms for data processing to reduce the impacts of noises but ignore whether these algorithms perform efficiently for bridge system which is a nonlinear system, and the problem about the impacts of varying operational condition and environment on damage identification precision. Also, for damage diagnosis, how to solve the problems of identification sensitivity and locating precision are not essentially solved.

2.6.1 Problems of Data Processing in BSHM

In vibration data based BSHM system, measurement noises widely exist in acquired vibration-data, and are derived from thermal, magnetic and electric effect of data acquiring devices and observation error. These noises can bring difficulties to damage identification while the noise pollution of vibration-data is large, because noises can cover the characteristic changes caused by damages. In order to reduce the impacts of noises on damage identification to avoid wrong results of damage identification, many kinds of de-noising methods had been employed for data processing in BSHM system, such as wavelet transform de-noising algorithm in the BSHM of Golden Gate Bridge, empirical mode decomposition de-noising algorithm in the system of Jindo Bridge, ICA in reference [16], and etc.

Wavelet Transform (WT) is a common method for data processing in BSHM. In this algorithm, after wavelet decomposition, the wavelet transform coefficients of signal are bigger than the wavelet transform coefficients of noise. So a suitable number lambda can be found as threshold, when a wavelet transform coefficient is less than the threshold, this coefficient at this moment is mainly caused by noise; conversely, it is mainly caused by the signal. In order to determine appropriate threshold to reduce noise in the appropriate range, WT usually needs to estimate the range of characteristic frequency about true signal and noise firstly. If there is no prior knowledge about the range of characteristic frequency, it is difficult to get satisfied noise reduction.

ICA (Independent Component Analysis) is another application of data processing in BSHM. ICA is a famous blind source signals separation technology. In reference [16], FastICA is chosen to separate the singles from noises and others for de-noising, because of well known, fast, and representative. As we known, Fast ICA is a linear ICA algorithm, which is suitable to the processing of signal in linear mixing environments. Thus, there are some obvious disadvantages in the de-noising of non-linear signals, such as the vibration signals of bridge.

Empirical model decomposition (EMD) is employed as data processing to de-noise in many BSHM systems such as the BSHM on Jindo Bridge. It decompose the signal into many orderly Intrinsic Mode Functions (IMFs) arranged from high frequency to low frequency. This algorithm achieves de-noising by removing the first IMF from the decomposition IMFs, because the first IMF is caused by high frequency random noise. There two defects in this algorithm. First, the first IMF may contain the bridge signal components, which are the high frequency components of bridge signal possibly. Second, this algorithm only removed the high frequency part of the noises, thus the other IMFs remains noises.

In addition to above mentioned data processing methods in BSHM, many other den-noising algorithms are employed for data processing in BSHM. However, these data processing methods didn't regard the impact of varying operation condition and environment on damage indication, because these changes in the data caused by the varying operation condition and environment maybe regard as an effect of damage mistakenly. Therefore, how to separate changes caused by the variability from changes caused by real damage is also a challenge to the field implementation of a robust SHM system.

Based on above discussion, we can obtain follow problems summarization of existing data processing methods in BSHM.

1) The de-noising performance is not good in bridge system (nonlinear system) such as FastICA used in BSHM of reference [16] and wavelet transform in Golden

Gate Bridge system.

2) The impacts of varying operation condition and environment on damage identification are ignored by all these data processing method in BSHM.

To solve these above shortcomings, our data processing method should be able to: 1) effectively minimize the impacts of noises with satisfied reliability. 2) Effectively minimize the impacts of varying operation condition and environment on data analysis.

To achieve these goals, two data processing algorithms are proposed. The first is the optimization of de-noising performance by designing an improved post-nonlinear ICA de-noising algorithm. The second is designing a novel data normalizing algorithm based on data matching to eliminate the impacts of varying operation condition and environment on damage identification. The two algorithms are introduced in the chapter 3.

2.6.2 Problems of Data Analysis Method for Damage Detection

Currently, many methods have been proposed by different researchers to identify structural damage, such as model-based algorithms and feature-based algorithms, for BSHM. A fundamental difficulty with model based methods is that physical-parameters acquired from the model updating is likely to unrelated to the information of real damage (location and severity). Different to model-based algorithms, the feature-based algorithms detect the changings of structure based on some damage features without a particular structural-model. The Features used for damage identification are typically based on mode-shape derivative, natural frequency, and stiffness-matrix etc. Cheng et al. [16] proposed a feature based algorithm by using ICA (independent component analysis) to denoise and FFT to detect the changes in characteristic frequency. Based on the results, the bridge structure damage has been able to detect. However, the algorithm in [16] cannot detect the severity and location(s) of damage. Farrar et al. [18, 20] evaluated the sensitivity of some features to all kinds of damages based on data sampled on the real bridge. It was proved that the features based on modal property were not good at damage identification.

Lately, SPR (statistical pattern recognition) techniques have been studied in expectation of seeking a more high-performance method for distributed damage detecting. Sohn et al. [21] developed an attractive damage diagnosis for mechanical systems. In [21], ARX (a, b) models of the reference data segments and the unidentified data are constructed to obtain their model residuals. Hence, ARX residual sequences of reference and unidentified data can be obtained, which are ϵ_r and ϵ_u respectively. The researchers define the ratio $\sigma(\epsilon_u)/\sigma(\epsilon_r)$ as DSF

(damage-sensitive-feature). A changing of damage indicator's values is regarded as the damaged. A statistical detecting scheme and the damage features obtained by all data samples were designed to detect the novelty of structure and locate damage. The main lack of model residual based algorithms is that the sensitivity of the DSF is easily affected by noise, varying environment and model type easily. [22] reported an application of AR model residuals based damage diagnosis algorithm in a concrete bridge. In [22], it successfully applied the AR model residuals in detecting structural change. An undamaged condition data set is applied for obtaining a reference AR model. The main lack of model residual based algorithms is that the sensitivity of the DSF is easily affected by the noise, varying environment and model type easily.

Based on above discussion, we can obtain following problems summarization of existing damage diagnosis algorithm.

1) The physical-parameters acquired from the model updating is likely to unrelated to the information of real damage (location and severity) in model based methods.

2) In feature based algorithms, the global feature-based algorithms, such as the algorithm in [16], cannot minor damage sensitively and locate damage. The damage feature in not good sensitivity is another problem in feature based algorithm such as algorithm in [18, 20].

To deal with these above problems, our damage diagnosis algorithm should able to: 1) identify the damages in sensitivity and accuracy; 2) detect damage severity and locate damages efficiently. To reach these goals, a novel two-stage bridge structure damage diagnosis algorithm is introduced in the chapter 4.

2.6.3 Problems of Nondestructive Testing Method for Local Damage Detection

NDT (Non-destructive Testing) based local damage diagnosis algorithm comprises assessing the health condition of systems and components without destruct them by using a large number of analysis techniques utilized in science research and industry production. In last the past few decades, many nondestructive testing techniques and systems are developed to obtain the specific information of damages.

In [31], a NDT method based on stress wave is proposed. In this method, impacting the material surface is used to generate stress waves to propagate through the material at the sound speed and reflect from various surfaces, such as internal crack and boundaries surfaces between adjacent different materials. The time used for stress wave to propagate a required distance can be utilized to detect the location of decay in bridge structure. When stress waves through decay part, its propagation speed is smaller than in healthy part. Thus, based on the size of material and the time propagate time the location of decay will be obtained.

The ultrasonic inspection techniques contain the characteristics of the stress wave with high frequency (bigger than 20 KHz) transmitting through material. In [24], ultrasonic-wave is used to detect the rebar corrosion progression. A nonlinear ultrasonic based NDT method is presented by Shah in [25] to detect the concrete. The main lack of using ultrasonic inspection for bridge structural detection is difficulty to effectively obtain ultrasonic coupling between the surface of bridge and transducer. Another defect of ultrasonic inspection in bridge structural NDT is to touch the bottom surface of bridge deck to transmit and receive ultrasonic wave. Due to the significant attenuation of stress waves with high-frequency, the propagating distance of stress wave is short. Thus, the ultrasonic wave based DNT method can only effectively detect decay and other defects in very limited area, which limits ultrasonic waves to be applied in bridge structures with large, heavy cross sections.

The radiography technique uses a radiographic source placed on one side of an object to send radial and a recorder, for example a film, on the other side to record the received radial. The condition of bridge structural has been investigated by radiographic techniques based NDT methods are applied to detect the bridge structural heath condition in laboratory and field. However, portability of equipment is the main problem in field bridges. Another lack of radiographic techniques based NDT methods is difficulty in accesssing bottom surface of a bridge deck to place the recorder. In [26], X-ray mapping is used to evaluate the penetration of alkalis. Also we must note the hazard of radial in radiographic techniques to humans. A NDT method based on analyzing the surface waves in multichannel is proposed in [27]. However, it is expensive and time consuming.

Microwave inspection techniques are based on the propagation characteristic of electromagnetic-waves. Ground penetrating radar is travel microwave inspection technique. It uses an antenna intergrade transmitter and receiver to send wave and receive the reflected wave. Then based on the reflected wave techniques can obtain the time difference of two or three difference surfaces. The time difference can be used to detect the location and size of damages or defects. Chen and Wimsatt [28] used a 400 MHz antenna to detect the subsurface health conditions in pavements. Yehia et al. [29] studied many different type NDT techniques, such as ground penetrating radar technique and impact echo technique, designed to detect the health conditions of concrete deck in bridges. Field data complexities and difficulties in data interpretation limit the application of the abovementioned techniques. When testing methods based on electromagnetic waves were used in the past, several serious problems were encountered. Conventional electromagnetic wave-based testing methods, such as microwave and ground-penetrating radar, need the total reflected waveform to calculate the location of subsurface voids using time delay. However,

considering the frequency limitations of the oscilloscope and A/D converter, it might be difficult to clearly capture the waveform at high frequencies (higher than 1 GHz). In addition, it is difficult to separate the incident and reflected waves.

Based on above discussion, to order to solve these problems of existing NDT technologies, our NDT system should have the following function: 1) detect the location and the damage severity which has not only high accuracy, but also resolution; 2) detect and locate damages economically and efficiently. To reach these goals, we then introduce the idea of standing-wave based structure nondestructive testing system for local damage information detection in the chapter 5.

References

[1] D. Balageas, C. Fritzen, and A. Güemes, “Structural Health Monitoring”, ISET Ltd., London, UK. (2006)

[2] K, Wong, “Monitoring Hong Kong’s Bridges Real-Time Kinematic Spans the Gap.” GPS world, Vol. 12, No. 7, pp10-18. (2001)

[3] J. Caicedo, E. Clayton, and S. Dyke, “Structural Health Monitoring for Large Structures using Ambient Vibration.” Proceeding of the ICANCEER Conference, Hong Kong, August 15-20.(2002)

[4] E. Cross, K. Koo, J. Brownjohn, , and K. Worden, “Long-Term Monitoring and Data Analysis of the Tamar Bridge.” Mechanical Systems and Signal Processing, Vol.35, No.1-2, pp.16-34.

[5] Z. Sun, G. Li, , and S. Geng. “Study on Stayed-Cable Health Monitoring.” Advanced in Intelligent Systems and Computing, Vol. 180, pp.1091-1098. (2013)

[6] S.N. Pakezad, “Design and Implementation of Scalable Wireless SensorNetwork for Structural Monitoring”, Journal of Infrastructure Systms, Vol.4, No.1, pp.89-101. (2008)

[7] S. Jang, H. Jo, K. Mechitove, J. Rice, “Structural Health Monitoring of a Cable-Stayed Bridge using Smart Sensor Technology: Deployment and Evaluation.” Smart Structures and Systems, Vol. 6. No.5, pp.439-460.(2010)

[8] K. Chebrolu, B. Raman, and N. Mishra, “BriMon: A Sensor Network System for Railway Bridge Monitoring”, Proceedings of the 6th international conference on Mobile systems, applications, and services, pp.2-14, New york, USA. (2008)

[9] M. Maroti, B. Kusy, G. Simon, and A. Ledeczi, "The flooding time synchronization protocol". in Proc. of the 2nd International Conference on Embedded Networked Sensor Systems 2004, Baltimore, MD, ACM Press, pp. 39-49, New york, USA. 2004(2004)

[10] A. Woo, T. Tong, and D. Culler, “Taming the underlying challenges of reliable multi-hop routing in sensor networks”. SenSys 2003 Los Angeles, California.

[11] K. Cock, and B. Moor, “subspace indentification methods”, Control systems, robotics, and Automation, Vol.5.

[12] T. Li, H. Xiao, and H. Ogai, “A Multi-hop Wirelss Sensor System for Bridge Health Monitoring”, IEEJ transactions on Electronics, Information and Synstems, Vo.131, No.10, PP.1760-1766. (2011)

[13] S. Ganeriwal, R. Kumar and M. B. Srivastava, "Timing-sync protocol for sensor networks". in Proc. of the SenSys 2003, Los Angeles, CA, Nov. 2003.

[14] K. Lae, E. Serpedin, and K. Qaraqe, “A New Approach for Time Synchronization inWireless Sensor Networks: Pairwise Broadcast Synchronization”, IEEE Transactions on Wireless Communications, Vol.7, No.9, 3318-3322. (2008)

[15] S. Cho, H. Jo, etc, “Structural health monitoring of a cable-stayed bridge using wireless smart sensor technology: data analyses”, Smart Structures and Systems, Vol. 6, No.5-6, PP.461-480. (2010)

[16] J. Cheng, “Bridge diagnosis system by using wireless sensor network and independent component analysis,” Master’s thesis, Waseda University (2005)

[17] Sohn H, Farrar CR, “Damage diagnosis using time series analysis of vibration signals,” Smart Mater Struct Vol.10, pp.1–6 (2001)

[18] Farrar CR, Jauregui DA, “Comparative study of damage identification algorithms applied to a bridge: I. Experiment,” Smart Mater Struct, Vol.7, pp704–719 (1998)

[19] Farrar CR, Jauregui DA, “Comparative study of damage identification algorithms applied to a bridge: II Numerical study,” Smart Mater Struct, Vol.7, pp.720–731 (1998)

[20] Farrar, C.R., Duffey, T.A., Doebling, S.W., Nix, D.A, “A statistical pattern recognition paradigm for vibration-based structural health monitoring,” 2nd International Work shop on Structural Health Monitoring, Stanford, CA (1999)

[21] R. Koushik, and H. Ogai, “Damage Detection of Bridge Using Wireless Sensors”, 2012 IFAC Workshop on Automation in Mining, Mineral and Metal Industries, Vol.2, Part 1, pp.107-111. (2012)

[22] Peter Carden, E., Brownjohn, James M. W., “ARMA modelled time-series classification for structural health monitoring of civil infrastructure,” Mechanical Systems and Signal Processing, Vol. 22, No. 2, pp.295-314 (2007)

[23] Ch. Hellier: “Handbook of Nondestructive Evaluation”, McGraw-Hill. p. 1.1. ISBN 0-07-028121-1. (2003)

[24] S. Sharma and A. Mukherje: “Monitoring corrosion in oxide and chloride envroments using ultrasonic guided waves,” Journal of Materials in Civil Engineering, Vol. 23, No.2, pp.207–211 (2011)

[25] A. A. Shah and S. Hirose: “Nonlinear ultrasonic investigation of concrete damaged under uniaxial compression step loading,” Journal of Materials in Civil Engineering, Vol.22, No.5, pp.476–483 (2010)

[26] A. S. M. Kamal and M. Boulfiza: “Durability of GFRP Rebars in simulated concrete solutions under accelerated aging conditions,” Journal of Composites for Construction, Vol.15, No.4, pp.473–481 (2011)

[27] G.Cascante, H. Najjaran, and P. Crespi: "Novel methodology for nondestructive evaluation of brick walls: fuzzy logic analysis of MASW tests," Journal of Infrastructure Systems, Vol.14, No.2, pp.117–128 (2008)

[28] D. H. Chen and A. Wimsatt: "Inspection and condition assessment using ground penetrating radar," Journal of Geotechnical and Geoenvironmental Engineering, Vol.136, No.1, pp.207–213 (2010)

[29] S. Yehia, O. Abudayyeh, S. Nabulsi, and I. Abdelqader: "Detection of common defects in concrete bridge decks using nondestructive evaluation techniques," Journal of Bridge Engineering, Vol.12, No.2, pp.215–224 (2007)

[30] M. Whelan, M. Gangone, K. Janoyan, " Highway Bridge Assessment Using an Adaptive Real-time Wireless Sensor Network", IEEE Sensors Journal, Vol.9, No.11, pp.1405-1413. (2009)

[31] "Stress-Wave Probing of Electric Field Distributions in Dielectrics", Phys. Rev. Lett. 47, 1483 – 1487. (1981)

[32] R.C. M, "Bridge diagnosis by using wireless sensor network and Transfer Function," Master's thesis, Waseda University. (2009)

Chapter 3

Improved Nonlinear ICA based Data Processing Method

3.1 Introduction

In vibration based bridge structural health monitoring (BSHM) system, the main purpose of BSHM is to evaluate the health condition of bridge structure by analyzing the vibration data of bridge. The key issue of this type BSHM system is how to detect the damages in sensitive and accuracy by analyzing the vibration data. Attribute to use more and more advanced hardware facilities for BSHM system, the measurement errors is reduced significantly. However, these devices cannot make the acquired vibration-data avoid the measurement noises, which can affect the precision of damage diagnosis significantly by covering the characteristic changes caused by damages. Otherwise, during deploying a BSHM system on a field bridge which is exposed to outside varying operation condition and environment, the changes in the data caused by the variability of operation condition and environment maybe regard as an effect of damage mistakenly. Therefore, design of a data processing method to de-noise and eliminate the impacts of varying operation condition and environment is an indispensable mean for detecting damages accurately.

In the research, to deal with these problems, a two-stage data processing method, including a new de-noising algorithm and a novel environment impact reduction method, is proposed to efficiently de-noise in nonlinear system and reduce the impact of varying operation condition and environment on data analysis. To achieve efficiently de-noising an improved post-nonlinear geometric-linearization ICA algorithm is designed for data processing in nonlinear system. After de-noising, in order to reduce the impact of varying operation condition and environment, a novel environment impact reduction method based on similarity matching is proposed. The simulation and experiment results of the two methods show better performance.

3.2 Overview of Proposed Data Processing Method

In order to effectively solve above discussed noisy vibration data problem and varying environment (complex working condition) impact, a two-stage data process method is proposed in this charter. The proposed diagnosis scheme consists of the two stages shown in Figure 3.1.

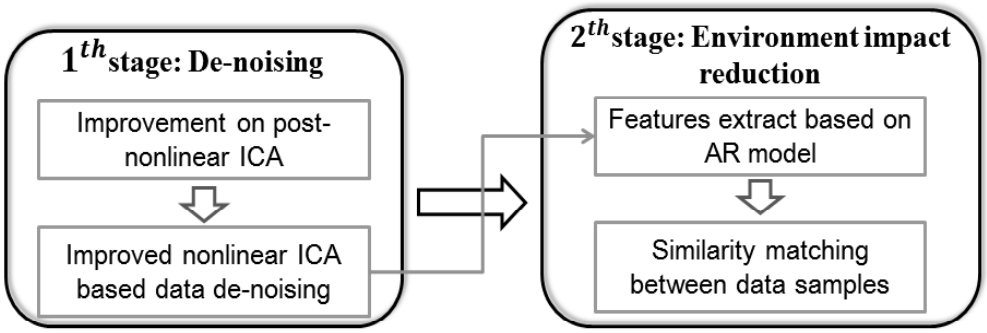

Figure 3.1 Two-stage data process method

The method of first stage is designed to reduce the impact of noises, and the method of second stage is proposed to reduce the impact of varying environment and operation condition. In the first stage, to achieve efficiently de-noising in nonlinear system (bridge system), an improved post-nonlinear geometric-linearization ICA based de-noising method is designed for processing vibration data. In this improved ICA algorithm, compensation based scheme is proposed to reduce the linearization error caused by the linearization scheme of the post-nonlinear geometric ICA. In the second stage, in order to reduce the impact of varying environment, a novel environment impact reduction method based on similarity matching is proposed. In the method, data samples are divided into two set, health condition data set and unknown condition data set. AR model is used to extract the features of each data samples in the two sets. Based on these features, a data matching scheme based on Euclidean distance is designed to obtain the data sample pair (one data sample of health condition data set and anther in unknown condition data set) measured in a similar environment. In this way, the change of structure caused by varying environment is reduced effectively.

To summarize, the data process scheme includes data de-noising and impact reduction of varying environment and operation condition. Formulations for the two stages are presented in the following subsections.

3.3 Improved Nonlinear-ICA based De-noising Method

3.3.1 Post-nonlinear Geometric ICA

Post-nonlinear (PNL) mixtures are proposed first by Taleb. The PNL model consists of two stages, the linear stage and the nonlinear stage. In [1], a post-nonlinear ICA, named pgICA (post-nonlinear Geometric ICA), is proposed and divided the demixing process into the two stages. Since the linear ICA algorithms are mature comparing with nonlinear ICA, the advantage of pgICA is it can utilize any kind of linear ICA algorithms in the second stage, to deal with various problems.

The pgICA algorithm consists of two stages: a geometry based linearization stage and a demixing stage by linear ICA algorithm. *m* blind source signals is presented in equation (3.1). Equation (3.2) formulates the linear mixing and nonlinear mixing of ICA, and the equation (3.3) shows vector *x*. In equation (3.2) the nonlinear function is defined as *f* and *A* is defined as the $n \times m$ full rank matrix. A separation system is needed to be established to obtain the source signal *s*. Thus, we need to search a mapping $G: R^n \rightarrow R^m$ such as equation (3.4), where *y*, shown in equation (3.5), represents the estimates of source signal *s*; *g* and *w* represents the inverted nonlinear-function (linearization function) and inverted-matrix. The two levels of pgICA are shown as Figure 3.2.

$$s = [s_1(t), s_2(t), \cdots, s_m(t)]^T \tag{3.1}$$

$$v = As,\ x = f(v) = f(As) \tag{3.2}$$

$$x = [x_1(t), x_2(t), \cdots, x_n(t),]^T \tag{3.3}$$

$$y = G(x) = g(Wx) \tag{3.4}$$

$$y = [y_1(t), y_2(t), \cdots, y_m(t),]^T \tag{3.5}$$

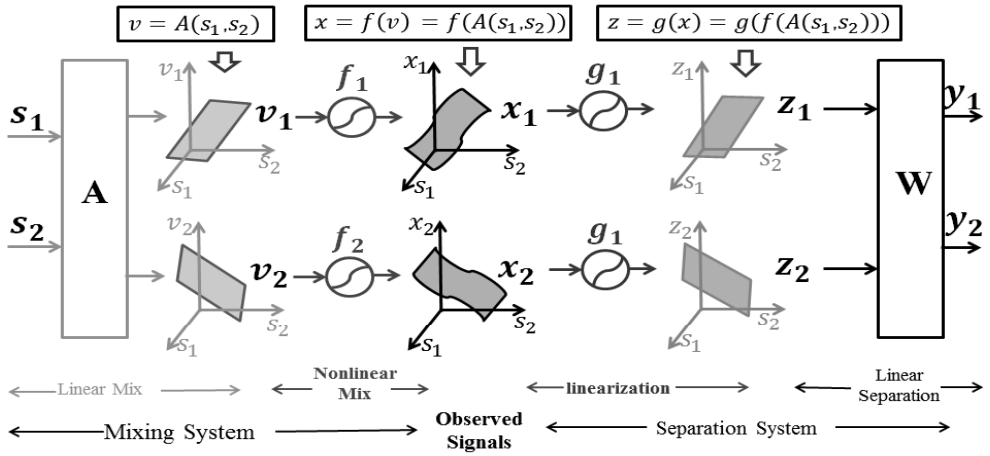

Figure 3.2 Two levels of the pgICA

A geometric viewpoint is applied in the pgICA to deal with the nonlinear problem. Generally, a linear-mixture signal and a nonlinear-mixture signal are able to be denoted by plane and curved surface in three-dimensional space respectively, such as the signal v and signal x in Fig 3.2. In this way, firstly the distribution of inputs is represented in a 3D space by pgICA. And then the distribution of inputs is geometrically transformed to planes by pgICA, and linear-mixture corresponded to that plane is funded. In the geometric transformation, the notation "companion points" is given to the points that belong to the 3D plane, which have equal position in x and y coordinate axis (unknown values). To recognize such points, the mixture's time-index is used to find a companion point; when $t = t_1$, a sample of nonlinear-mixture signal x_i is denoted as $x_1(t_1)$. Thereafter, ($s_1(t_1)$, $s_2(t_1)$, $x_1(t_1)$) is the coordinates of the point in the surface of signal x_1, which is point $p_1 = (s_1(t_1), s_2(t_1), s_1(t_1))$. Otherwise, a "fake plane" Γ_k is used as a referenced plane and the other surfaces Γ_i are transformed by this "fake plane". When a surface is chosen as the fake plane in this time transforming, the fake plane may change to another in the next transforming process period. At last, a linear ICA is used to de-mix the transformed linear-mixture to obtain the source signals.

To introduce pgICA, the process in detail for two observed signals, signal x_k and signal x_i, is given to introduce the method. There are two case needs to be considered. Case 1: observed signals have a linear mixture signal and a nonlinear mixture signals. Case 2: observed signals only contain nonlinear mixture signals. The steps are shown as follow.

(1) In case 1, randomly select a linear mixture signal x_k (plane) as reference plane Γ_k to linearize other surface. In Case 2, randomly select a nonlinear mixture signal x_k, (surface) as a fake plane named Γ_k. The other surface is called Γ_i, and $cont$ = 0. The processes of geometric linearization of case 1 and case 2 are shown as Fig 3.3 and Fig 3.4 respectively. The different between case 1 and case 2 only exist in this step. Other steps of the two cases are the same. So, we only give the flowchart of case 2 in Fig 3.5 for explaining.

(2) Pick two random points $p_{k1} = (s_1(t_1), s_2(t_1), x_k(t_1))$ and $p_{k2} = (s_1(t_2), s_2(t_2), x_k(t_2))$ from Γ_k. Locate their respective companion points q_{i1} and q_{i2} in the surface Γ_i.

(3) Select an arbitrary point $p_{kc} = (s_1(t_c); s_2(t_c); x_k(t_c))$ between p_{k1} and p_{k2}, and its companion point q_{ix} in Γ_i and q_{ic} on straight line $q_{i1}q_{i2}$. Get the value $z_i(t_c)$ of point $q_{ic} = (s_1(t_c); s_2(t_c); z_i(t_c))$ using equation (3.7).

$$z_i(t_c) = \frac{x_k(t_c) - x_k(t_1)}{x_k(t_2) - x_k(t_1)} (x_i(t_2) - x_i(t_1)) + x_i(t_1) \qquad (3.7)$$

(4) Update $x_i(t_c)$ by computing $x_i^{new}(t_c)$ using equation (3.8). μ belongs to [0, 1].

$$x_i^{new}(t_c) = \mu z_i(t_c) + (1 - \mu) x_i^{old}(t_c) \qquad (3.8)$$

(5) If $cont \leq N_k$ then $cont = cont + 1$ and go to step 2. Else, $cont = 0$ and compute the error using equation (3.9) and then go to next step. $N_k$is the amount of points updated in every iteration.

$$\epsilon = \frac{1}{nN_k}\sum_{i=1}^{n}\sum_{j=1}^{N_k}(x_i^{new}(j) - x_i^{old}(j))^2 \tag{3.9}$$

(6) If $\epsilon > \xi$ (stopping threshold of linearizing) go to (2). Else, the linearizing process is stopped. Go to the next step.

(7) Sort the linearized signal z_i according to an ascending order and name the sorted signal as z_i^s. Smooth z_i^s by using the averaging function, equation (3.6).

$$\tilde{z}_i(t) = \frac{1}{L}\sum_{j=-(L-1)/2}^{(L-1)/2} Z_i^s(t+j) \tag{3.6}$$

(8) Restore the original order of the smoothed signal $\tilde{z}_i$ to produce signal z_i. This nonlinear geometric transformation algorithm for n observations is the same as when $n = 2$. Then the signal x_k is used to transform other signals. After linearizing all signals, the signal x_k is transformed by the plane of signal z_i. Then use linear ICA to separate these linearized signals.

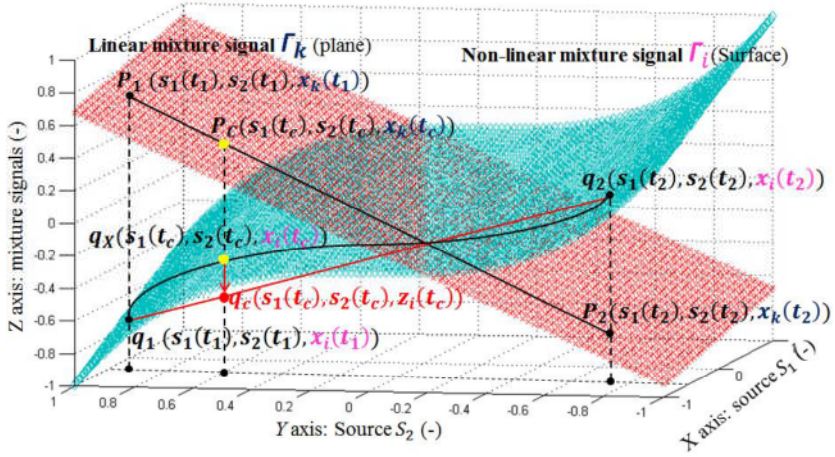

Figure 3.3 Geometric linearization process of the pgICA in case 1

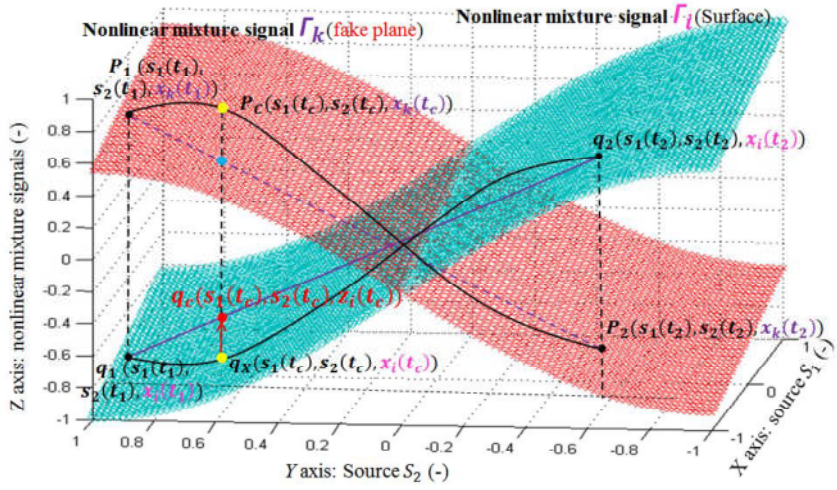

Figure 3.4 Geometric linearization process of the pgICA in case 2

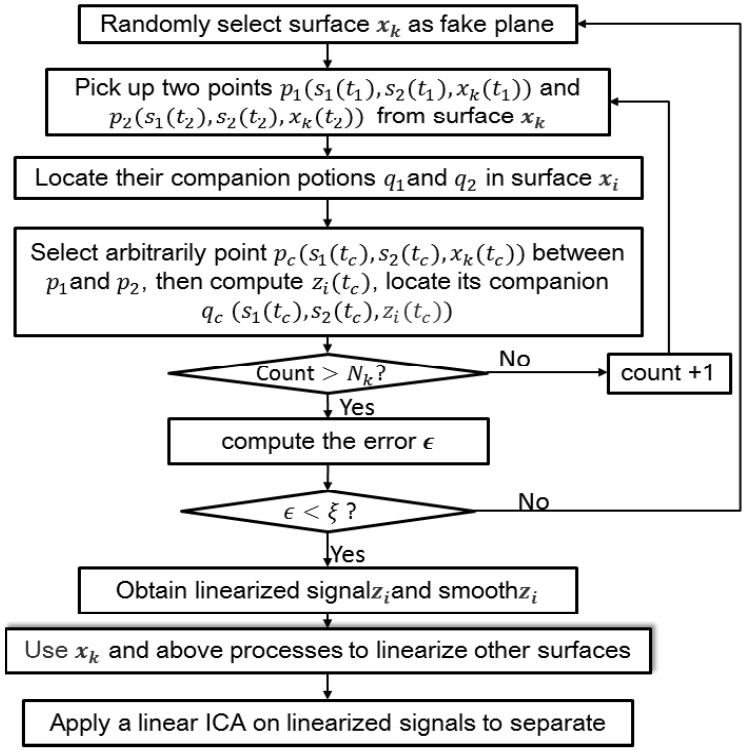

Figure 3.5 Flowchart of pgICA

3.3.2 Problem of Post-nonlinear Geometric ICA

We have previously [1] discussed three issues related to unavailability while using the geometric linearizing technique in pgICA. The first and second issues are solved in [1]. The third issue relates to vagueness in the point $q_c \in$ line q_1q_2. Due to the unknown first-two coordinates, if $p_c \in$ line p_1p_2 can't be ensured. Thus, as introducing in [1], the Proposition 2's reverse can't been hold always. It means not only one point can satisfy Proposition 2. The completed solution has not been found in [1] to remove the vagueness. A local transforming and a position update algorithm is applied in [1] to lower the vagueness.

In local transformation, we averagely divided the surface into small cells according to the amplitude of the observed signal. However, this could result in the number of samples in one cell being far smaller or bigger than the number in other cells, due to non-linear distortion of cells. As a result, the algorithm would not work. To address this, we have improved the local transformation. We arrange the amplitudes of observed signals in ascending order. Based on this, we determine the total number of cells, named CellNum. The surface is divided into CellNum cells. Thus, the number of samples in each cell is the same, but the amplitude of signal in every cell is different. The geometric linearization transformation is carried out in these cells. In this way, the problem of local transformation is solved.

In addition, a position update algorithm is applied to lessen the inaccuracy in [1]. In

this algorithm, in order to replace the operation of pulling q_x to the right position q_c, a learning-rate $\mu < 1$ is utilized for updating q_x. The transformation takes longer, but it converges to a plane in steady. Equation (3.8) shows the updating-function. In order to easily understand this linearization algorithm, a transversal cut over line p_1p_2 of the 3D plane is projected to the YZ axis as shown in Figure 3.6, where these points are p_1(-, -, $x_k(t_1)$), p_2(-, -, $x_k(t_2)$), p_c(-, -, $x_k(t_c)$), p'_c(-, -, $z_k(t_c)$), q_1(-, -, $x_i(t_1)$), q_2(-, -, $x_i(t_2)$), q_x(-, -, $x_i(t_c)$), q'_c(-, -, $z_i(t_c)$), and q_c(-, -, $z'_i(t_c)$).

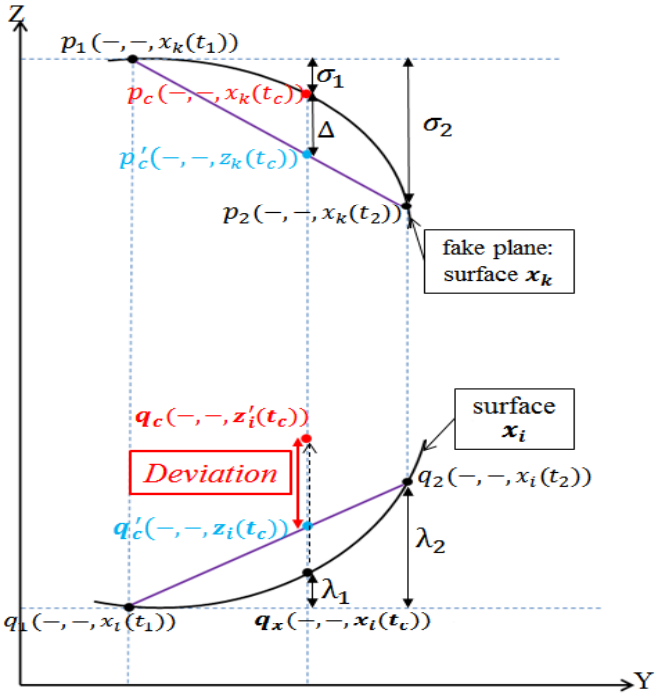

Figure 3.6 3D plane projected to YZ axis

From Fig 3.6, we can get equation (3.10), where $x_i(t_2)-x_i(t_1) > 0$. As shown in Figure 3.6, q_x is under the line q_1q_2. In the original geometric linearization algorithm, the reference plane is a real plane, but there is no real plane in the practical pgICA; pgICA utilizes a fake plane, resulting in an error. $z_i(t_c)$ is the value of t_c when the reference plane is the fake plane. Based on the above discussion and equation (3.7), we can get equation (3.11).

$$x_k(t_c) = z_k(t_c + \Delta)(\Delta > 0) \tag{3.10}$$

$$\begin{aligned} z'_i(t_c) &= \frac{x_k(t_c)-x_k(t_1)}{x_k(t_2)-x_k(t_1)}(x_i(t_2) - x_i(t_1)) + x_i(t_1) \\ &= \frac{z_k(t_c)+\Delta-x_k(t_1)}{x_k(t_2)-x_k(t_1)}(x_i(t_2) - x_i(t_1)) + x_i(t_1) \\ &> z_i(t_c) = \frac{z_k(t_c)-x_k(t_1)}{x_k(t_2)-x_k(t_1)}(x_i(t_2) - x_i(t_1)) + x_i(t_1) \end{aligned} \tag{3.11}$$

As shown by equation (3.11) and Figure 3.5, using q'_c instead of q_x leads to "move too much" phenomenon, which creates the point q_c. When $\Delta < 0$, $x_i(t_2)-x_i(t_1) < 0$, and q_x is under the line q_1q_2, this problem still exists.

$$z_i'(t_c) = \frac{z_k(t_c)+\Delta-x_k(t_1)}{x_k(t_2)-x_k(t_1)}(x_i(t_2)-x_i(t_1))x_i(t_1)$$

$$= \frac{z_k(t_c)-x_k(t_1)}{x_k(t_2)-x_k(t_1)}(x_i(t_2)-x_i(t_1)) + x_i(t_1) \quad + \Delta\frac{x_i(t_2)-x_i(t_1)}{x_k(t_2)-x_k(t_1)}$$

$$= z_i(t_c)+\Delta\frac{\lambda_2}{\sigma_2} = z_i(t_c)+\Delta k_2 \tag{3.12}$$

3.3.3 Improvement of Post-nonlinear Geometric ICA

To solve this problem, a compensation algorithm is proposed for pgICA. From equation (3.11), we can obtain equation (3.12). Equation (3.12) shows the value of q_c equal to q'_c (ideal value) plus a floating up and down deviation. If a method can reduce the deviation, we can calculate the position of q_c more accurately and transform the surface to a plane more accurately. Thus, we can limit the value of λ_2 and σ_2 to make the transformation more accurate.

Herein, we decribe our compensation algorithm in detail. We set

$$k_1 = \frac{\lambda_1}{\sigma_1} = \frac{x_i(t_1)-x_i(t_c)}{x_k(t_1)-x_k(t_c)} \tag{3.13}$$

$$k_2 = \frac{\lambda_2}{\sigma_2} = \frac{x_i(t_1)-x_i(t_2)}{x_k(t_1)-x_k(t_2)} \tag{3.14}$$

As shown in Figure 3.6, when $k_1 = k_2$, we get a perfect line $q_1\ q'_c\ q_2$. We can use this information to compensate the "move too much" phenomenon. By analyzing the position relation between point p_c and line p_1p_2, the position relation between q_c, q'_c and line q_1q_2, and by equation (3.12), we obtain the compensation algorithm as shown in equation (3.15) and equation (3.16). The new compensated $z'_i(t_c)$, named $z^c{}_i$(tc), is obtained from the $z'_i(t_c)$ calculated in equation (3.11). Note that the $z_i(t_c)$ in equation (3.7) is the same as the $z'_i(t_c)$ in equation (3.11).

When $k_2 > 0$ and $|k_1| > |k_2|$,

$$z_i^c(t_c) = z_i'(t_c) - (z_i'(t_c) - x_i(t_c))k_2 \tag{3.15}$$

When $k_2 < 0$ and $|k_1| < |k_2|$,

$$z_i^c(t_c) = z_i'(t_c) + (z_i'(t_c) - x_i(t_c))k_2 \tag{3.16}$$

We set $\Delta' = z'_i(t_c) - x_i(t_c)$ and take it into equation (3.12), and we get equation (3.17) and (3.18). We use the position of q_x and q'_c to compensate for the inaccuracy in the position of q_c caused by the "move too much" phenomenon.

$$z^c{}_i(t_c) = z_i(t_c) + (\Delta - \Delta')k_2 \tag{3.17}$$

$$z^c{}_i(t_c) = z_i(t_c) + (\Delta + \Delta')k_2 \tag{3.18}$$

Based on this compensation algorithm, we improve the pgICA and obtain the improved algorithm, named post-nonlinear compensated geometric ICA (pcgICA). The flowchart and steps of pcgICA are shown as follows and Fig 3.7.

(1) Use the improved local transformation algorithm described above to divide

surfaces into small cells.

(2) Select a fake plane named Γ_k. The other surface is called Γ_i.

(3) Pick two random points $p_{k1} = (s_1(t_1); s_2(t_1); x_k(t_1))$ and $p_{k2} = (s_1(t_2); s_2(t_2); x_k(t_2))$ from the surface Γ_k. Locate their respective companion points p_{i1} and p_{i2} in the surface Γ_i.

(4) Select an arbitrary point $p_{kc} = (s_1(t_c); s_2(t_c); x_k(t_c))$ between p_{k1} and p_{k2}, and its companion point q_{ic} in Γ_i. Find the value $z'_i(t_c)$ of point $p_{ic} = (s_1(t_c); s_2(t_c); z'_i(t_c))$ using equation (3.7).

(5) Use equation (3.15) and (3.16) to get the compensated value $z^c_i(t_c)$ of point q_{ic}.

(6) Compute $x_i^{new}(t_c)$ using equation (3.8).

(7) If $cont \leq N_k$ then $cont = cont + 1$ and go to step 2. If $cont = 0$, go to next step.

(8) Compute the error using equation (3.9). If $\epsilon > \xi$, go to (2). Otherwise, the linearizing process is stopped. Go to next step.

(9) Sort the linearized signal z_i in ascending-order, and smooth the sorted-signal using the averaging function, equation (3.6).

(10) Restore the original order of the smoothed signal $\tilde{z}_i$ to produce signal z_i, which are utilized for the inputs of the linear-ICA. The plane of signal z_i is utilized as the fake-plane for transforming other signals the signal x_k.

(11) Use FastICA to separate the linearized signals.

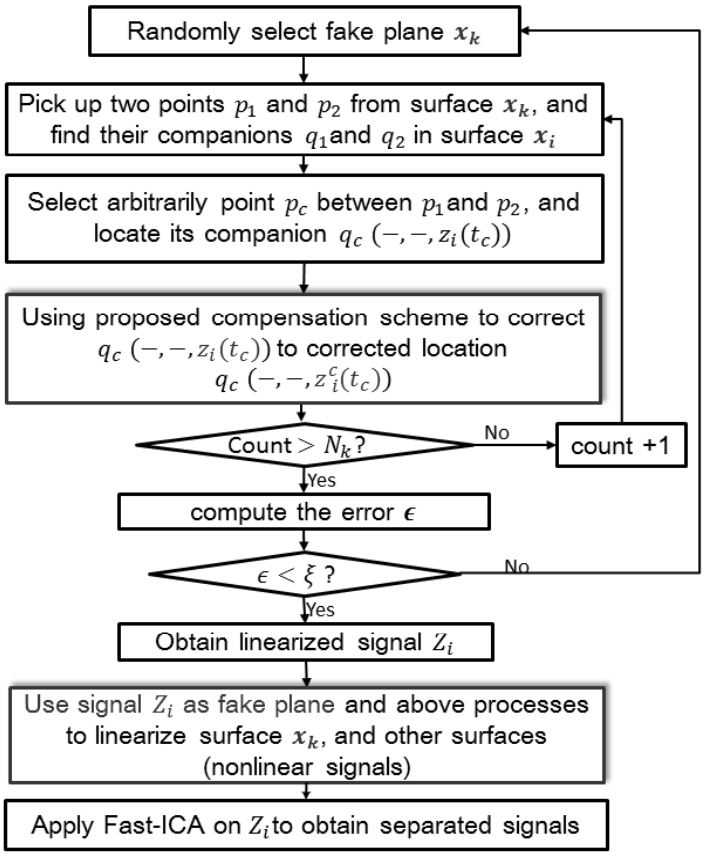

Figure 3.7 Flowchart of improved pgICA (pcgICA)

3.3.4 Improved nonlinear ICA based De-noising Method

This proposed de-noising method is consists of these steps shown as follows. The flowchart of this method is shown as Figure 3.7

- Step 1: Using proposed compensation scheme to improve the linearization process of post-nonlinear geometric ICA.
- Step 2: Use the improved nonlinear ICA to separate the signals of the bridge from others (such as noise, car, and etc.). In this improved ICA, Fast-ICA is chosen for the linear separation process, since it is well known, fast, and representative.
- Step 3: After signal separation, Fast-ICA calculates the power value to check which signal is the most powerful and can represent the bridge's vibration. Power value calculation is important for linear ICA and is useful for choosing the signal that represents the bridge's vibration. The most powerful signal is considered to be the bridge's signal, because our sensors are set directly on the bridge. In this way, the acquired vibration data is de-noised and used for damage diagnosis.

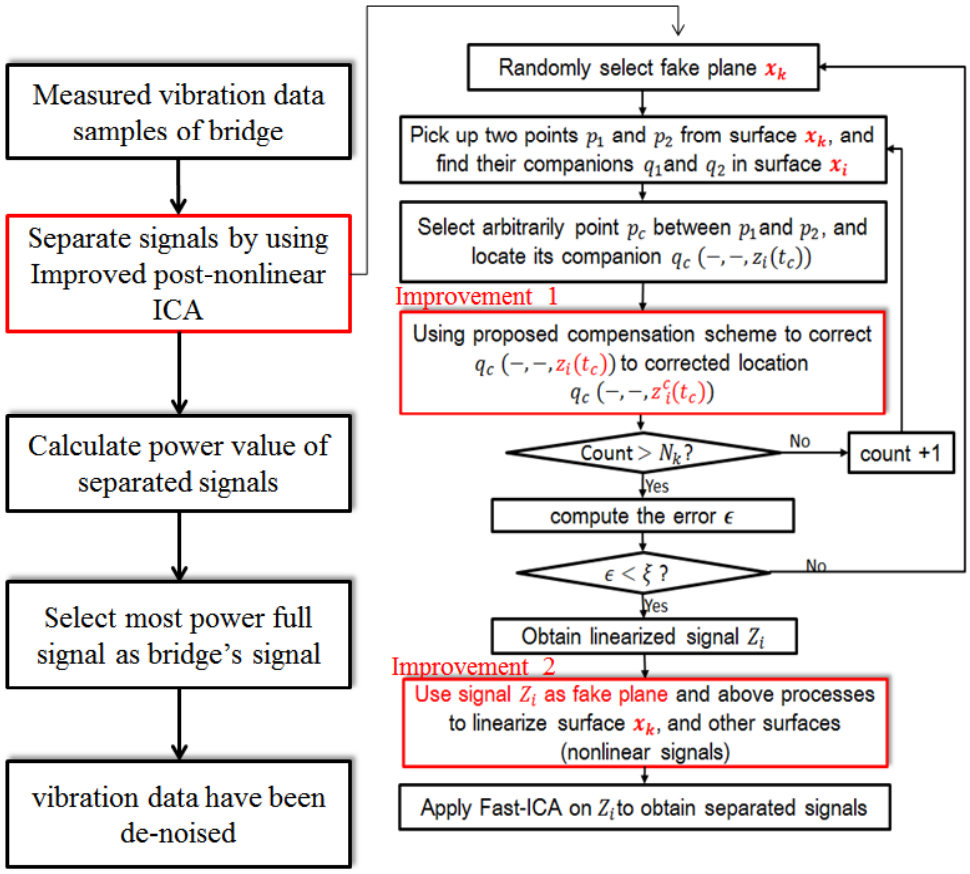

Figure 3.7 Flowchart of improved pgICA based de-noising method

3.4 Experiments of Improved Nonlinear ICA

3.4.1 Simulation 1 of Improved Nonlinear ICA (pcgICA)

Two signals are used in this simulation, s_1(t) is a sinusoidal signal shown as equation (3.19), and s_2(t) is a noise uniform distributed in [−1, 1]. Two linear mixtures, v_1 and v_2, are generated by mixing matrix A is used to generate the linear-mixture v_1 and linear-mixture v_2. Matrix A is composed of the random-numbers of [−1, 1] shown as equation (3.20). Equation (3.21) is used to distort the two linear-mixtures to produce the observations x_1 and x_2. In this simulation, the sample size N equal to 3000, the μ equal to 0.2, the window size of smoothing-function L equal to 151, and the error-threshold ξ equal to 0.002. The number of cells CellNum = 10.

Figure 3.8 shows the 3D plots of linear mixtures v_1 and v_2. Since v_1 and v_2 are the linear mixtures of source signals s_1 and s_1, they are planes. Figure 3.8 shows the 3D plots of the nonlinear mixtures x_1 and x_2, which are obtained by non-linear mixing. Figure 3.9 shows the linear mixtures z_1 and z_2. The mixtures z_1 and z_2 are linear signals because the geometric linearization algorithm of pcgICA was used to linearize the nonlinear mixtures signals x_1 and x_2. Thus, in Figure 3.9, the signals z_1 and z_2 are planes. After linearizing signals, the FastICA is utilized for z_i to separate and obtain the source-signal's estimates y_i. The source signals s_1, s_2, nonlinear mixture signals x_1, x_2, and separated signals y_1, y_1 are shown in the Figure 3.10. Figure 3.10 shows the separated signal well reflects the characteristic of the source signal.

The correlation-coefficient between a source-signal s_i and its estimate s_i',$\mathrm{r}(s_i, s_i')$, is used to measure the performance. The correlation-coefficient was computed by using equation (3.22). The estimate of the i^{th} source-signal s_i belongs to the outputs $y_i(\mathrm{i} = 1, 2, 3, \cdots, \mathrm{n})$, and the correlation-coefficient's absolute, $|\mathrm{r}(y_i, s_i)|$, is the biggest. We utilized the index, $\mathrm{r}(s_i, s_i')$, to compare FastICA, pgICA and pcgICA. Table 3.1 shows the results. the table shows our algorithm pcgICA performs better than others. Compared to FastICA and pgICA, the correlation-coefficient of our method is improved 37.4% and 8.1%, respectively. Thus, the results indicate that the linearization algorithm of our algorithm is more accurate than that of pgICA.

$$s_1(t) = \sin(0.22t) \tag{3.19}$$

$$\mathrm{A} = \begin{bmatrix} 0.1503 & -0.0454 \\ -0.0987 & 0.2075 \end{bmatrix} \tag{3.20}$$

$$x_1(t) = (v_1(t) + v_1^3(t))/10$$
$$x_2(t) = (3v_2/10) + \tanh(3v_2(t)) \tag{3.21}$$

$$r(s, y) = \frac{\sum_{t=1}^{N} s(t)y(t)}{\sqrt{\sum_{t=1}^{N}(s(t))^2 \sum_{t=1}^{N}(y(t))^2}} \tag{3.22}$$

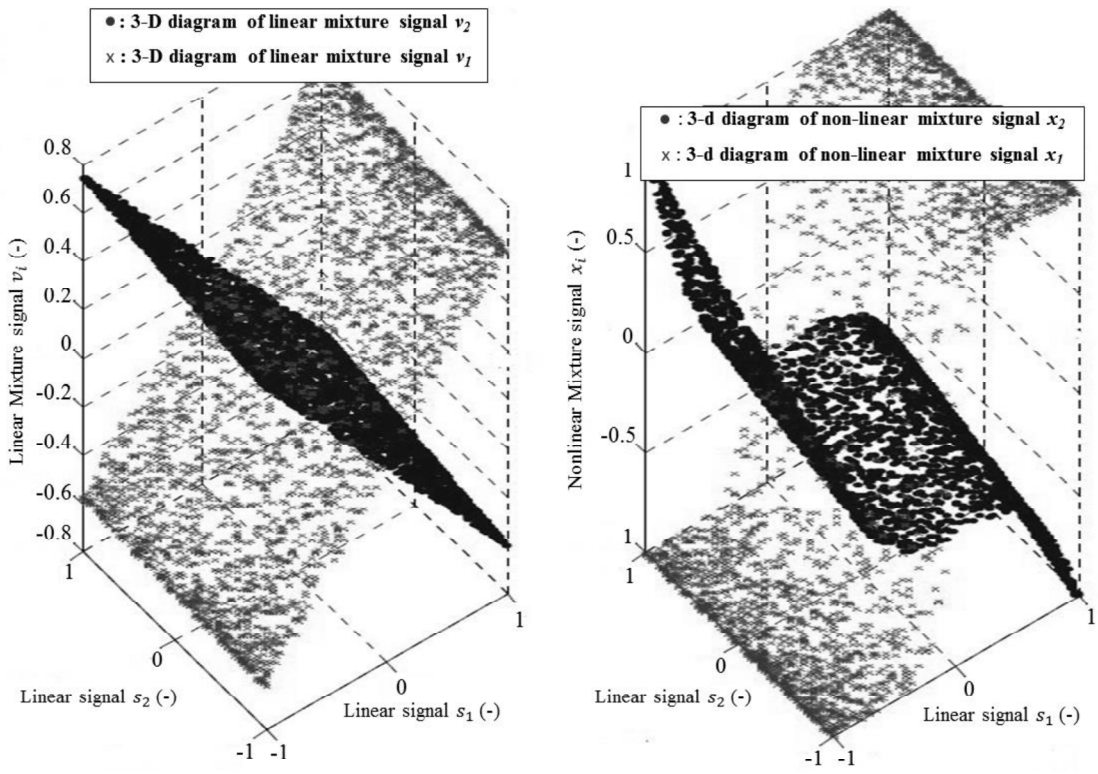

Figure 3.8 3-D diagram of linear signals v_1, v_2 and nonlinear signals x_1, x_2

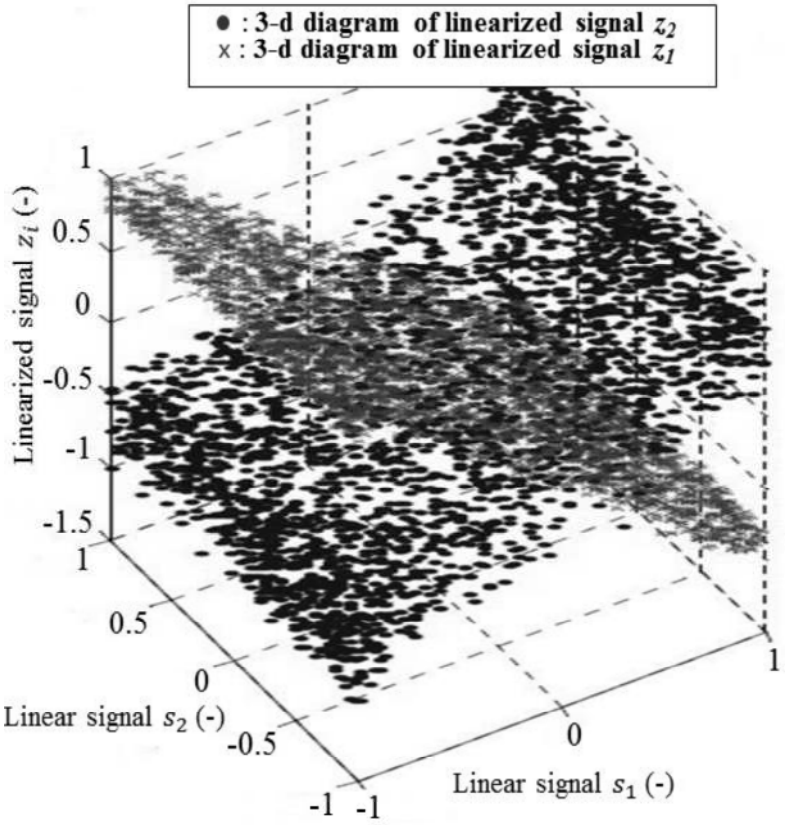

Figure 3.9 3-D diagram of Linearized signals z_1 and z_2

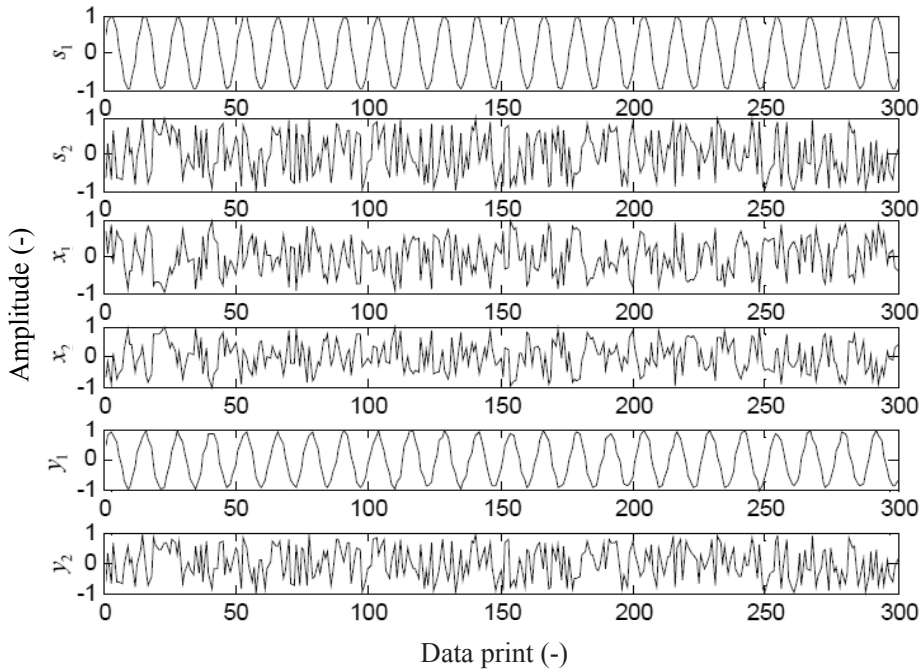

Figure 3.10 Source signals s_1, s_2, nonlinear mixture signals x_1, x_2, and separated signals y_1, y_1

Table 3.1. Correlation coefficient comparison

algorithm	$r(s_1, s_1')$	$r(s_2, s_2')$
FastICA	0.91	0.53
pgICA	−0.95	−0.91
pcgICA (our algorithm)	−0.99	−0.98

The signal-noise-ratio (SNR) is also used to measure the performance. The SNR was computed by using equation (3.23). Table 3.2 shows the SNR results of FastICA, pgICA and pcgICA. The table shows our algorithm pcgICA performs better than others. Compared to FastICA and pgICA, the SNR of our method is improved 51.8% and 16.3%, respectively. Thus, the results indicate that the linearization algorithm of our algorithm is more accurate than that of pgICA.

$$SNR(i) = 10 \lg \frac{s_i^2}{(s_i - s_i')^2} \tag{3.23}$$

Table 3.2. SNR comparison

algorithm	SNR(s_1') dB	SNR(s_2') dB
FastICA	13.57	8.01
pgICA	19.37	15.25
pcgICA (our algorithm)	21.417	18.84

3.4.2 Simulation 2 of pcgICA

Source signals used in this simulation are shown as Figure 3.11, which are from http://www.bsp.brain.riken.jp/ICALAB/ and choose the Speech4.mat data. Linear mixture matrix A is used to generate the linear-mixture signal v_1, v_2, v_3,

and v_4. Matrix A is composed of the random-numbers of [−1, 1] shown as equation (3.24). Equation (3.25) is nonlinear mixture function to distort the four linear-mixtures to produce the observations x_1, x_2, x_3, and x_4. In this simulation, the sample size N equal to 5000, the μ equal to 0.2, the window size of smoothing-function L equal to 151, and the error-threshold ξ equal to 0.01.

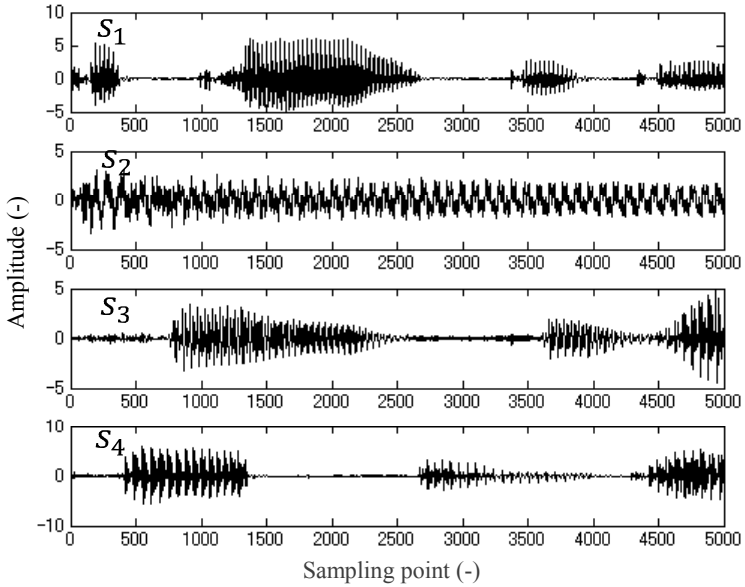

Figure 3.11 Source signals of simulation 2

$$A = \begin{bmatrix} -0.7056 & -0.2723 & -0.8562 & -0.4275 \\ 0.3966 & 0.1866 & -0.2596 & 0.0014 \\ -0.7758 & 0.7012 & 0.1318 & -0.4642 \\ 0.8582 & -0.2290 & 0.3806 & -0.8994 \end{bmatrix} \tag{3.24}$$

$$\begin{aligned} x_1(t) &= \tanh(2v_1(t)) \\ x_2(t) &= v_2(t) + 0.1v_2^3(t) \\ x_3(t) &= v_3^3(t) \\ x_4(t) &= v_4(t) + \tanh(3v_4(t)) \end{aligned} \tag{3.25}$$

Figure 3.12 shows the mixed signals x_1, x_2, x_3, and x_4. To show the advantage of improved pgICA, I compare my method with Fast-ICA and pgICA. Figure 3.13, Figure 3.14, and Figure 3.15 shows the separated signals of using Fast-ICA, pgICA, and improved pgICA (pcgICA) respectively. Compare these three result figures with the source signals Figure 3.11, the separated signals of using pcgICA is more better than other two methods. To further verify the advantage of pcgICA, the results of correlation-coefficient between a source-signal s_i and its estimate s_i',$\mathrm{r}(s_i, s_i')$ are

shown in the table 3.3. The table shows our algorithm pcgICA performs better than others. Compared to FastICA and pgICA, the correlation-coefficient of our method is improved 0.39 (51.8%) and 0.17 (16.7%) averagely, respectively. Compare with the results of simulation 1, Table 3.1, the more complex (more mixture signals) mixture data is, the greater advantage my method has. Thus, the results indicate that the linearization algorithm of our algorithm is more accurate than that of pgICA.

Table 3.3. Correlation coefficient comparison

Method	$r(s_1, s'_1)$	$r(s_2, s'_2)$	$r(s_3, s'_3)$	$r(s_4, s'_4)$
Fast-ICA	0.41	0.35	-0.54	-0.62
pgICA	0.68	−0.62	-0.64	0.87
Improved pgICA	0.76	−0.84	-0.91	0.99

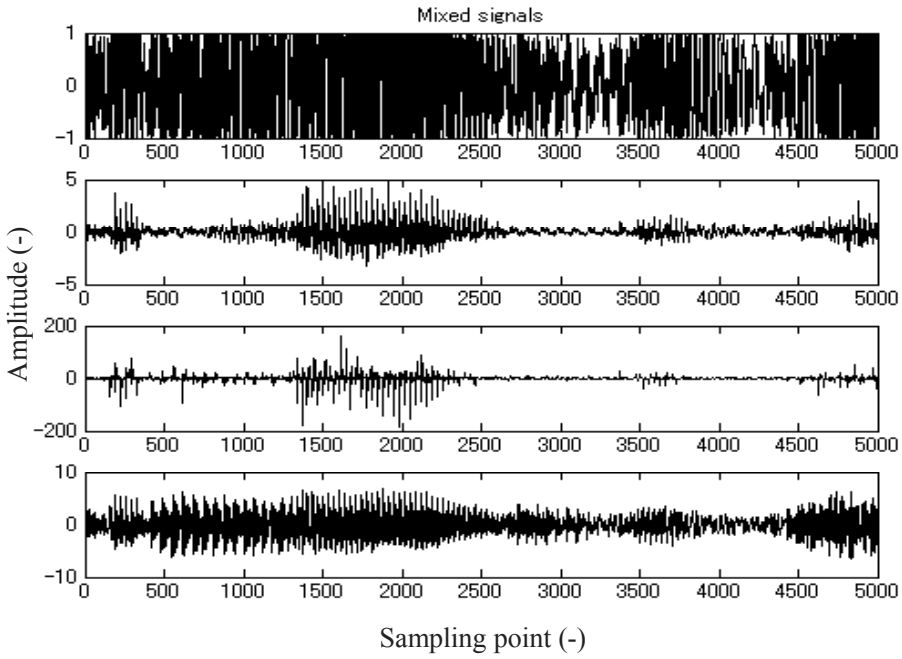

Figure 3.11 Mixed signals of simulation 2

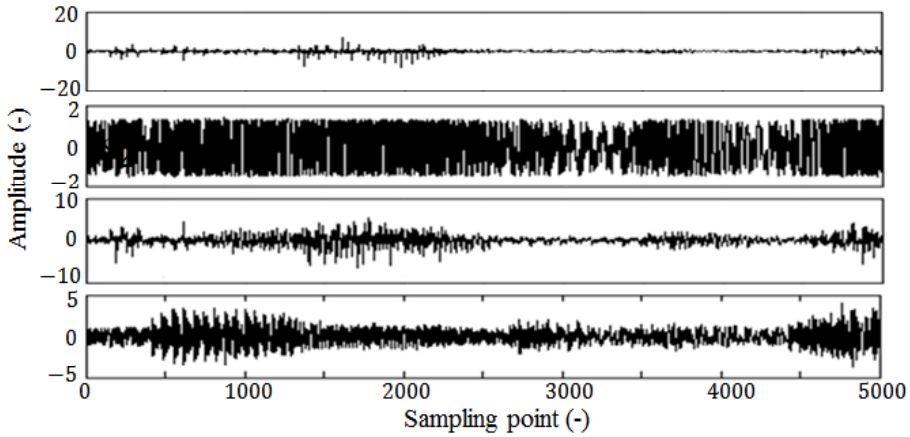

Figure 3.12 Separated signals of Fast-ICA

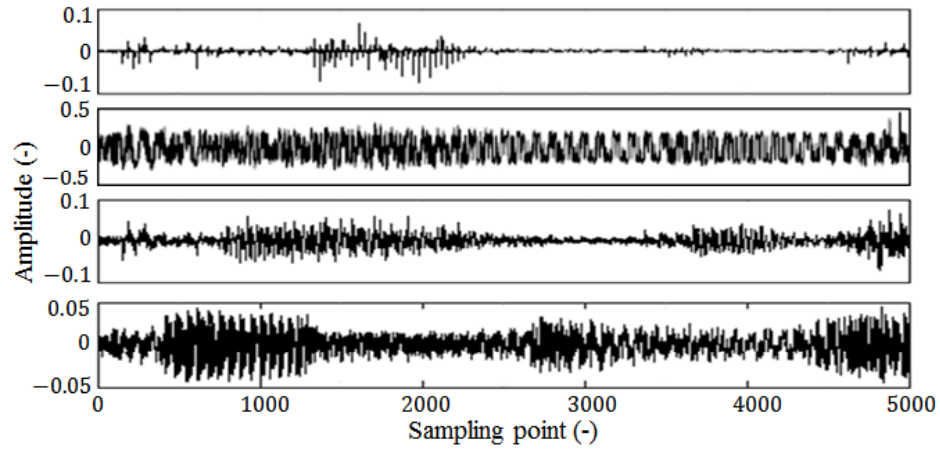

Figure 3.12 Separated signals of pgICA

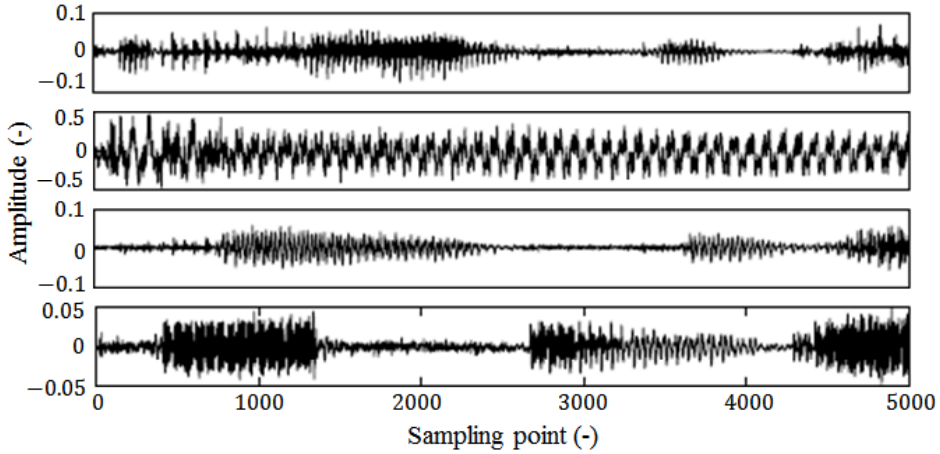

Figure 3.13 Separated signals of pcgICA

3.4.3 Experiment of Improved Nonlinear ICA

3.4.3.1 Data of Nakajima Bridge Experiment

The Seiran Bridge was selected for our research because it satisfied all the demand conditions, healthy, made of steel, and easy for the placement of a sensor node. In this experiment, the vibration was sampled using accelerometer sensors. Data from the bridge pier and beam were measured. The location of sensors is described in Figure 3.14 and Table 3.4. The acquired original data are as follows. Original sampling frequency was 200Hz, and the number of samplings was 15,000. In this experiment, from 9:30 to 16:00, we successfully took 10 times measurements, and once measurement every half an hour. In order to avoid data corruption case by transmutation, we repeatedly perform 3 times data acquiring per times measurement.

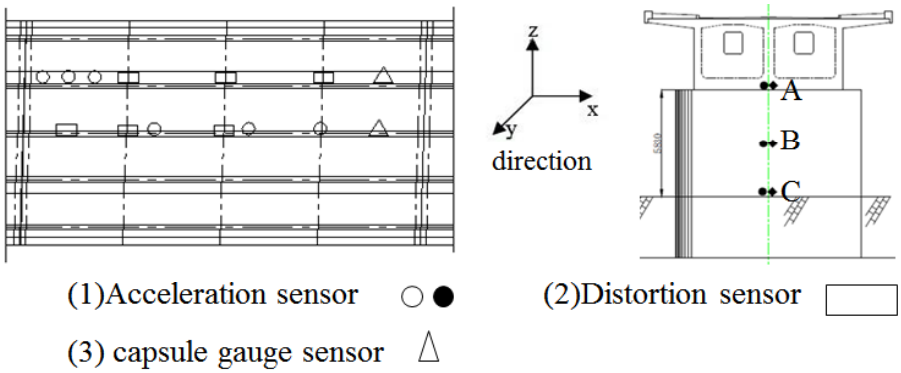

Figure 3.14 Deployment of sensors on beam and pier

3.4.3.2 Performance Evaluation of De-noising Method

In order to shown the performance of pcgICA in field bridge experiment, it is use to analyze the data of this field bridge experiment to obtain the signal of bridge. As is well known, if we directly use FFT to obtain the spectral pre-analysis of the original signal, the result will show many frequencies due to various kinds of noise. Thus, the spectral pre-analysis is used to shown the de-noising performance. We describe the analysis results of the data in x-axis and y axis from the sensors A, sensor B, and sensor C deployed on the pier of bridge, and at 10:30 a.m. Here, we arbitrarily select 8,000 samples of original data as analysis target.

The chosen data samples of the x-axis data in sensors A, B, and C are shown in Figure 3.15. The FastICA of Hyvarinen was used in the linear-stege of pcgICA and pgICA, where the nonlinear function is chosen as $g(\mu) = \mu^3$, randomly choosing W in initial, and the value of the stopping criterion ξ equal to 0.0001. Figure 3.16 show the separation result of pcgICA.

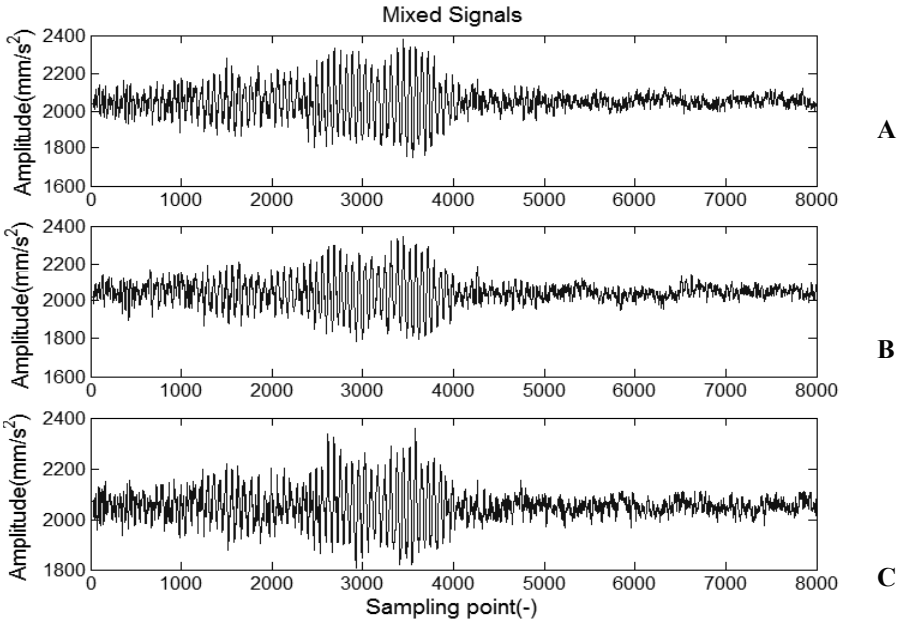

Figure 3.15 8000 data samples of original data in x-axis

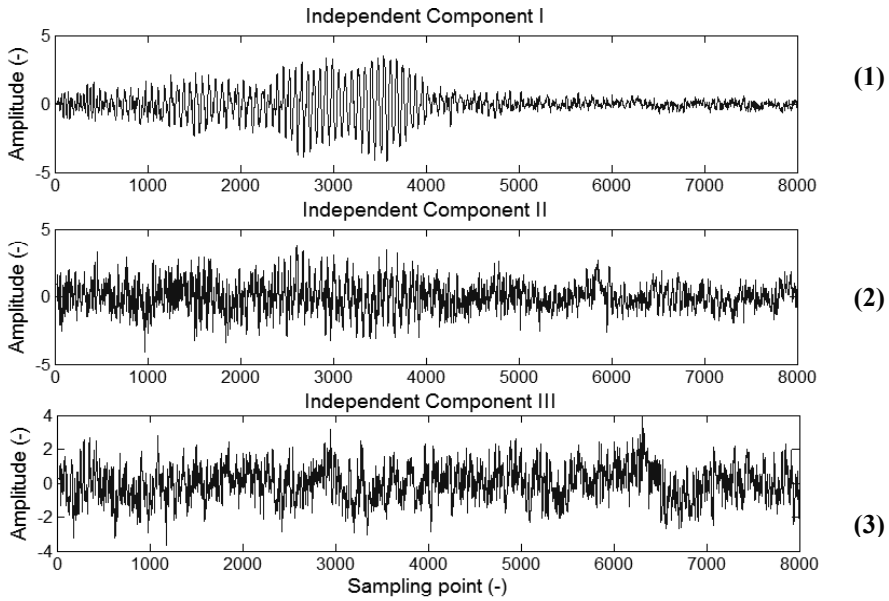

Figure 3.16 Signals separated by x-axis data using pcgICA

By using the eigenvalue analysis of FastICA, the first demixed-signal contains the most powerful and biggest eigenvalue in the x-axis. It is considered as the signal of the bridge, because our sensors were set directly on the bridge. The power values of the separated signals are shown in Figure 3.17. Thus, the first separated signal is chosen for spectral analysis, and the result shows its frequency in the x-axis is equal to 3.2 Hz, as shown in Figure 3.18. The spectral analysis results of other signals (car, noise) are shown in Figure 3.19 and Figure 3.20. From Figure 3.21, we can see that the FFT results of the two signals are not clear enough to obtain their frequency. When we use ICA to separate the signal of the bridge, we cannot perfectly separate other signals from the bridge signal. However, ICA can considerably reduce the effect of noises, as verified by Figure 3.18 and Figure 3.21.

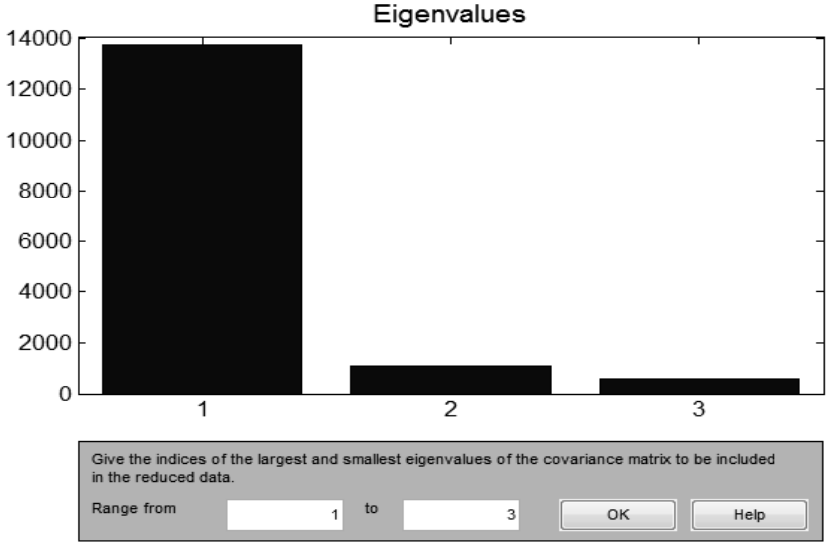

Figure 3.17 Power values of three separated signals

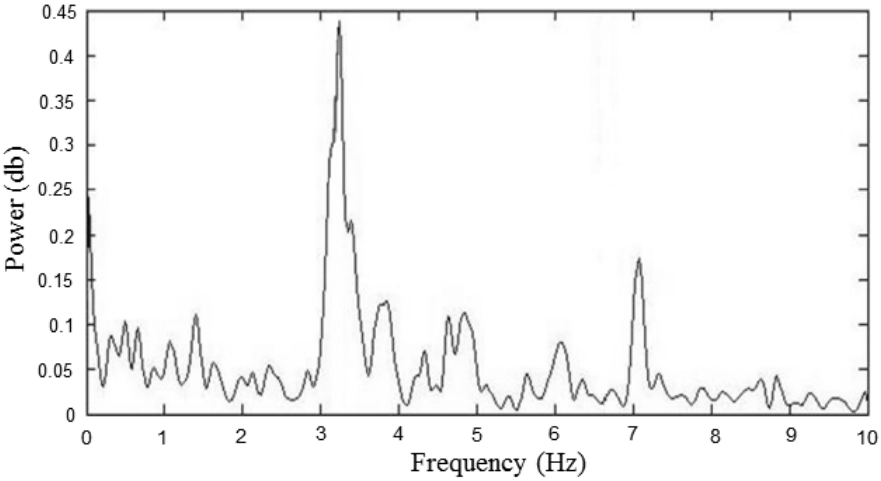

Figure 3.18 Spectral analysis of separated signal 1 in x-axis

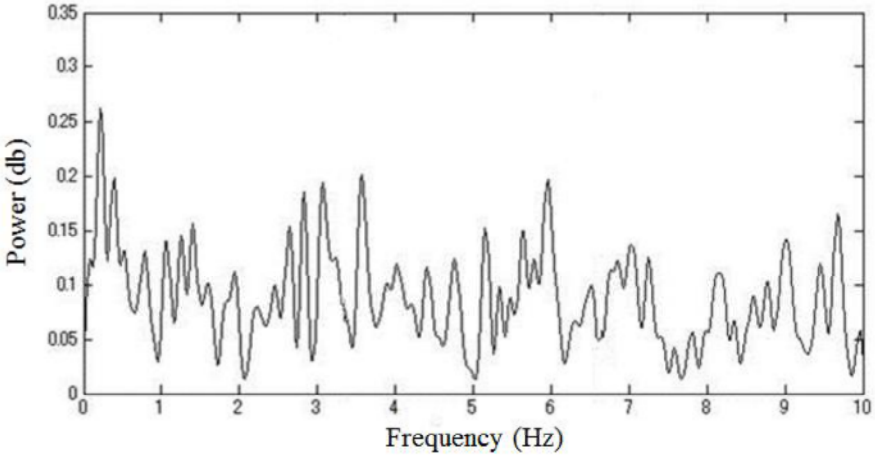

Figure 3.19 Spectral analysis of separated signals 2 in x-axis

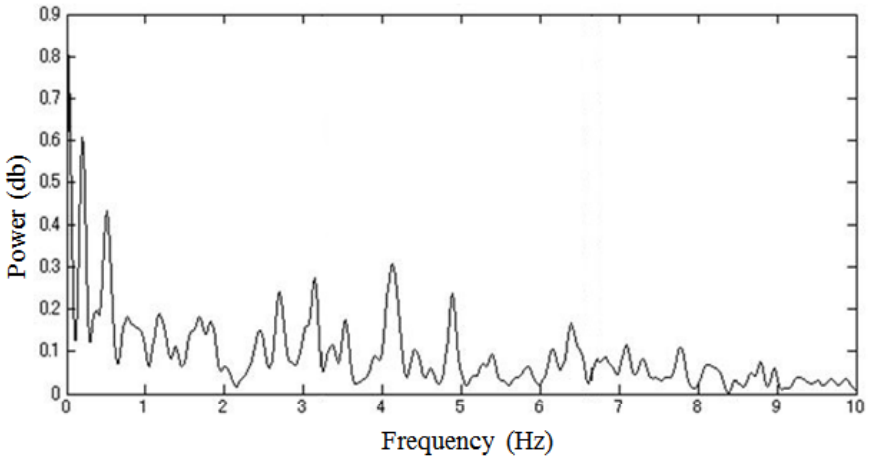

Figure 3.20 Spectral analysis of separated signals 3 in x-axis

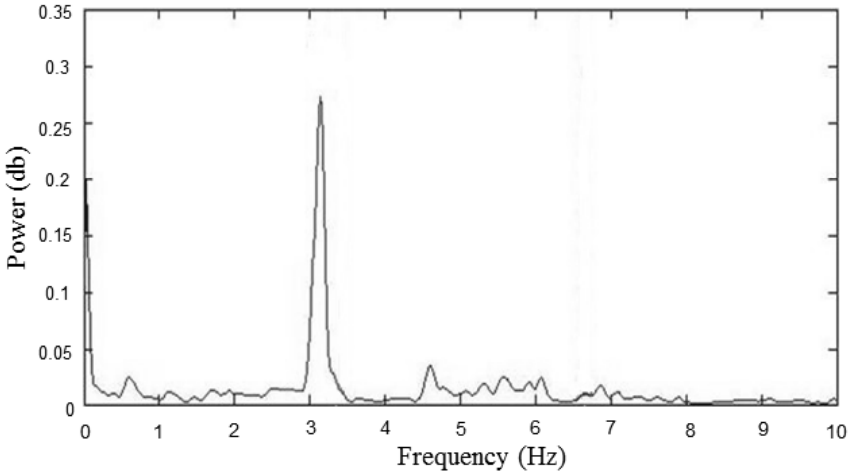

Figure 3.21 Spectral analysis of separated signal 1 in y-axis

By using the accessory eigenvalue-analysis of FastICA, the second demixed-signal contains the most powerful and biggest eigenvalue in y-axis. Thus, it can be look as the signal of bridge and selected for spectral analysis. Figure 3.21 shows the result of using FFT, where the frequency of the signal in y-axis is equal to 3.2 Hz. Because of few noises in the signal, the primary frequency is acquired cleanly and easily.

In order to verify the effectiveness of ICA in various potential excitations, before performing this experiment our research group implements many bridge diagnosis simulations and experiments by using ICA, FFT and Spectral analysis. These simulation experiments are described in [4] [5]. In these simulations, we adopted identical excitation for identification such as the fixed size impact (300N), the fixed speed wind (10 m/s, 20m/s, 30m/s and 40m/s) and the fixed weight vehicle running in fixed speed. These excitations were added on the undamaged bridge and damaged bridge. The analysis result shows that the identified characteristic frequency of healthy bridge keeps no change with the increase of the wind, impact or vehicle running speed. Also, the characteristic-frequency is reduced when corrosion existing. Thus, these simulations and bridge experiments verify the effectiveness of ICA in the situation of running vehicle as excitation. Although the bridge vibration signal and vehicle vibration signal seem dependent, the analysis results of these simulations and experiments show ICA can separate the bridge vibration signal from other vibration signals or noise successfully. It means the basic assumption of independent between bridge vibration and vehicle vibration doesn't affect the results.

Comparing FastICA and pgICA with pcgICA

In order to show the advantage of the pcgICA algorithm, a comparison between the pcgICA, pgICA, FastICA, and wavelet threshold based de-noising method in the same signals is presented in this subsection. The comparison between the four methods in

x-axis is shown in Figure 3.22, Figure 3.23, Figure 3.24, and Figure 3.25. Figure 3.26, Figure 3.27, Figure 3.28, and Figure 3.29 show the comparison between the four methods in y-axis. The results of Fast-ICA and wavelet threshold based method show that although the frequency of the bridge is found to be 3.2 Hz, the FFT result does not clearly distinguish which frequency belongs to the bridge. Even in the case, the noise degrees are too large to difficultly search the bridge's frequency. As is well known, the result of the spectral analysis of a bridge's signal needs to be as clear as possible. Figure 3.25 and Figure 3.29 indicate that pcgICA is better than Fast-ICA, wavelet threshold based method and pgICA in this regard.

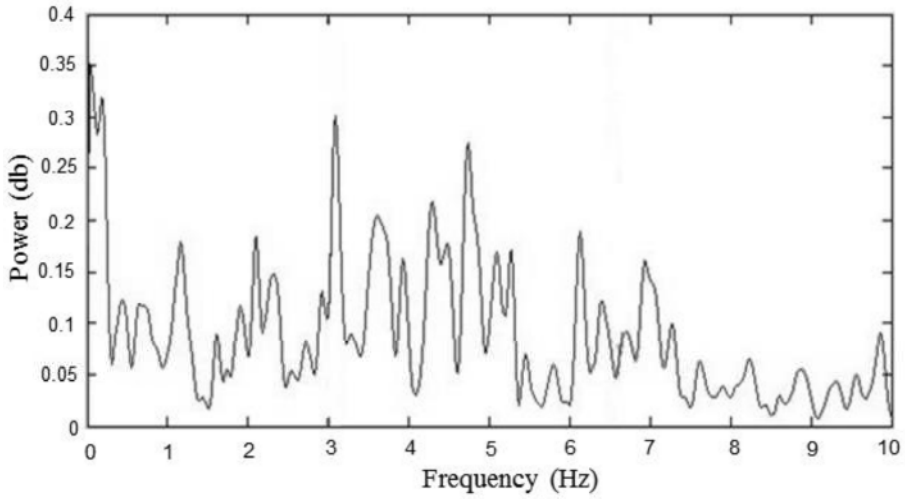

Figure 3.22 Results of FastICA in x-axis

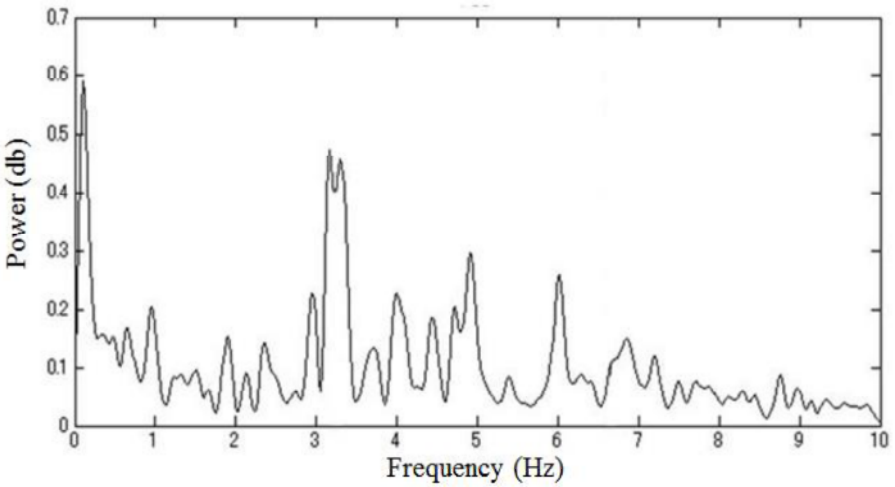

Figure 3.23 Results of Wavelet threshold based method in x-axis

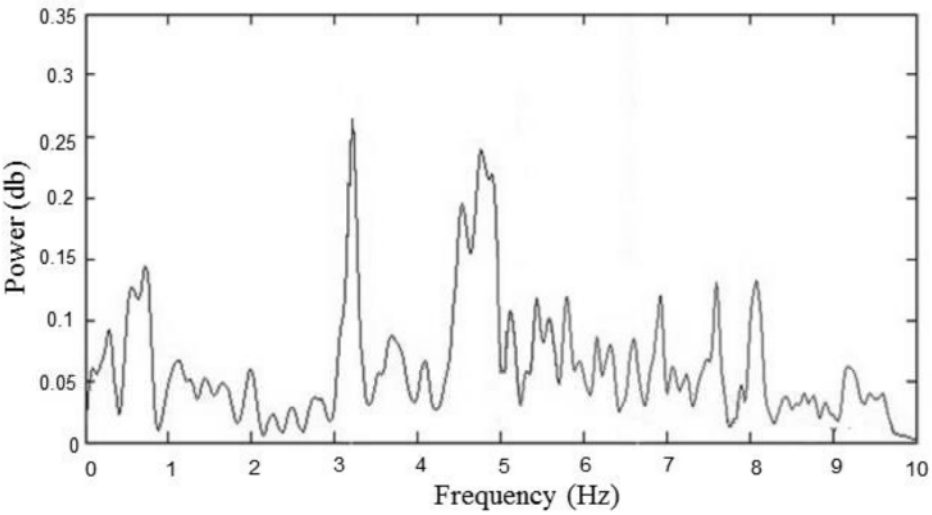

Figure 3.24 Results of pgICA in x-axis

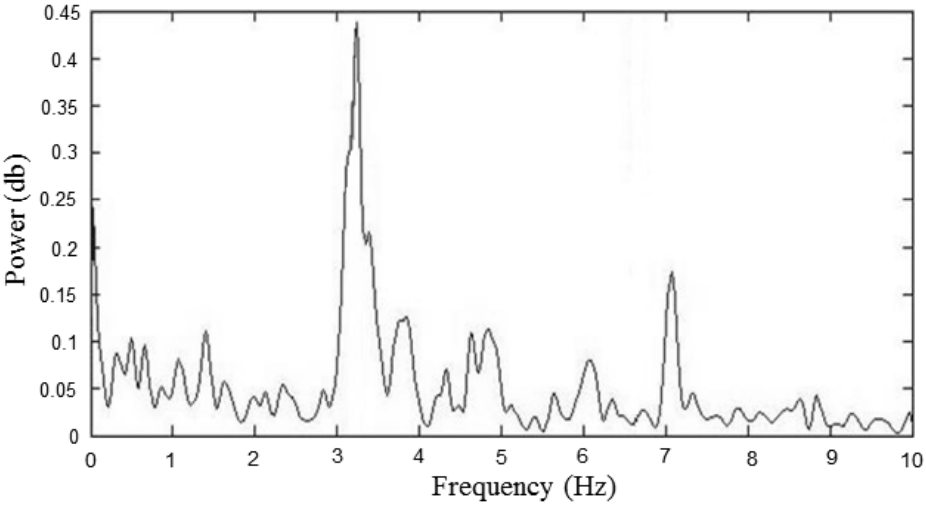

Figure 3.25 Results of improved pgICA (pcgICA) in x-axis

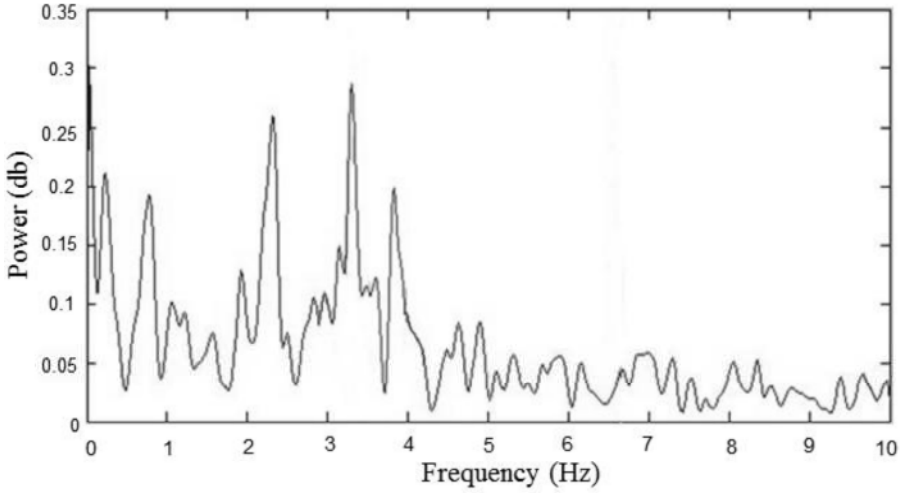

Figure 3.26 Results of Fast-ICA in y-axis

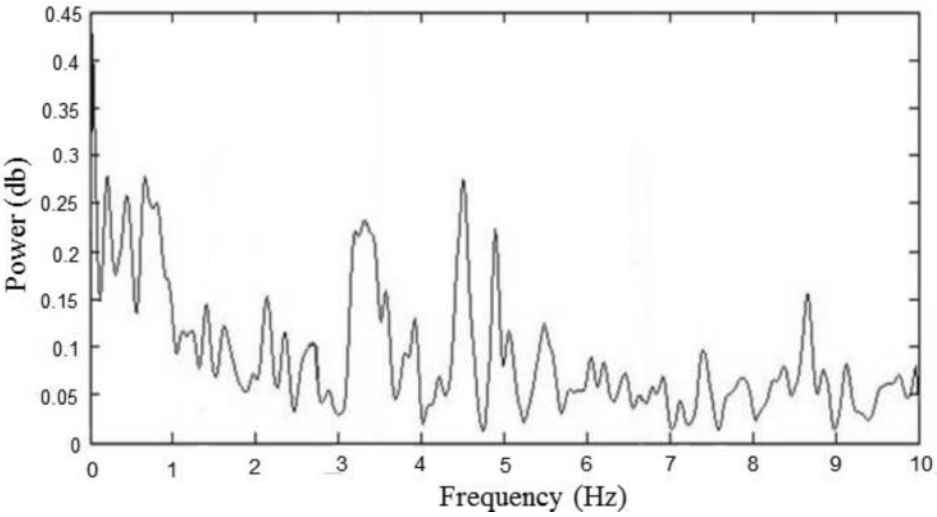

Figure 3.27 Results of Wavelet threshold based method in y-axis

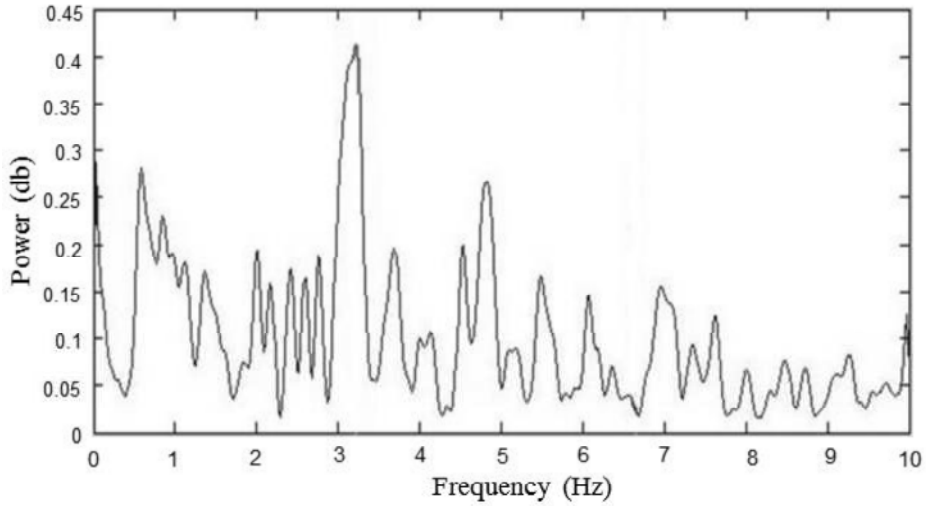

Figure 3.28 Results of pgICA in y-axis

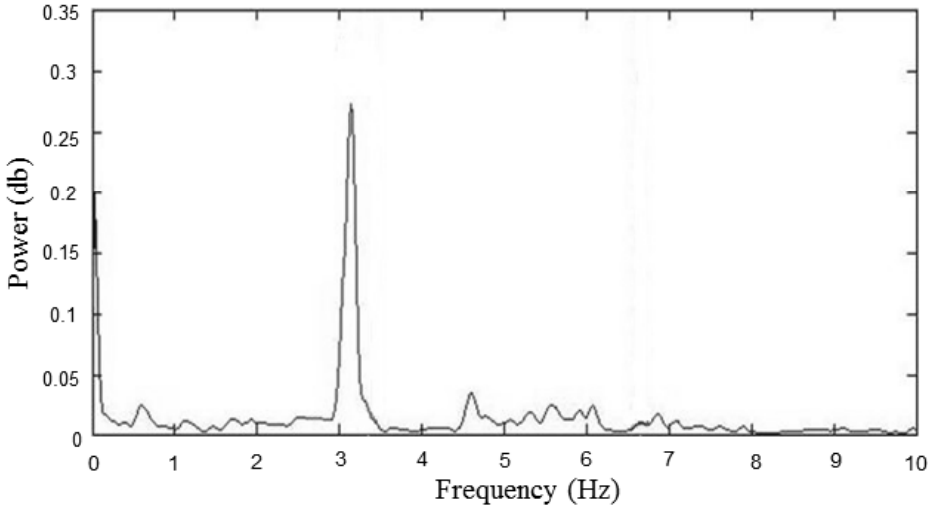

Figure 3.29 Results of pcgICA in y-axis

3.5 Similarity Matching based Environment Impact Reduction Method

3.5.1 Overview of Environment Impact Reduction Method

As discussed in section 2.6, the varying environment and operation conditions can affect the dynamic vibration data of bridge structure significantly. Therefore, the acquired data needs to be processed to eliminate the influences of the varying environment and operation conditions. However, although environment such as wind and temperature can be simultaneously measured with structural responses, it is difficult to acquire the quantitative measurement of operation conditions such as traffic-flow in BSHM. To solve this problem, a novel environment impact reduction method based on similarity matching is proposed. The flowchart of proposed method is shown in the Figure 3.30. By using our proposed scheme it is no need to measure the condition of environment and operation when the vibration data is sampled. The data recorded in the undamaged condition should cover as many conditions of environment and operation as possible.

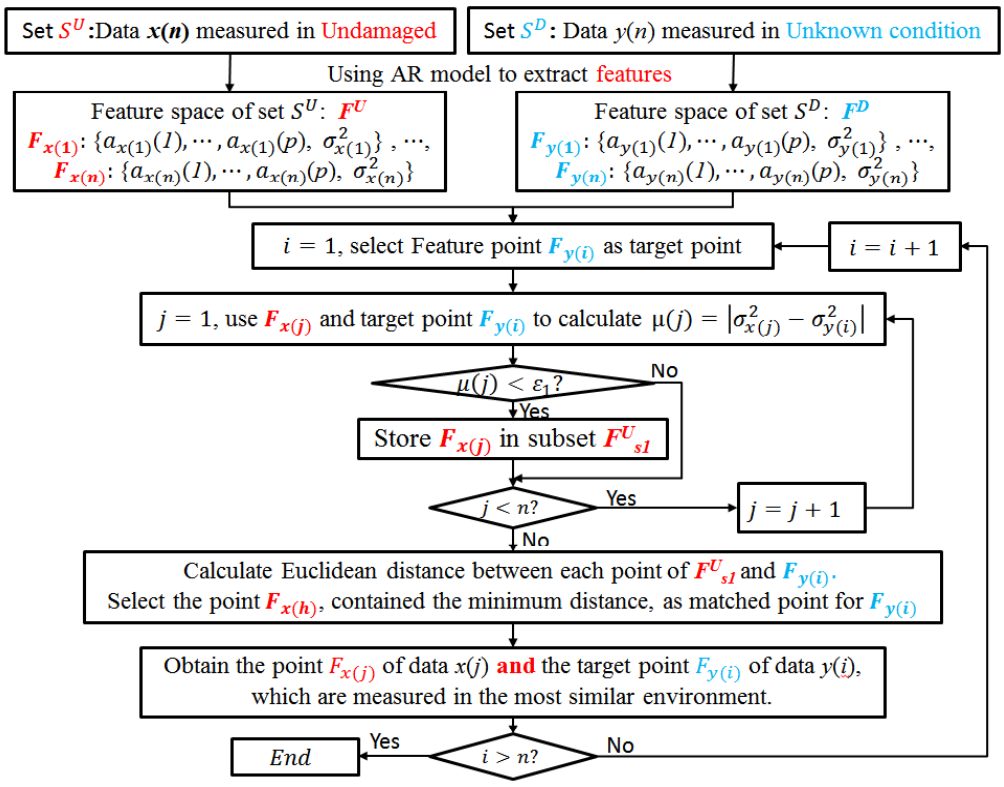

Figure 3.30 Flowchart of proposed method

3.5.2 Data Samples Set Partition Procedure

In order to eliminate expediently, two data samples sets are generated, which are used for the health condition and the unknown condition of the bridge respectively.

The set of data samples corresponded to the health condition is defined as S^U, while the S^D is defined as the set in unknown condition. For data sample S^D, the elimination scheme is used to search a referenced data-sample of S^U that is likely to have been sampled under similar environment and operation conditions.

3.5.3 Similarity Matching Procedure

Practically, our proposed elimination scheme is a similarity matching process. A finding is implemented on many data-samples to get the data samples within a distance (defined by user) between it and a target data-sample. In this scheme, data samples are transformed to a number of features by using AR model. And then the similarity-measures are employed to search the data sample matched to the target data-sample. Thus, the random data-samples in S^D is represented by $\mathrm{y}(n)$, and the random data-samples in S^U is represented by $x(n)$. Here, an autoregressive model (AR) is applied to constructed models for $\mathrm{y}(n)$and $x(n)$, which are shown as equation (3.26) and (3.27), where the AR mode's order is p, $a_x(k)$ is the coefficient of AR, also $a_y(k)$ is AR's coefficient, $u_x(n)$ $u_x(n)$represents the white-noise inputs containing the variance of σ_x^2, and $u_y(n)$ is defined as the white-noise inputs containing variances of σ_y^2. In the meaning of second-order statistics, the character of a time-series is able to be presented by the AR's coefficients and the corresponded-input. Thus, we can regard $\{a_x(k), \sigma_x^2\}$ or $\{a_y(k), \sigma_y^2\}$ to a type of feature of $x(n)$ or $\mathrm{y}(n)$. Since measured-data is divided into many data samples, only one of the data samples from a given set is selected to create the AR model, in order to reduce the modeling times. After modeling all the data-samples of S^U and S^D by using Equation (3.19) or (3.20), we obtain two feature spaces, F^U and F^D, which correspond to S^U and S^D respectively. So any data can find a mapping with a point $\{a_x(k), \sigma_x^2\}$ or a point $\{a_y(k), \sigma_y^2\}$ in F^U or F^D.

$$x(n) = -\sum_{k=1}^{p} a_x(k)x(n-k) + u_x(n) \tag{3.26}$$

$$y(n) = -\sum_{k=1}^{p} a_y(k)y(n-k) + u_y(n) \tag{3.27}$$

Thereafter, similarity matching is performed by searching a point $\{a_x(k), \sigma_x^2\}$, which is similar to a target point $\{a_y(k), \sigma_y^2\}$ of F^D (the target point is mapped by certain data in F^D) in space F^U. The hierarchical similarity search algorithm "hierarchy scan," presented in [2], is applied to search for the aforementioned data point. The adaptive similarity-measures and a hierarchical-scan are implemented in the extracted-features of data samples S^U. σ_x^2 or σ_y^2 also can be looked as the input for a linear system, and equation (3.21) is used for finding a certain target-point $\{a_y(k), \sigma_y^2\}$ to choose a less part of features in F^U. In equation (3.21), ε_1 is a specified-difference from σ_x^2 to σ_y^2. Therefore, we obtain a subset $F^U{}_{s1}$, including the

feature points which satisfy equation (3.21). The value of ε_1 is based on the matching speed and accuracy we demand. For example, if we want more accuracy, we need make the value smaller, which will make subset F^U_{s1} contain more points.

Thereafter, the next similarity-measure is utilized for further seeking in subset F^U_{s1}. In equation (3.22), ε_2 represents a similarity-coefficient containing specified value. The value of ε_2 is determined in almost the same manner as that of ε_1. The value of ε_2 is within [−1, 1]. Thus, only a small fraction of F^U_{s1} can pass the test, and these passed feature points constitute a smaller subset, F^U_{S2}. At last, the Euclidean-distance from the target-point to every feature point of F^U_{S2} is calculated, and the feature point with the minimum Euclidean distance, shown as equation (3.23), is regarded as the one matched to the target-point. Thus, a matched data-sample pair is constituted by the data sample corresponded to the target-point of F^D and the point of F^U which matched to the target-point. All the data samples in S^D are matched by performing the above similarity matching process to obtain their data sample pairs.

$$\left|\sigma_x^2 - \sigma_y^2\right| \leq \varepsilon_1 \tag{3.21}$$

$$\frac{\sum_{j=1}^{p} a_y(j)a_x(j)}{\sqrt{\sum_{j=1}^{p} a_y^2(j)}\cdot\sqrt{\sum_{j=1}^{p} a_x^2(j)}} \geq \varepsilon_2 \tag{3.22}$$

$$\min\left[\sum_{j=1}^{p}(a_y(j) - a_x(j))^2\right]^{\frac{1}{2}} \tag{3.23}$$

3.6 Performance Evaluation of Environment Impact Elimination Method

In order to shown the performance of similarity matching based environment impact elimination method, the data of 10 times measurements are used. In order to display the influence of varying operation condition and environment on bridge structure properties such as characteristic frequency, the pcgICA and FFT are used to obtain the characteristic frequencies of 10 times measurements. Here, we still choose the data in x-axis and y axis from the sensors A, sensor B, and sensor C, from 9:30 to 4:00. The temperatures of 10 times measurements are shown in table 3.4. The calculated characteristic frequencies of 10 times measurements are shown in the Figure 3.31. From Figure 3.31, the frequency decrease with the temperature increase. The frequency variation is up to 4.55%, which means the varying environment can affect the characteristic frequencies of bridge structure significantly.

Table 3.4 10 times measurements

Measurement Number	Measurement Time	Temperature (Degree)	Measurement Number	Measurement Time	Temperature (Degree)
1	9:30	11.4	7	13:30	24.4
2	10:00	12.2	8	14:00	21.3
3	10:30	13.6	9	14:30	19.3
4	11:00	16.1	10	15:00	16.4
5	11:30	18.7	11	15:30	14.1
6	12:00	25	12	16:00	12.5

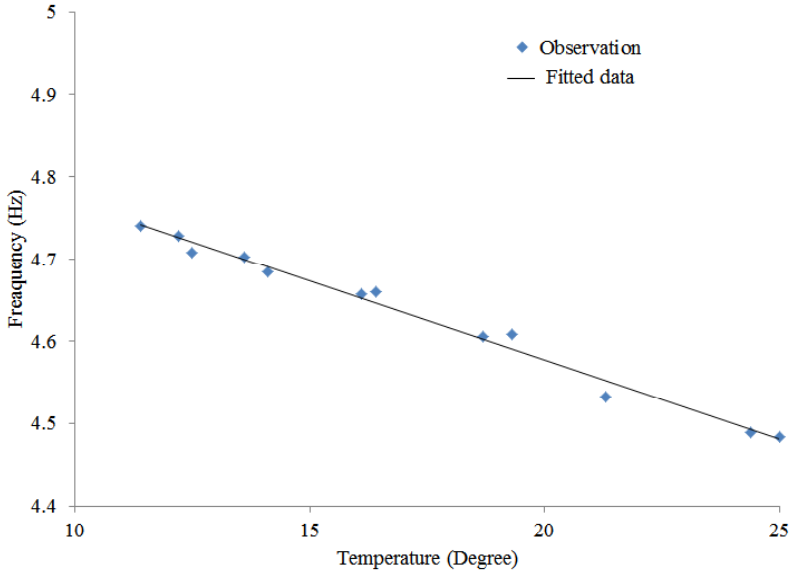

Figure 3.31 Frequency vs temperature

In order to further shown the impact of the varying environment on structure frequency, the data of second measurement is used as the reference to obtain the frequency variation between it and the other measurements. The frequency variation is shown as the black points in Figure 3.33. To verify the effectiveness of our proposed elimination method, we employ the data of first 6 measurements as undamaged condition, and the data of others 6 measurements are use as unknown condition. Our proposed method is applied to obtain the matched data pairs. The matched results are shown in Figure 3.32. After data matching, FFT are used to obtain the frequency of the data in the two conditions. The frequency variation of this case is shown as the read points in Figure 3.33. From Figure 3.33, we can get that by using our elimination method the frequency variation is very small, about 0.013% per degree. Our proposed method can effectively reduce the impact of the varying environment.

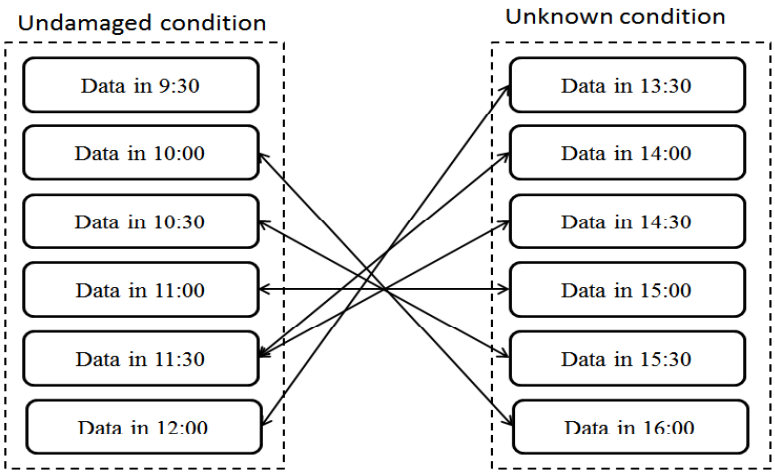

Figure 3.32 Matched results

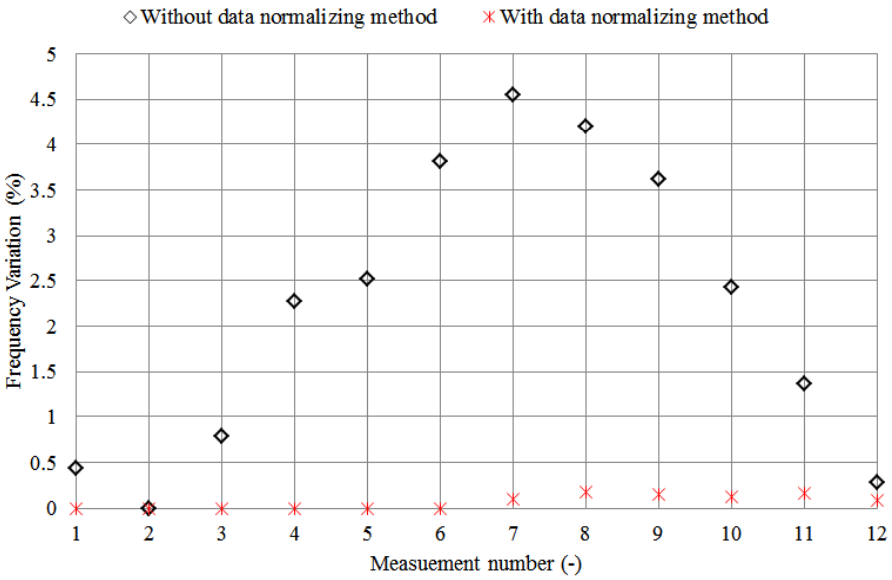

Figure 3.33 Frequency variations in using and without using proposed method

3.7 Summary

In vibration based BSHM, The key issue of this type BSHM system is how to detect the damages in sensitive and accuracy by analyzing the vibration data. Attribute to use more and more advanced hardware facilities for BSHM system, the measurement errors is reduced significantly. However, these devices cannot make the acquired vibration-data avoid the measurement noises. Otherwise, during deploying a BSHM system on a field bridge, the changes in the data caused by the variability of operation condition and environment maybe regard as an effect of damage mistakenly. Therefore, design of a data processing method to de-noise and eliminate the impacts of varying operation condition and environment is an indispensable mean for detecting damages accurately.

In the research, to deal with these problems, a new data processing method, including a new de-noising algorithm and a novel data normalizing algorithm, is proposed. To achieve efficiently de-noising an improved post-nonlinear geometric-linearization ICA algorithm (pcgICA) is designed for data processing in nonlinear system. In this improved ICA algorithm, compensation based scheme is processed to reduce the geometric-linearization error caused by the original linearization scheme of the post-nonlinear geometric ICA (pgICA).

After de-noising, in order to eliminate the impact of varying operation condition and environment on data analysis, a novel environment impact elimination method based on AR model and similarity matching is proposed. In this algorithm, acquired vibration data samples are divided into two sets, undamaged condition data set S^U and unknown condition data set S^D. AR model is used to extract the features of each data samples in the two sets. Based on these features, a similarity matching scheme based on Euclidean distance is designed to obtain the data sample pair, one sample of S^U and one of S^D, which are sampled in a similar operation and environment condition. Thus, the change caused by varying operation condition and environment is eliminated.

To verify the advantage of our algorithm, pcgICA, it is compared with FastICA and pgICA by calculate the correlation-coefficient and signal-noise-ratio (SNR) in simulation. Comparing with FastICA and pgICA, the average correlation-coefficient of pcgICA is improved by 0.39 (62.1%), and 0.17 (16.7%) respectively, the SNR is improved by 51.8% and 16.3% respectively. In Nakajima bridge experiment, the results shows pcgICA also is better than FastICA and pgICA. To verify the effectiveness of the proposed environment impact emilination algorithm, the data of Nakajima bridge experiment is used. The results shows using our method can effectively eliminate false damage detection caused by varying environment. It means our proposed method is efficient.

Reference

[1] T.V. Nguyen, J.C. Patra, A. Das, and G.S. Ng, “Post nonliear blind source separation by geometric linearization,” In
Networks, Vol. 1, pp. 244–249 (2005)

[2] Li CS, Yu PS, Castelli V. HierarchyScan, “a hierarchical similarity search algorithm for database of long sequences,” 12th international conference on data engineering, New Orleans, Louisiana, pp. 546–553 (1996-2)

[3] C. Zang, M.I. Friswell, and M. Imregun, “Decomposition of time domain vibration signals using the independent component analysis technique,” 3rd International Conference on Identification Engineering System, Swansea, UK, pp. 434–445

[4] J. cheng, M. Hsieh, Y. Yeh and H. Ogai, “Development of Bridge Diagnosis Technology by Independent Component Analysis”, SUCE-ICASE 2006 International Joint Conference, pp. 4692-4697, Busan, South Korea (2006)

[5] L. Zhong, H. Song and B. Han, “Extracting Structural Damage Features: Comparison Between PCA and ICA”, Intelligent Computing in Signal Processing and Pattern Recognition Lecture Notes in Control and Information Sciences, Vol. 345, pp. 840-845 (2006)

[6] Haitao Xiao, Sheng Luo, Harutoshi Ogai, “A Novel Bridge Structure Damage Diagnosis algorithm based on Post-nonlinear ICA and Statistical Pattern Recognition”, IEEJ Transactions on Electronics and Electronic Engineering, Vol.10, No.3, May, 2015.

Chapter 4

Time-series Modeling based Damage Detection Method

4.1 Introduction

After data processing, the accuracy and sensitivity of damage diagnosis algorithm directly determines the performance of BSHM system. How to identify damages sensitively and how to accurately detect the damage severity and location become major problems in vibration data based BSHM system. To deal with these problems, many vibration data based damage diagnosis algorithms are designed. However, most of these algorithms detect damages of bridge structure by comparing the vibration data in current status condition with the vibration data in health condition. Actually, there is no vibration data corresponding to health condition or difficult to obtain in many old bridges. Thus, how to detect damages by only using the data in current state is another problem. The backgrounds promoted design of advance and sensitivity damage diagnosis algorithm. In this chapter, a novel two-stage bridge structure damage diagnosis algorithm is proposed to evaluate the health of bridges, including damage identification and damage servility and location detection. In the first stage, after data processing, FFT is used to obtain the characteristic frequency of bridges. By comparing the frequency in a healthy state with an unknown state, we detect the structural novelty (damage identifying).

In second stage, to detect the severity and location of damage, a statistical damage detection algorithm, called Time-series modeling based damage diagnosis algorithm, is proposed. ARMA model is used to establish models for the processed data to perform feature extraction, where PCA (principal component analysis) is employed to reduce the amount of features. A new damage sensitive feature index with high sensitivity, D_{index}, is proposed to obtain the severity and location of damages.

4.2 Overview of Proposed Damage Detection Method

Generally vibration data of structure excited by environment are acquired and used in structure damage diagnosis. Thus, there is an assumption for the proposed damage detection algorithm: The monitoring system can only obtain the output vibration data because of free input excitations (environment excitations or random traffic loading). The proposed diagnosis scheme consists of the two stages shown in Figure 4.1.

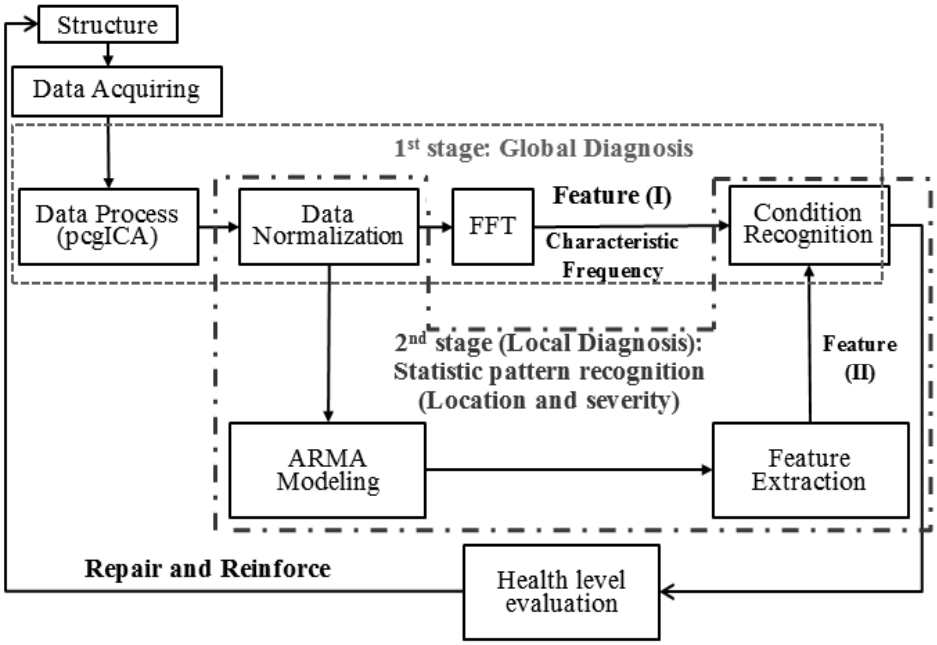

Figure 4.1 Proposed two-stage damage detection method

The first stage detects the novelty of the bridge structure, and the second stage detects the severity and location(s) of damages. In the first stage, after de-noising and normalizing, FFT is used to extract the characteristic frequency of healthy state and unknown state for the structural novelty detection. The second stage is utilized to locate damages and detect the severity sensitively. In this stage, a statistical damage identification algorithm, called time-series modeling based Damage Diagnosis Algorithm, is proposed. At first, the data samples are used to establish ARMA model. Based on the model, the pattern vectors perform feature extraction, where PCA is utilized to carry out the effective curtailment of the multi-feature. These features and Mahalanobis distance are used to extract the damage-sensitive-features (DSFs). In DSF extraction, there two cases need to be considered: First case containing the vibration data in health condition and the second case without that data. In 1th case, the features of the data sample in health condition are chosen as reference to be used for calculating Mahalanobis distance. In 2nd case, the features of any one data sample

in unknown condition are chosen as reference. Based on the DSFs, a new sensitive DSF index, D_{index}, is proposed to obtain a diagnosis of structure condition, or identify the severity and location of damages.

To summarize, the diagnosis scheme includes global and local structure damage detection. Formulations for the two stages are presented in the following subsections.

4.3 Process of First Stage

After processing data by de-noising and normalizing, the first stage of our algorithm, global structure damage detection, is used to detect bridge damage. The first stage damage detection consists of four steps shown as Figure 4.3. These steps are as follows.

STEP ONE: Use pcgICA to separate the signals of the bridge from others (e.g., noise, car, and wind signals). Herein, FastICA is chosen for the linear separation phase of pcgICA. Note that the vibration of the bridge is excited by vehicles or other ambient excitations. In this system, the excitation is the input, and vibration data of the bridge is the output. They seem to be related, but actually they are statistically independent, as verified by many research results. We calculate the power value to check which signal is the most powerful and can represent the bridge's vibration. Power value calculation is important for linear ICA and is useful for choosing the signal that represents the bridge's vibration. The most powerful signal is considered to be the bridge's signal, because our sensors are set directly on the bridge.

STEP TWO: Perform similarity matching based environment impact reduction method to obtain data sample pairs.

STEP THREE: Use FFT to obtain the bridge's characteristic frequency in the undamaged and unknown conditions. Then, compare the extracted frequency in the data sample pair to determine the global structure health condition of bridge. Change in characteristic frequencies means there is damage on the bridge. We then proceed to the second stage, local structure damage detection, to locate damages and detect the severity of damage.

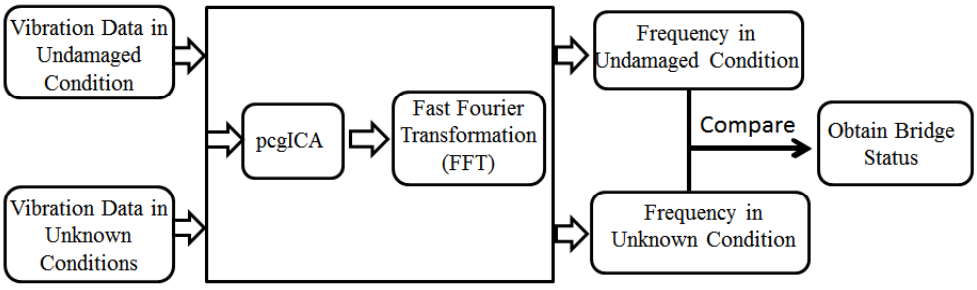

Figure 4.2 First stage of the two-stage damage diagnosis algorithm

4.4 Second Stage: Time-series Modeling based Damage Detection Algorithm

In this structure damage diagnosis stage, we propose a novel structure damage diagnosis algorithm called the time-series modeling based damage diagnosis algorithm. Four steps consist of the damage diagnosis algorithm shown as Figure 4.3.

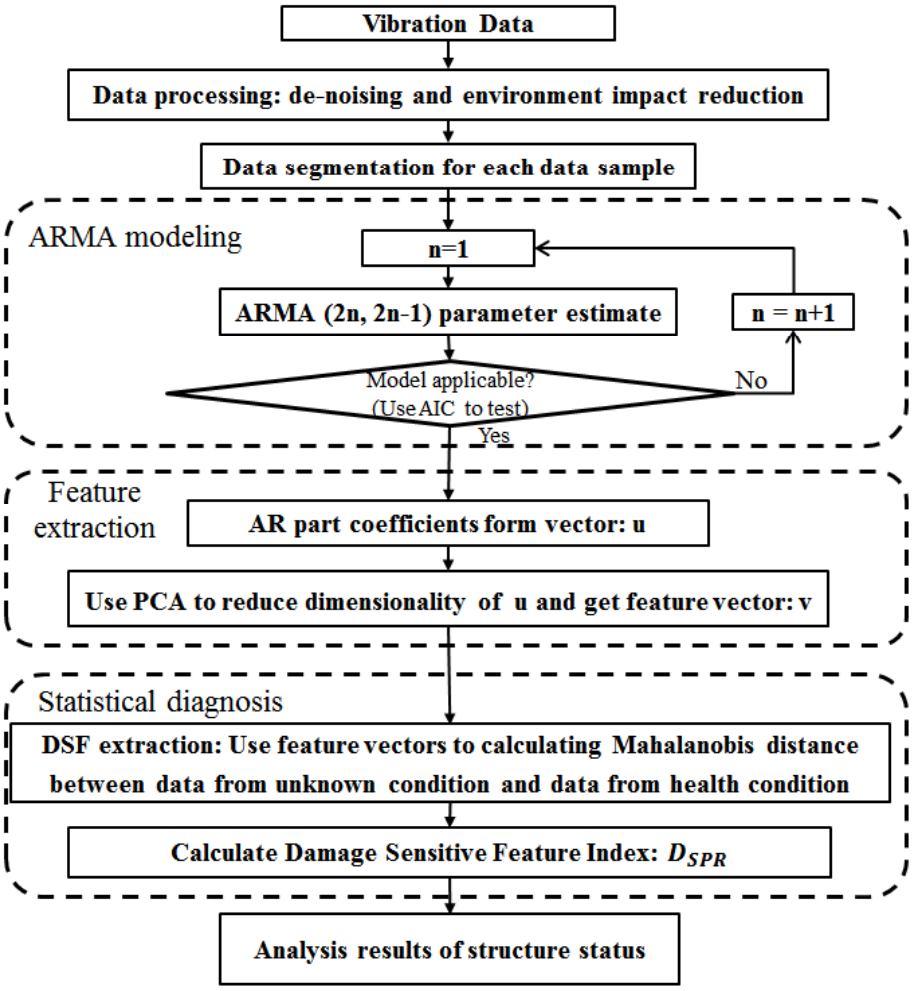

Figure 4.3 Four steps of SDD

STEP ONE: The data is processed by the data process method proposed in chapter 3. S^U and S^D are obtained.

STEP TWO: After processing the data samples, ARMA is chosen and applied for each data sample to establish the ARMA model.

STEP THREE: In a bridge system, the inherent characteristics of the system can be characterized by the parameters of the ARMA's AR part. Thus, we can apply the parameters of ARMA's AR part to extract the damage sensitive feature (DSF). To extract the DSFs quickly and accurately, PCA (Principal Component Analysis) is applied to carry out the effective curtailment of the multi-feature parameters.

STEP FOUR: Statistical discrimination is carried out based on the DSFs of data samples. A damage sensitive feature index (D_{index}) is proposed to compare the DSF coming from the damaged condition with that coming from the undamaged condition. Thus, we can use the damage-sensitive-feature index D_{index} to detect the severity of damages and locate damages.

4.4.1 Data Normalizing

In this stage, each data sample is further normalized by following equation (4.1) to differentiate the effect of structural alteration from some trivial outfitted amendments. $x_{ij}(t)$ represents the normalized-data, $X_{ij}(t)$ is the j^{th} data sample of i^{th} sensor's data, μ_{ij} is the mean of data sample $X_{ij}(t)$ and σ_{ij} is the standard-deviation of $X_{ij}(t)$.

$$x_{ij}(t) = \frac{X_{ij}(t) - \mu_{ij}}{\sigma_{ij}} \tag{4.1}$$

4.4.2 ARMA Modeling

4.4.2.1 ARMA Model

After normalization, an ARMA (p x q) model is established as equation (4.2) for each normalized data sample, $x_{ij}(t)$.

$$x_{ij}(t) - \sum_{k=1}^{p} \varphi_k \, x_{ij}(t-k) = \varepsilon_{ij}(t) - \sum_{k=1}^{q} \theta_k \, \varepsilon_{ij}(t-k) \tag{4.2}$$

Where φ_k and θ_k are the kth coefficient of AR part and MA part, severally, $\varepsilon_{ij}(t)$ represents residual-term or error-term (when this equation correctly interpret the time series' structure and rule, $\varepsilon_{ij}(t)$ is the white-noise containing zero-mean and variance of σ_a^2.). This ARMA (p x q) model contains two parts: the auto regressive (AR) and the moving average (MA). The AR part denotes that the value of $x_{ij}(t)$ is associated with the value in previous p steps, and the MA part denotes that $x_{ij}(t)$ is associated with the noise in previous q steps. When the backward shift operator B, which is defined as B^k $\omega(t) = \omega(t\text{-}k)$, is drawn in equation (4.2), the equation (4.3) is obtained. So equation (4.2) can be transformed to equations (4.4) and (4.5).

$$(1 - \varphi_1 B - \varphi_2 B^2 - \cdots - \varphi_p B^p) x_{ij}(t) = (1 - \theta_1 B - \theta_2 B^2 - \cdots - \theta_q B^q) \varepsilon_{ij}(t);$$

$$\varphi(B) = 1 - \varphi_1 B - \varphi_2 B^2 - \cdots - \varphi_p B^p;$$

$$\theta(B) = 1 - \theta_1 B - \theta_2 B^2 - \cdots - \theta_q B^q \tag{4.3}$$

$$\varphi(B) x_{ij}(t) = \theta(B) \varepsilon_{ij}(t) \tag{4.4}$$

$$x_{ij}(t) = \frac{\theta(B)}{\varphi(B)} \varepsilon_{ij}(t) \tag{4.5}$$

When the $\varepsilon_{ij}(t)$ is set as system input and the $x_{ij}(t)$ as the output, the ARMA (p x q)

can be described as a system with a transfer function, θ(t) / φ(t). Therefore, determining the order of this model, p and q, and the coefficient, φ_k and θ_k, is a process in model establishing and identification.

Using $\varphi(B)$ and $\theta(B)$ in equation (4.5) for factorization, we obtain equations (4.6) and (4.7), where λ_k and η_k are the characteristic root of the AR and MA parts respectively. From the point of view in system, λ_k is the pole of transfer function of system and denotes the inherent characteristic of the system. η_k is the zero point of transfer function of system and denotes the connection between the system and the environment. Thus, $\varphi(B)$ denotes the inherent characteristic of system. Compared with AR model ARMA model is more complete, higher model precision, and clearer in the physical interpretation of parameter, because ARMA fully considers the influence of external factors (MA part). Thus, ARMA model has better ability to identify small changes in the structure inherent characteristics.

$$\begin{aligned}\varphi(B) &= (1-\lambda_1 B)(1-\lambda_2 B)\cdots(1-\lambda_p B)\\ &= \prod_{k=1}^{p}(1-\lambda_k B)\end{aligned} \tag{4.6}$$

$$\begin{aligned}\theta(B) &= (1-\eta_1 B)(1-\eta_2 B)\cdots(1-\eta_1 B)\\ &= \prod_{k=1}^{q}(1-\eta_k B)\end{aligned} \tag{4.7}$$

4.4.2.2 ARMA Modeling

In this thesis, (2n, 2n-1) modeling method [1] is used to establish ARMA (2n, 2n-1) model. The order p and q in ARMA is determined by using Akaike's Information Criterion (AIC) [1]. The parameters of ARMA are estimated by the long regression residuals method [1].The searching scheme is shown as Figure 4.4. The processes of model establish is shown as Figure 4.5. There are three steps in this model establish method, which are shown as follow.

(1) TEP ONE: From $n = 1$, use the long regression residuals method [1] for data $\{x_{ij}(t)\}$ to fit ARMA (2n, 2n-1) model.

(2) STEP TWO: Use AIC to test whether this model is applicable. If not applicable, let $n = n + 1$, and go to fit ARMA (2n, 2n-1) model again until the model applicable. Then go next step.

(3) STEP THREE: Reduce order of AR part, and do above two steps again to test whether there is a more small AR part's order can be applicable. If yes, get the final ARMA model contained smallest AR part's order. Else, use the ARMA model obtained in the step two.

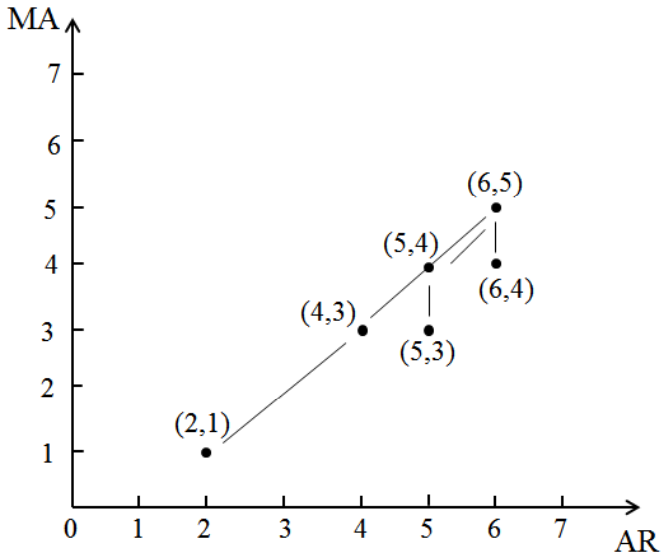

Figure 4.4 Searching scheme of (2n, 2n-1) modeling method

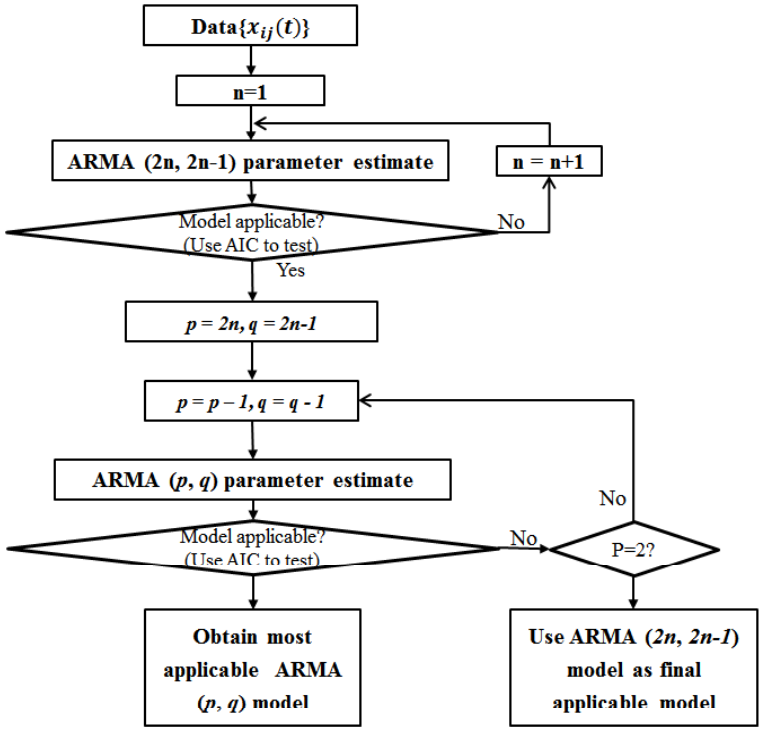

Figure 4.5 Processes of ARMA modeling

Akaike's Information Criterion (AIC)

In this ARMA model, the model residue error can be present by equation (4.8).

$$\varepsilon_t = x_t - \sum_{i=1}^{p} \varphi_i x_{t-i} + \sum_{j=1}^{q} \theta_j \varepsilon_{t-j} \tag{4.8}$$

After calculating the residue $\{\varepsilon_t\}$(t=p+1, p+2,⋯, N) by using equation (4.8), the residue sum of squares *S* is calculate by equation (4.9) and variance of residue σ^2 is obtained by equation (4.10).

$$S = \sum_{t=p+1}^{N} \varepsilon_t^2 \tag{4.9}$$

$$\sigma^2 = \frac{1}{N-p-2}\sum_{t=p+1}^{N} \varepsilon_t^2 = \frac{S}{N-p-2} \tag{4.10}$$

Then based on the equation (4.9) and equation (4.10) we can get the AIC, shown as equation (4.11), where N is the length of data, n represents the amount of model order, n= p + q. Thus, when we use AIC to determine the order of model, increase the fitting order n, the σ^2 will decrease. Therefore, when the AIC (n) get the minimum, the order n is best fitting order. In this way we can get the value of p and q.

Long Regression Residuals Method

After using AIC to get the order of model, the long regression residuals method [1] is applied to estimate the parameters of ARMA model. As described in [1], the parameter of AR model is a linear estimation, but the estimation of ARMA is a nonlinear estimation because the $\{\varepsilon_t\}$ is unknown. Thus, the idea of long regression residue method is that: firstly, use data $\{x_t\}$ to fit AR(p) model and calculate the residue $\{\varepsilon_t\}$ of AR model. Then use this residue $\{\varepsilon_t\}$ as the residue of ARMA and use the linear regression method, least square method, to estimate the parameters of ARMA model.

According above idea, use data $\{x_t\}$ to fit AR (n) model at first, and obtain the AR model parameters $\varphi_i(i = 1,2,\cdots,n)$.

$$\varepsilon_t = x_t \sum_{i=1}^{n} \varphi_i x_{t-i} \tag{4.11}$$

Then, we calculate the residue of AR model by equation (4.11). Thus, the residue sequence $\{\varepsilon_t\}(t = n+1, n+2, \cdots, N)$ is obtained.

The residue sequence $\{\varepsilon_t\}$ is regard as the observed value of MA part of ARMA model. Then, take the observed value and $\{x_t\}$ into ARMA (p, q) model, and calculate the parameter of ARMA (p, q) model. For example, when the least square method is used to estimate parameters, take $\{x_t\}$ and $\{\varepsilon_t\}$ into ARMA (p, q), and the equation (4.12) can been got:

$$\begin{cases} x_{n+p} = \sum_{i=1}^{p} \varphi_i x_{n+p-i} + \varepsilon_{n+p} \sum_{j=1}^{q} \theta_j \varepsilon_{n+p-j} \\ x_{n+p+1} = \sum_{i=1}^{p} \varphi_i x_{n+p+1-i} + \varepsilon_{n+p+1} \sum_{j=1}^{q} \theta_j \varepsilon_{n+p+1-j} \\ \vdots \\ x_N = \sum_{i=1}^{p} \varphi_i x_{N-i} + \varepsilon_N \sum_{j=1}^{q} \theta_j \varepsilon_{N-j} \end{cases} \tag{4.12}$$

Use matrix to represent equation (4.12), shown as equation (4.13).

$$\mathbf{y} = \mathbf{X}\boldsymbol{\beta} + \mathbf{a} \tag{4.13}$$

Where:

$$\mathbf{y} = \begin{bmatrix} x_{n+p} & x_{n+p+1} & \cdots & x_N \end{bmatrix}^T$$

$$\mathbf{a} = \begin{bmatrix} a_{n+p} & a_{n+p+1} & \cdots & a_N \end{bmatrix}^T$$

$$\boldsymbol{\beta} = \begin{bmatrix} \varphi_1 & \varphi_2 & \cdots & \varphi_p & -\theta_1 & -\theta_2 & \cdots & -\theta_q \end{bmatrix}^T$$

$$\mathbf{X} = \begin{bmatrix} x_{n+p-1} & x_{n+p-2} & \cdots & x_n & \varepsilon_{n+p-1} & \varepsilon_{n+p-2} & \cdots & \varepsilon_{n+p-q} \\ x_{n+p} & x_{n+p-1} & \cdots & x_n & \varepsilon_{n+p} & \varepsilon_{n+p-1} & \cdots & \varepsilon_{n+p+1-q} \\ \cdots & \cdots & \cdots & \cdots & \cdots & \cdots & \cdots & \cdots \\ x_{N-1} & x_{N-2} & \cdots & x_{N-p} & \varepsilon_{N-1} & \varepsilon_{N-2} & \cdots & \varepsilon_{N-q} \end{bmatrix}$$

Because ε_t of X are known, the least square estimation is shown as:

$$\boldsymbol{\beta} = (\mathbf{X}^{\mathrm{T}}\mathbf{X})^{-1}\mathbf{X}^{\mathrm{T}}\mathbf{y} \tag{4.14}$$

4.4.3 Feature extraction and dimensionality reduction

The analysis in subsection 4.4.2 shows that the parameters of the AR part denote the inherent characteristics of the system. Thus, the AR part can be used to extract the DSF. To identify damage, a new type of DSF is proposed based on Mahalanobis distance. In order to improve the speed of extraction, PCA is utilized before extracting. There are five steps to obtain the DSF, shown as Figure 4.6.

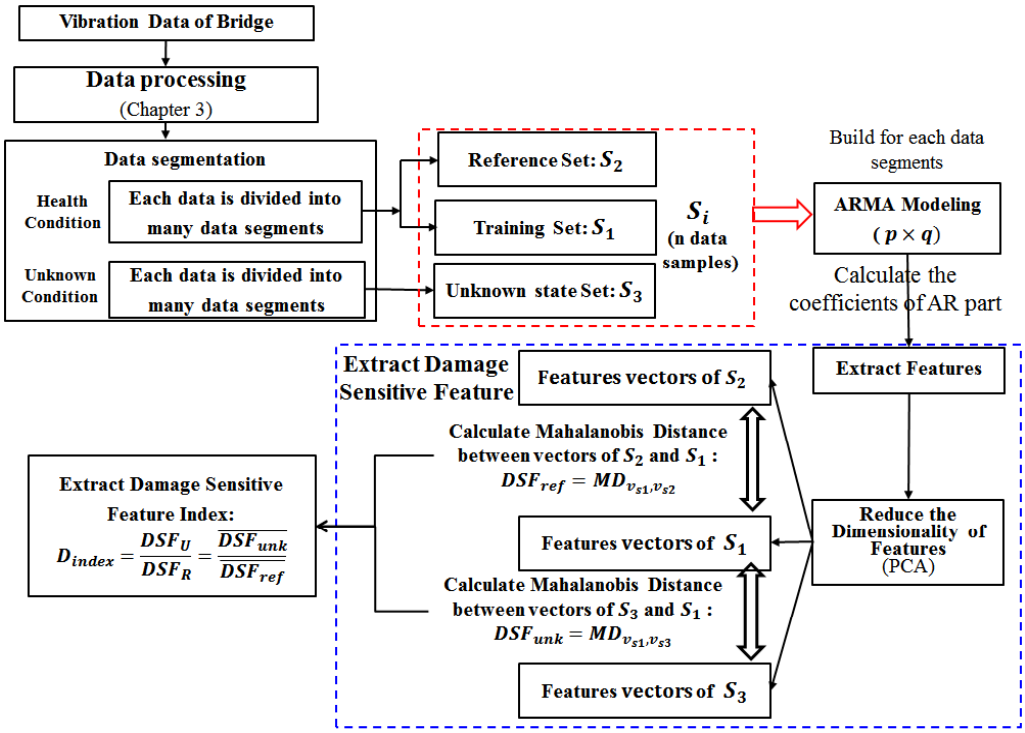

Figure 4.6 Processes of damage sensitive feature (DSF) extraction

STEP 1: The data is processed by proposed data process method in chapter 3. In the 1th case, containing the data acquired in health condition, many data sample pairs

(target data sample-matched data sample) are obtained, which means the matched data sample corresponding to the target data sample (in S^D) is searched in S^U. Each data of S^U and S^D are divided in to many segments. These segments of data in S^U are divided into two parts, one part used for the training data samples set S_1, and the other used for the reference data samples set S_2. The data that contains the target data sample and correspond to the unknown condition is divided into two parts. The second part is used for the pending data sample set S_3. In the 2th case without the data acquired in health condition, we arbitrarily choose and divided a node's data into two parts one part used for the training data samples set S_1, and the other used for the reference data samples set S_2. Other nodes' data in the same time measurement is preform the same processes as 1th case. We set the number of data samples in S_1, S_2, and S_3 as n.

STEP 2: Use the data samples of these three sets to establish their ARMA models.

STEP 3: Record all order parameters of the AR part of each data segment's ARMA model in S_1 as vector $\mathbf{u_i}$ (i = 1, 2, …, n). Thus, we can get the ($n \times p$) matrix **U** of S_1:

$$\mathbf{U} = \begin{bmatrix} u_{11} & \cdots & u_{1n} \\ \vdots & \ddots & \vdots \\ u_{p1} & \cdots & u_{pn} \end{bmatrix} \triangleq [\mathrm{u}_1, \mathrm{u}_1, \cdots, \mathrm{u}_n];$$

$$\text{Where } \mathbf{u_i} = [u_{1i}, u_{2i}, \cdots, u_{pi}]^T \qquad (i = 1, 2, \cdots, n)$$

We use PCA to analyze the matrix **U** = ($\mathbf{u_1}$, $\mathbf{u_2}$, …, $\mathbf{u_n}$) and obtain P principal components of **U**. The k^{th} principal component Y_k shown as equation (4.15). From equation (4.15), we get equation (4.16), where Σ is the covariance of **U**, $\lambda_1 \geq \lambda_2 \ldots \geq \lambda_P$, and e_i is the characteristic root of Σ and orthonormal unitization characteristic vector. Then we do the same process as S_1 to S_2, and S_3.

$$\begin{gathered} \boldsymbol{Y_k} = \boldsymbol{e_k^T X} = e_{1k}\boldsymbol{X}_1 + e_{2k}\boldsymbol{X}_2 + \cdots + e_{pk}\boldsymbol{X}_p, \\ (k = 1, 2, \cdots, p) \end{gathered} \tag{4.15}$$

$$\begin{cases} \mathrm{Var}(\boldsymbol{Y_k}) = \boldsymbol{e_k^T \Sigma e_k} = \lambda_k, & (k = 1, 2, \cdots, p) \\ \mathrm{Cov}(\boldsymbol{Y_k}, \boldsymbol{Y_l}) = \boldsymbol{e_k^T \Sigma e_l} = 0, & (k \neq l) \end{cases} \tag{4.16}$$

STEP FOUR: Extracting the first m principal components (m < p, usually, 1 < m < 4 can contain the 80%–90% principal information of matrix **U**) instead of original data to carry out dimensionality reduction. Thus, three $n \times m$ principal matrices are obtained from S_1, S_2, and S_3 respectively.

STEP FIVE: Record the $n \times m$ principal matrix from training data sample set S_1 as m dimension population G. Its mean vector is μ, and covariance is Σ. We define the Mahalanobis distance between each vector of the n × m principal matrix of s_2 and s_3 (x) to the mean vector of population G as *DSF*, shown as equation (4.17). Thus, based on equation (4.17), we extract the DSF of the data samples.

$$\mathrm{DSF} = [(x - \mu)^T \Sigma^{-1} (x - \mu)]^{\frac{1}{2}} \tag{4.17}$$

4.4.4 Statistical Discrimination

Actually, even though there is no change in condition of the structure, the DSF can still be greater than *0* because of the nonlinear character or time-varying behavior of a bridge. Therefore, for statistical reliability, structure damage diagnosis should be performed based on a plenty of data-samples. Herein, a DSF-based statistical discrimination algorithm is proposed.

Firstly, all measured data are divided as in section 4.4.3. Thereafter, for each data sample in S_2 and S_3, the corresponding DSF is computed by using equation (4.17). By using these DSFs, a new damage sensitive feature index D_{index} is proposed as equation (4.18), where DSF_U is the mean value of DSF obtained by using the data samples of S_3. The DSF_R, named reference DSF, is the mean value of the DSF corresponding to the undamaged condition data sample set S_2. Thus, if the bridge structure changes, the D_{index} will be far larger than 1. In addition, the magnitude of D_{index} can be utilized to locate damages and determine the severity of damage, which will be verified in the simulation and experiments.

$$D_{index} = \frac{\mathrm{DSF}_U}{\mathrm{DSF}_R} = \frac{\overline{DSF_{unk}}}{\overline{DSF_{ref}}} \tag{4.18}$$

4.5 Simulation and Field Experiments

4.5.1 Numerical Simulation

To verify the validity of the presented algorithm in the second stage, a numerical simulation of a uniform beam model containing damages is performed. To clearly show the advantages of the diagnosis algorithm in the second stage, we use three equal spans girder model and stochastic white-noise as excitation, which are applied in simulation of many other statistic partner recognition based diagnosis algorithms, to implement simulation for my method. The model is shown in Figure 4.3, where the span length is 30 m, and the model is meshed into 10 elements in each span. The elastic module E= 2×10^5 MPa, the density ρ = 7850 kg /m^3, the section area A = $1.671 \times 10^{-3} m^2$, and the section inertia moment I = $1.652 \times 10^{-6} m^4$.

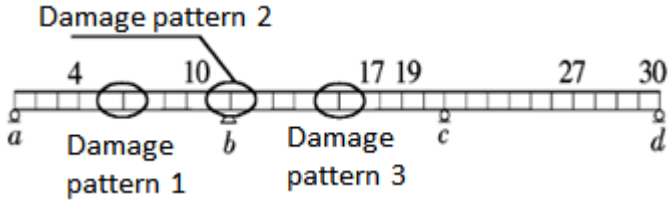

Figure 4.7 Three span girder model

Crack damage is simulated in an equivalent sub beam using a unit elastic modules discount function suggested in [2]. Considering the symmetry of the three-span girder model, damage patterns are designed in two cases. The first case contains four damage levels in the same position. In the second case, there are three different positions within the same damage level. In the first case, we reduce 10%, 20%, 35%, and 50% of the elastic module of the two units near the center of the left side span, respectively, for four damage patterns. In the second case, the damage conditions are as follows. For damage condition 1, reduce 10% of the elastic module in the damage 1 of Figure 4.7. For damage condition 2, reduce 10% of the elastic module in the damage 2 of Figure 4.7, maintaining the damage of condition 1. For damage condition 3, reduce 10% of the elastic module in the damage 3 of Figure 4.7, maintaining the damages of conditions 1 and 2.

In order to obtain a structural vibration data, the girder is loaded by a stochastic white-noise excitation. The vertical acceleration obtained from each of the 30 nodes is taken as the simulated monitoring data. The sampling frequency is set to 200Hz. To display the frequency change from the undamaged to the damaged condition, sensors sample 1000s. The first two orders of frequencies in the two conditions are shown in Table 4.1 (the data of node 10). From this table, we can find that the deviations of frequencies in the two conditions are less than 1% due to the structure changes.

Table 4.1 Frequency in damaged and undamaged conditions

Order	undamaged	Condition 1	2	3
1st	2.495	2.481	2.477	2.473
2nd	3.195	3.194	3.182	3.178

When we use our proposed algorithm to extract the structure damage feature, we only select the sampling data of posterior 150 s as simulated monitoring data because of the large size of the 1000 s sampling data. The simulated monitoring data obtained from the undamaged condition is divided into two groups, S_1 and S_2 (see sections 4.3.3 and 4.3.4). S_1 contains the data obtained during the prior 100 s, and S_2 contains the data obtained in the remaining 50 s. Meanwhile, the data obtained from all the damaged patterns during the posterior 50 s are used as S_3. All the simulated monitoring data in S_1, S_2, and S_3 are further divided into 100, 50 and 50 segments respectively (these are blocks, not seconds or points) to obtain data sample sets. Each segment consists of 1024 points, with 87.5% of data overlapped among adjacent segments. Thereafter, the data of nodes 4, 10, 17, 19, 27, and 30 are used to establish the ARMA and extract the DSFs and D_{SPR} by applying our algorithm.

The results from the first case are shown in Figure 4.8. When the structure changes, the D_{index} is larger than *1*, and the D_{index} sharply increases with the increase in damage level. When the damage level is small, such as in condition *1*, D_{index} also shows significant change. These results Figure prove that our index D_{index} is sensitive to the

damage of structure. The D_{index} of node 4 and that of node 10, which are close to the bridge damage, are significantly larger than the D_{index} of other nodes that are further away. Thus, we can locate the damage.

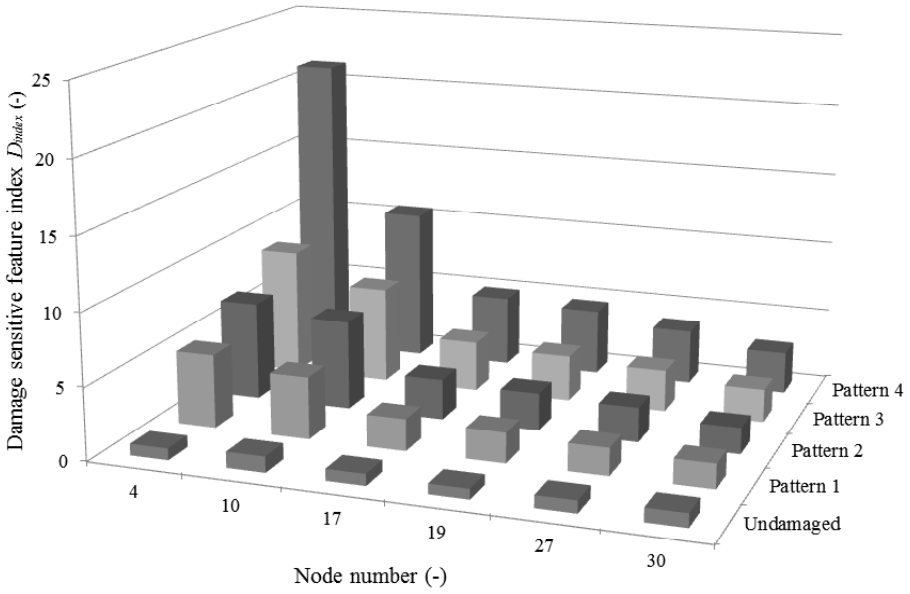

Figure 4.8 D_{index} for First case

Figure 4.9 shows the result of the second damage case. As noted above, the three span girder model contains several areas of damage in the second damage case. From Figure 4.9 shows obviously that significant difference exists in D_{index} obtained from the damaged and undamaged cases. From the bar graph of condition 2, we can find the D_{index} of nodes 4 and 10 are far larger than that of others. This indicates damage is located near those two nodes. Comparing with Figure 4.8, we find our D_{index} can locate the damage. From the bar graph of condition 3 in Figure 4.9, we can find the D_{index} of nodes 4, 10, and 17 are significantly larger than that of others, which means damage is located near the three nodes. Comparing the positions of these three nodes, we can guess there is damage between node 4 and node 10, within node 10, and within node 17. We can guess there is serious damage around node 10. After checking the position damages, we find the first guess is right, which verifies our algorithm can locate damage when there is damage in multiple locations.

Based on the discussion of the first and second damage cases, it can be concluded that the D_{index} index defined in this paper is sensitive to the damage of structure. Our algorithm can detect the severity and location of damage.

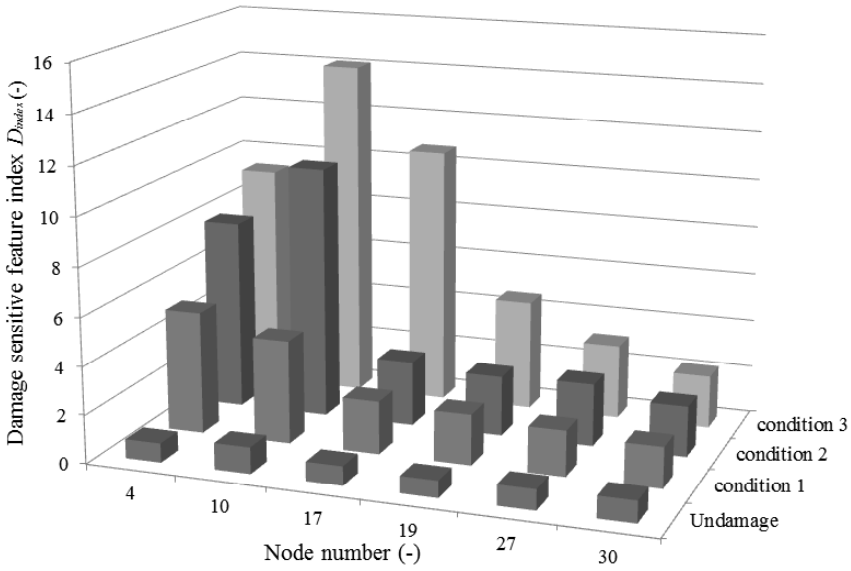

Figure 4.9 D_{index} for second case

4.5.2 Field Bridge Experiments

From 2008 to 2012, in order to test and improve the BSHM system, the system was tested on 10 bridges, using a variety of experiments, such as a large road bridge called Nakajima Bridge, in Fukuoka Prefecture. In this experiment, we applied the WSN to measure the vibration data of the bridge in an undamaged condition. To acquire data on the undamaged and damaged bridge, implemented an experiment is implemented on the Kando Bridge in Shimane Prefecture. To test the BSHM system through longer-term monitoring, we monitored Seiran Bridge in Kokura for four months. In this paper, we introduce the experiments on the Kando Bridge to verify the validity of the BSHM.

4.5.2.1 Kando Bridge Experiment

To acquire undamaged and damaged bridge data, an experiment was implemented on the Kando Bridge in Izumo in Shimane Prefecture. This bridge consist of a steel girder and a concrete deck slab, having five equal spans of length 50.8 m each, and pier-to-pier distance of 51.58 m. The bridge's length is 258m. The deck rests on braced steel girders of 2.1 m high placed at 2 m centerline distance. Figure 4.10 is a schematic diagram showing the location of damage and sensors on the bridge.

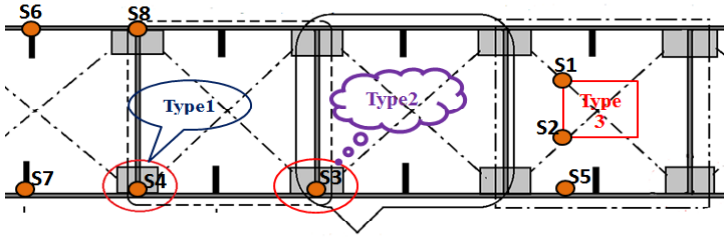

Figure 4.10 Locations of damage and sensors

The initial steps in this experiment were similar to those on the Nakajima Bridge; that is, the use of WSN to acquire acceleration data. Before we artificially damaged the bridge, (damaged by our), we collected data to serve as the measurement of the undamaged bridge condition (although this data may not reflect the actual bridge condition). In order to obtain significant vibration data in damage position we deploy some sensors beside the potential damage in this experiment. We need to declare that we deploy sensors on bridge according to a fixed spacing in other experiments such as Nakajima Bridge, Seiran Bridge, etc. We then induced damage to the bridge and collected additional measurement data, which is considered to represent the unknown condition. In this experiment, our proposed two-stage diagnosis algorithm is used to identify the damage to the bridge and verify the validity of our algorithm.

Damage was inflicted at three different places with six levels of severity. These damage types are as follows. Type I: the bearing between the abutment and bridge deck was damaged, shown in Figure 4.11. Type II: the gusset plate of the bridge deck located between piers P1 and P2 was damaged, shown in Figure 4.12. Type III: The concrete ceiling and the reinforcement were scratched out to damage the deck of the bridge as shown in Figure 4.13, where the cut depth of level-1 and level-2 are 3mm and 25mm respectively. The depth of level-3 in horizon is the same as the level-2, and the depth in vertical is equal to the level-1. The depth of level-4, level-5 and level-6 are 10mm, 10mm, and 30mm respectively.

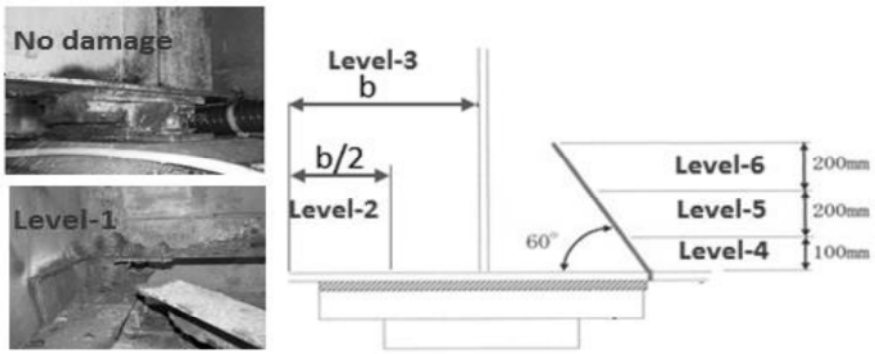

Figure 4.11 Abutment bearing damage

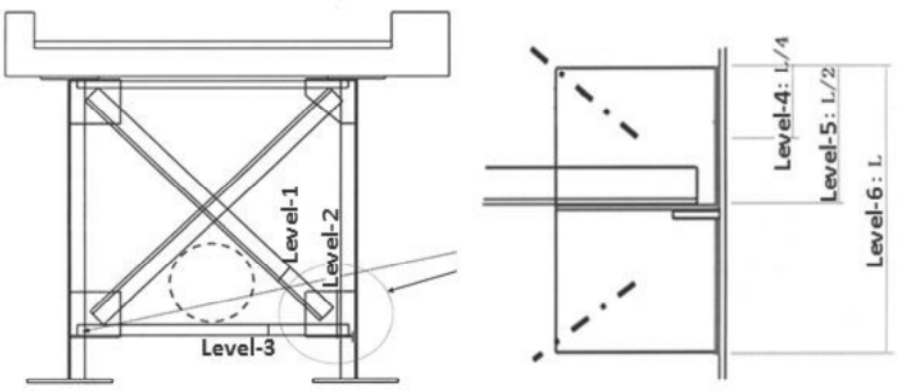

Figure 4.12 Gusset plate damage

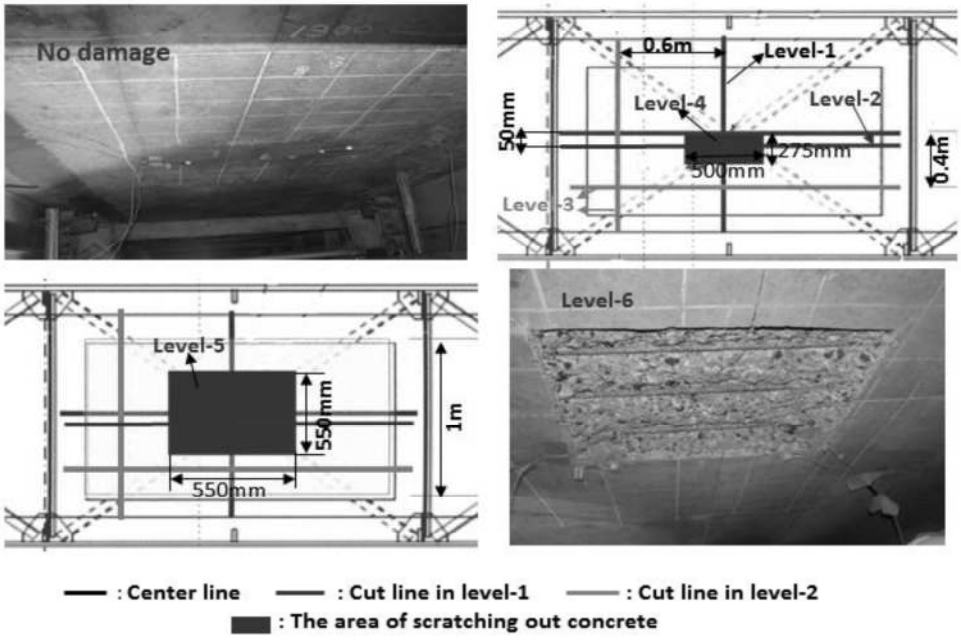

Figure 4.13 Concrete damage

After measuring the non-damaged Kando Bridge, we did three types of artificial damage to the bridge. Apart from ambient excitation, two types of external excitations were also used. The first one involved excitation using a loaded moving car, and the second one involved an impact with a 20 kg weight at 1 m high, at the same place. Typically, sensors for all damage cases are placed near the damage location in order to identify local changes. For damage types I, II, and III, eight sensors were deployed on the bridge as shown in Figure 4.10. In each level of damage, sensors measured the vibration of the bridge for each excitation. Thus, we obtained 57 measurements: three undamaged measurements and 54 unknown measurements.

To determine the modal properties of a system, a transfer function based approach is the most typical approach. For this approach, both input excitation and output responses are needed. In this bridge diagnosis, we can only obtain the output, since the system is excited by a moving car, hammer, or other ambient excitations. Thus, our two-stage diagnosis algorithm is proposed. Since the running car is the most common excitation in normal bridges, this paper only describes the results of the analysis of vibration data excited by the moving car.

4.5.2.2 Analysis Results of First Stage Algorithm

First, the pcgICA-based algorithm was used to obtain the change in frequency between the health condition and the damaged condition. Then, my method was utilized to obtain the severity of damages and locate damages. Because the vibration data were measured in almost the same environmental and operational conditions, we did not need to implement our proposed data normalization algorithm in this

experiment. The undamaged data and unknown data were divided into three data sample subsets as shown in section 4.4.3. Figure 4.14 shows the acceleration data of one axis in one sensor before and after damage. The upper picture shows the data of the healthy bridge, and the lower picture shows the data after doing steel frame damage.

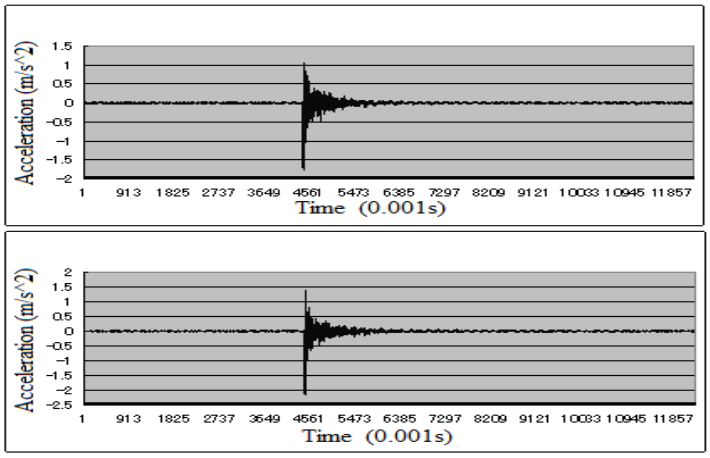

Figure 4.14 Acceleration data of one axis in one sensor

The results of the first stage of our diagnosis algorithm are tabulated in Table 4.3. It is observed from the characteristic frequency of type I in Table 4.3 that with an increase in damage severity the frequencies are decreasing, depicting the stiffness degradation of the structure. A similar trend of frequency drop is also observed from the type II data in Table 4.2. However, it may be noted that the percentage drop in the first two frequencies is less than in type I damage cases. It can also be noted that a slight increase in damage severity may not result in noticeable changes in frequencies from the type II of Table 4.2. This may be for various reasons, including change in damping and noise levels. As seen in Table 4.2, the type III damage shows degradation in frequency with an increase in damage severity, illustrating the contribution of web girder stiffness in structural frequencies. Most of the percentage drops are less than 3%, which indicates that the first stage can detect the structure change but is not sensitive enough to locate the damage. Thus, the second stage, using SDD, is proposed to detect the severity and location of damage.

Table 4.2 Frequency change for damage type I, type II, and type III

Severity	Type I frequency	Type II frequency	Type III frequency
0	2.443	2.442	2.442
1	2.443	2.442	2.436
2	2.415	2.413	2.432
3	2.388	2.406	2.432
4	2.371	2.406	2.395
5	2.315	2.36	2.362
6	2.271	2.353	2.356

4.5.2.3 Analysis Results of Second Stage Algorithm

In the second stage, the model order is determined by the method of section 4.4.2.2. In order to show the effect of de-noising, the model order using de-noising data and original data are shown in the Figure 4.15. Figure 4.15 shows the ARMA model is (8, 7) model using de-noised data, where the order of AR part is 8 and the order of MA is 7. In Figure 4.15, we can find the minimum AIC value of using non-de-noised data is at (10, 9). It means the model order determination is bad than using de-noised data, because high order will result in more parameters of AR part. This proves the important of de-noising in damage diagnosis again. The sampling frequency is 200Hz and sampling time is 15 seconds. Thus, every node can obtain 3000 length data. The sampled data obtained from the undamaged condition is divided into two groups, S_1 and S_2 (see sections 4.4.3). S_1 contains the data obtained during the 15 s, and S_2 contains the data obtained in the posterior 10s. Meanwhile, the data obtained from all the damaged patterns during the posterior 10s are used as S_3. All the simulated monitoring data in S_1, S_2, and S_3 are further divided into 40, 20 and 20 segments respectively (these are blocks, not seconds or points) to obtain data sample sets. Each segment consists of 400 points, with 83.75% of data overlapped among adjacent segments for S_1 and 80% for S_2 and S_3. Thereafter, the data of eight nodes in three type damager condition are used to establish the ARMA and apply the parameters of ARMA's AR part to extract the damage sensitive feature (DSF) (Mahalanobis distance) based on the equation (4.9). Finally, based on the result of DSFs, D_{index} of all nodes in tree type damages are obtained based on the equation (4.10).

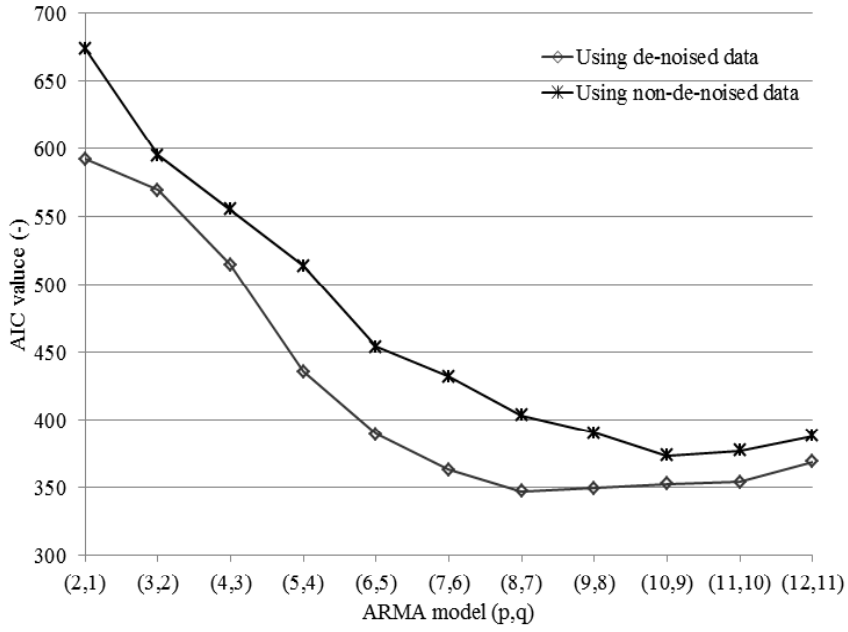

Figure 4.15 AIC results of de-noising data and non-de-noising data

Damage Type I

The extracted DSFs of all the data sample segments in the first type damage with six levels are shown in Figure 4.16, Figure 4.17, Figure 4.18, and Figure 4.19. Figure 4.20 shows the variation diagram of DSFs of sensor 4. From the five figures, we can get:

1) The DSFs of undamaged condition and six levels damage conditions exist obvious differences in the mean value and variance. In undamaged condition, the mean of DSFs and ripple of data are small, which means that the characteristic vector of undamaged condition is close to the reference population *G*. However, the DSFs of six levels damage in 8 sensors are increase and have large ripple, which means the characteristic vector of these conditions are far from G and has large discreteness.
2) The mean of DSFs of 8 sensors in six levels damage increase with the damage level increasing. Otherwise, the DSF growth of sensor 1, 2, 5 is not very big, but the DSFs of sensor 3, 4, 7, and 8 increase very obvious. Especially in sensor 4, the DSFs of six levels damage conditions shows far bigger than that of undamaged condition.

These results inosculate with the design of experiment, where, the sensor 4 is beside the damage and sensor 1, 2, 5 are far from the location of damage. However, it is difficult to intuitively the location and sensitivity of damages by using the distribution diagram of DSFs. To solve this, the equation (4.10) is used to get the damage sensitive feature index D_{index} of various damage levels and sensors. Figure 4.20 shows the damage severity feature index D_{index} of the undamaged condition and six levels damaged condition (the unknown condition is now known to be the damaged condition) in type I. From Figure 4.21, it can be observed that the value of D_{index} at sensor 4 is far larger than that at others, suggesting that the type I damage is very close to that sensor. From Figure 4.17 and Figure 4.20, a similar trend is observed, where sensor 4 is placed almost on the location of the bearing cut. In addition, the D_{SPR} at sensors 3, 7, and 8 is larger than at other sensors, and the D_{index} of sensor 3, 4, 7, and 8 obviously increase with the increase of damage level. In this way, we can obtain the sensitivity and location of damage accurately and intuitively.

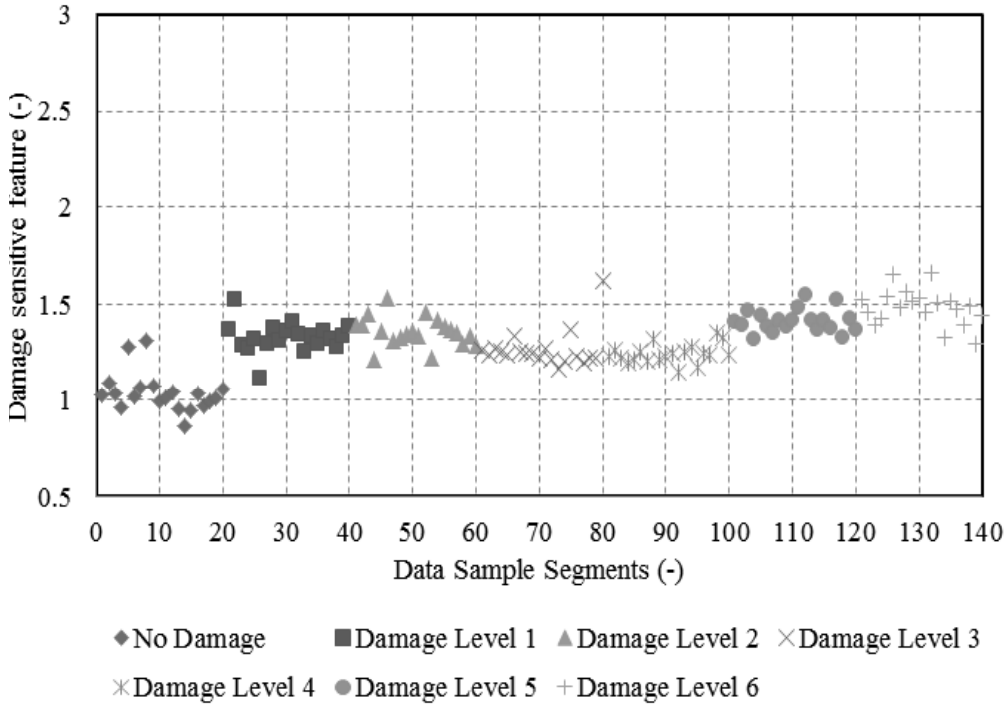

(a) Distribution diagram of DSF in sensor 1

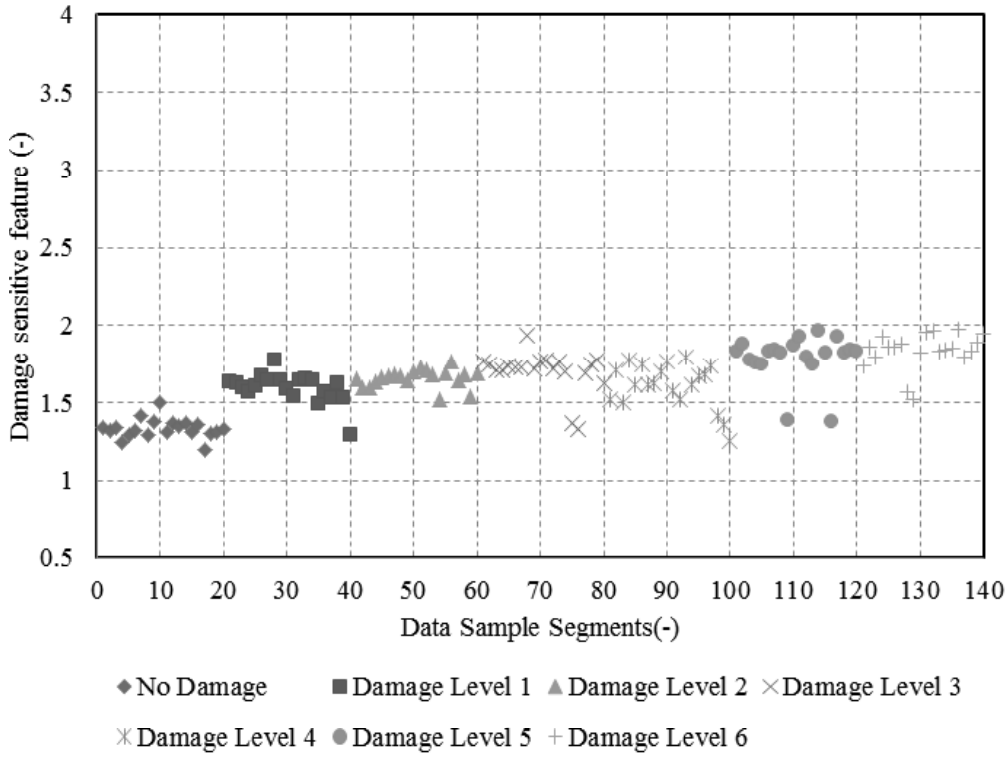

(b) Distribution diagram of DSF in sensor 2

Figure 4.16 Distribution diagrams of DSFs in sensor 1 and 2

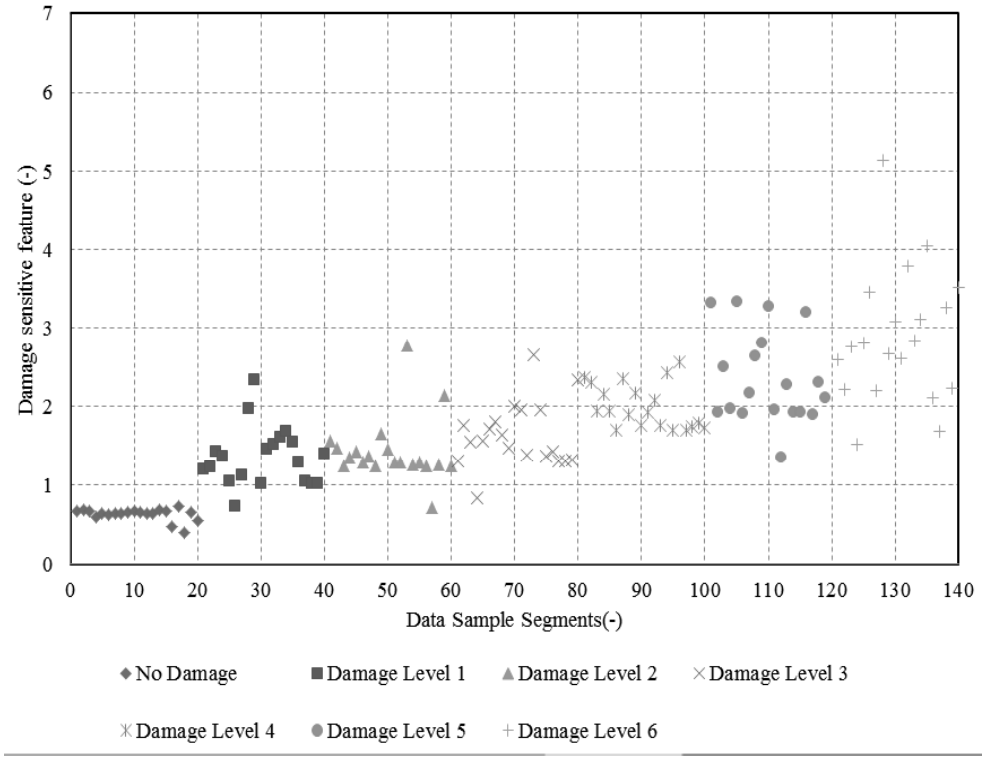

(a) Distribution diagram of DSF in sensor 3

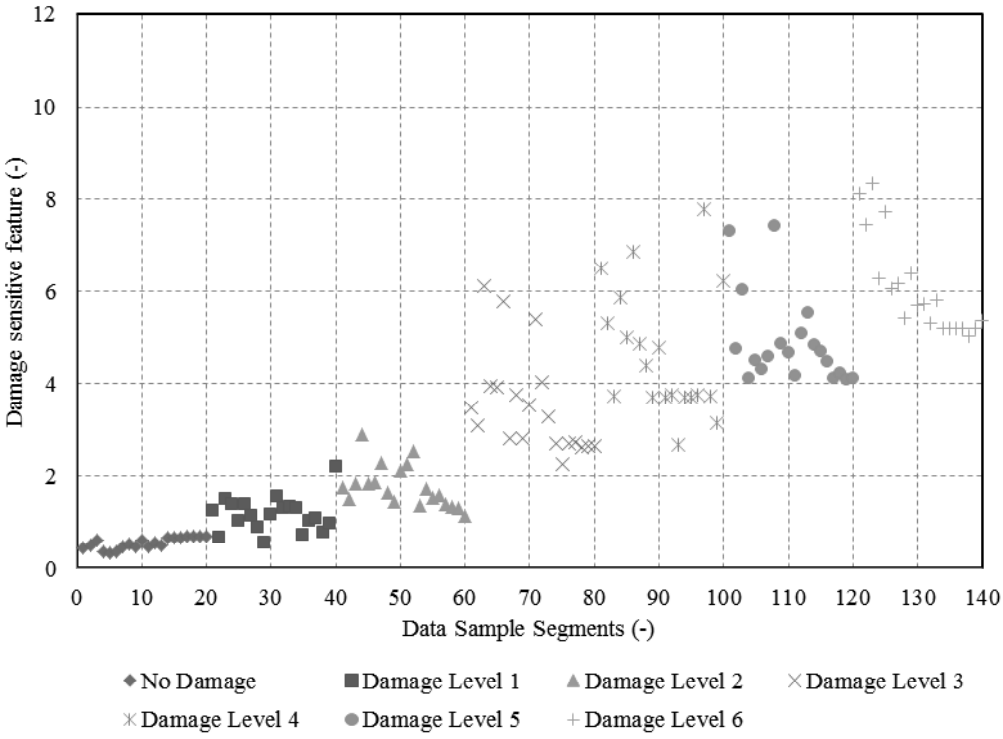

(b) Distribution diagram of DSF in sensor 4

Figure 4.17 Distribution diagrams of DSFs in sensor 3 and 4

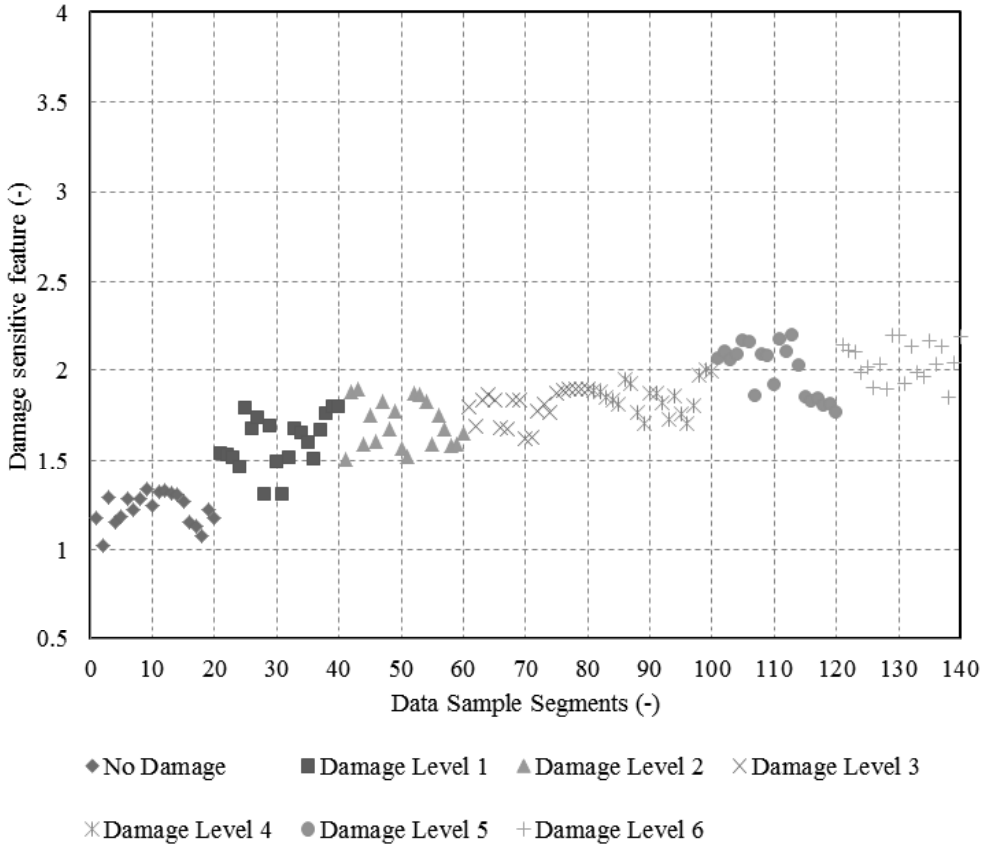

(a) Distribution diagram of DSF in sensor 5

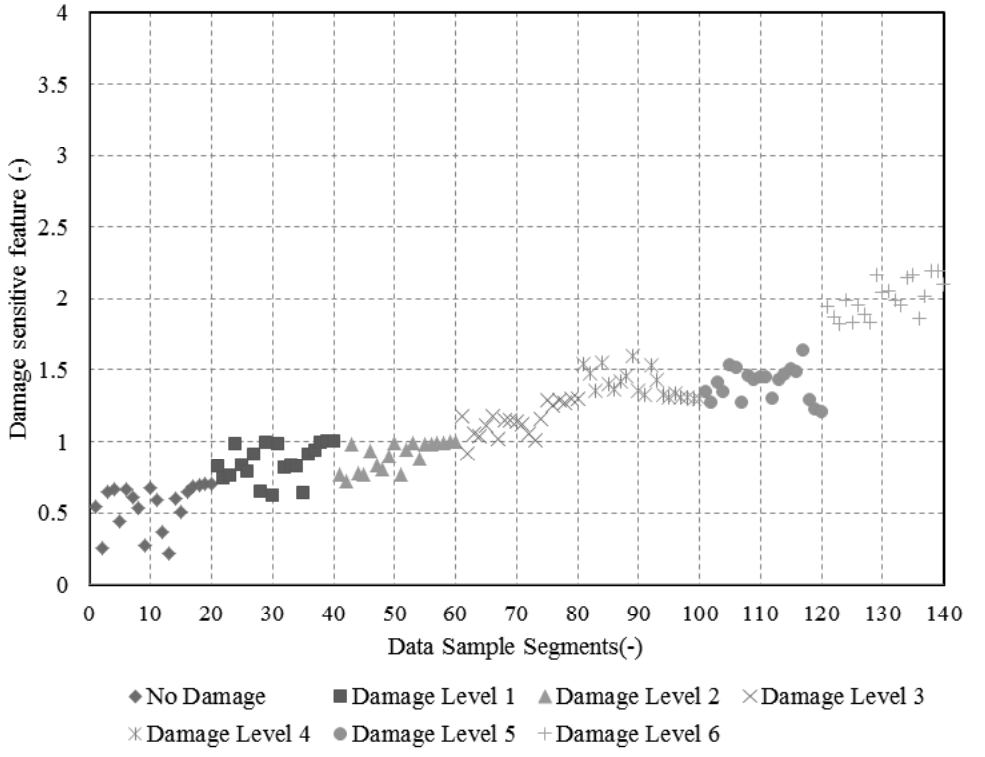

(b) Distribution diagram of DSF in sensor 6

Figure 4.18 Distribution diagrams of DSFs in sensor 5 and 6

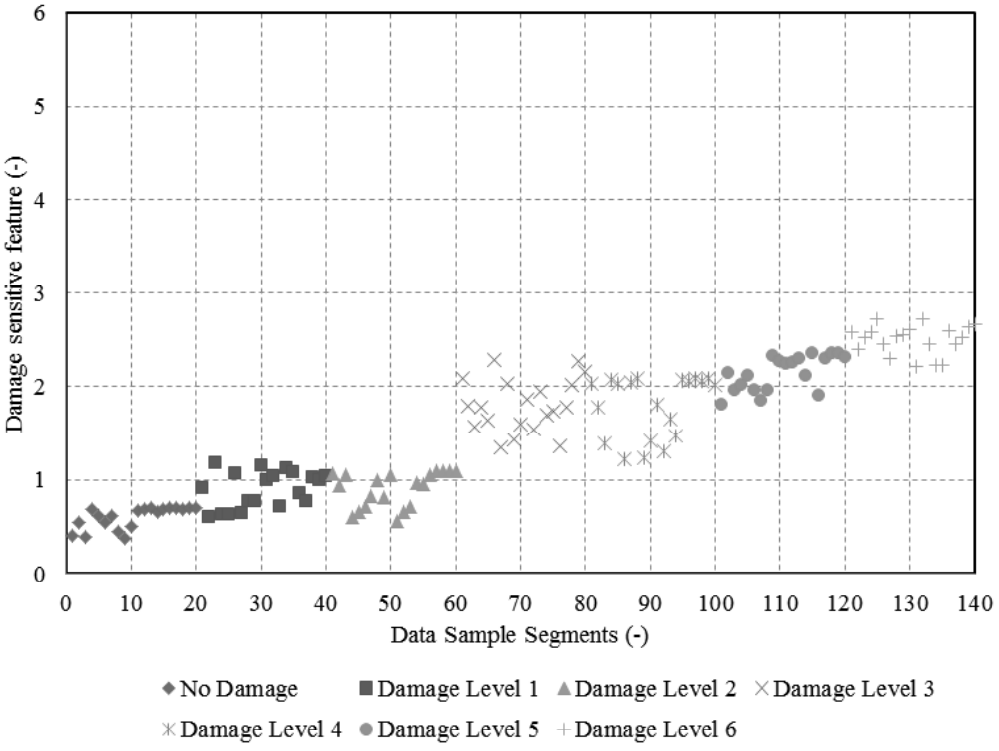

(b) Distribution diagram of DSF in sensor 7

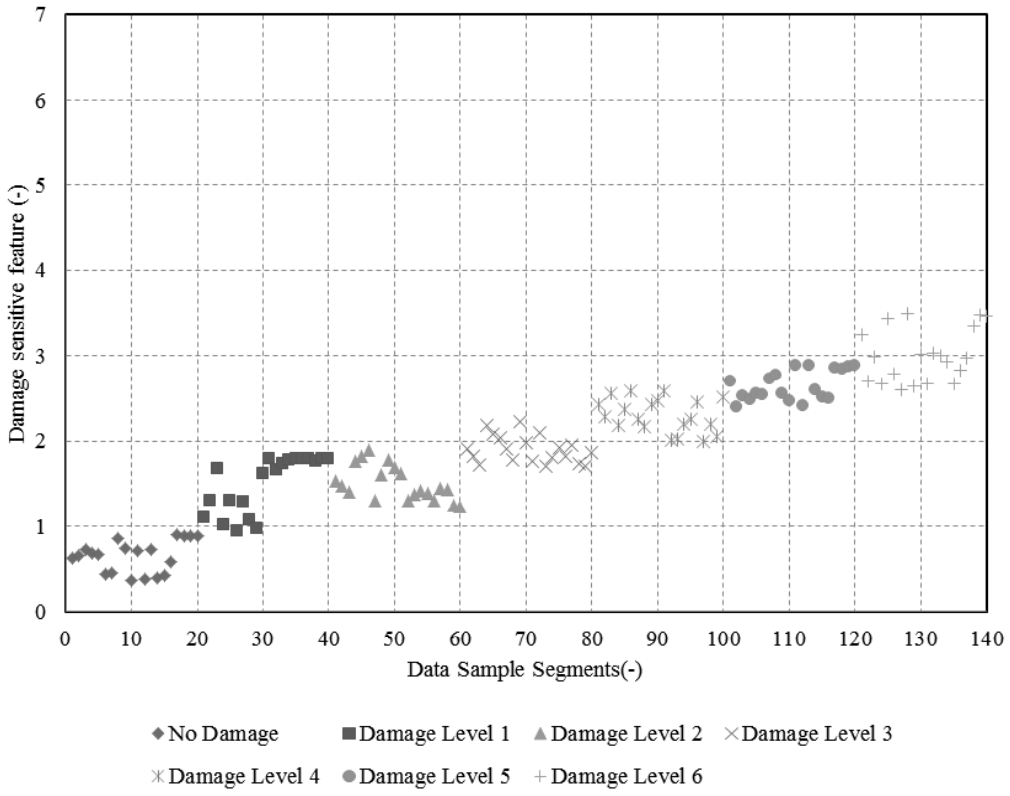

(b) Distribution diagram of DSF in sensor 8

Figure 4.19 Distribution diagrams of DSFs in sensor 7 and 8

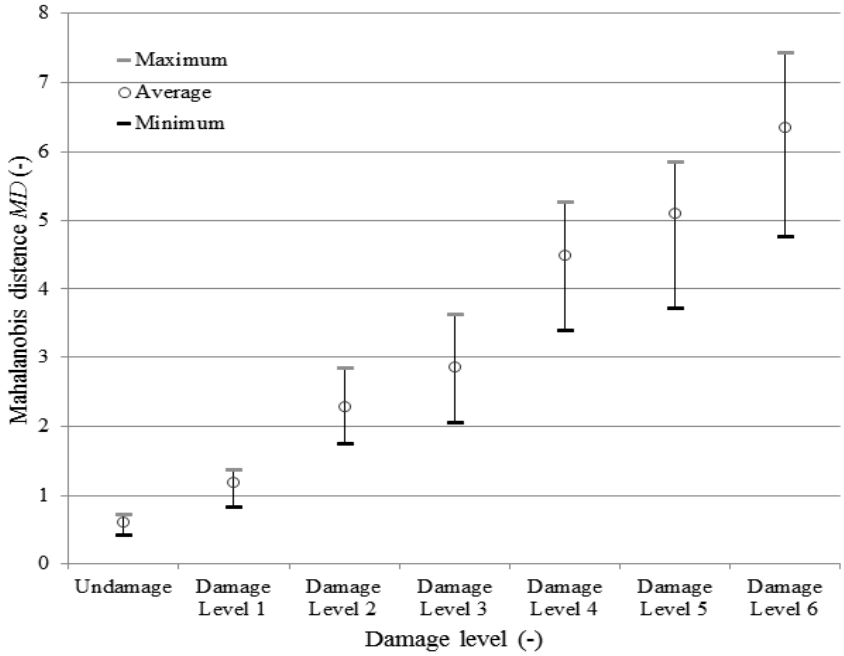

Figure 4.20 Variation diagrams of DSFs in sensor 4

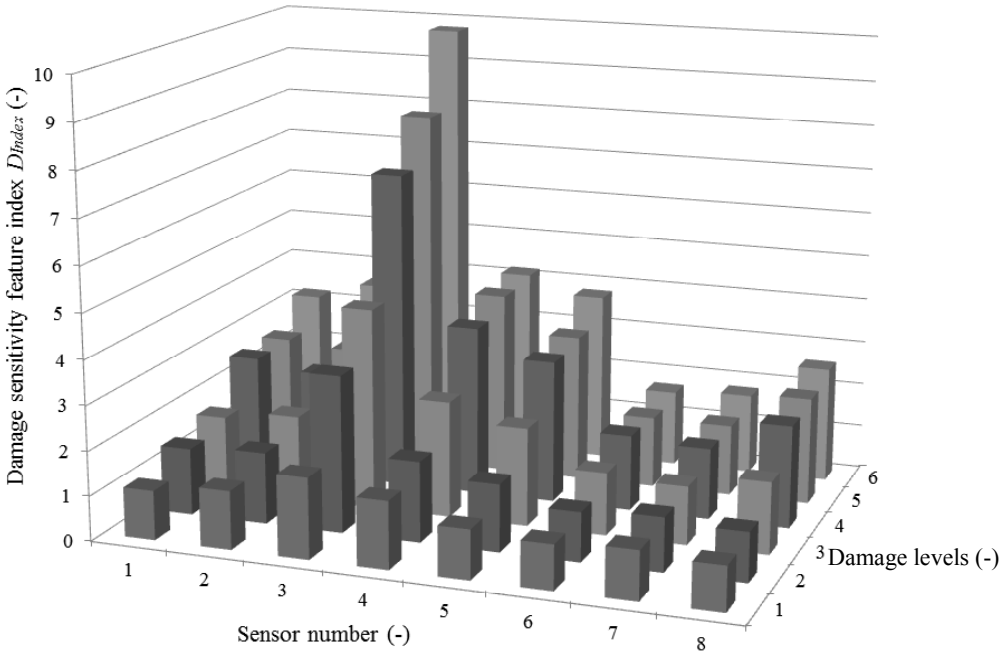

Figure 4.21 D_{SPR} for damage type 1

Damage Type II and III

In type damage II and III, we only to display the results of sensor 3's DSFs for damage II and that of sensor 1, and 2 for damage III, since these sensors are close to the damage II or damage III. Figure 4.22 shows the DSFs of sensor 3 in damage II. Figure 4.23, and Figure 4.24 give the DSFs of sensor 1, and 2 in damage III. From the three figures, we can get the DSFs of these sensors in six levels damage increase with the damage level increasing, and the DSF growth is very big. Especially in sensor 1 and 2 for damage III and sensor 3 for damage II, the DSFs of six levels damage

conditions shows far bigger than that of undamaged condition. These results also inosculate with the design of experiment.

The Figure 4.25 and Figure 4.26 show the damage severity feature index D_{index} in the undamaged condition and the damaged condition in damage type II and III. In Figure 4.25, the D_{index} of sensor 3 is far larger than others, which indicates that the type II damage is nearest to the location of sensor 3. Figure 4.10 confirms this. Figure 4.26 shows the type III damage is very close to sensors 1 and 2, and near sensor 5. From these figures, it can be observed that the D_{index} is a measure of damage severity. In other words, all the figures show that D_{index} is increasing with severity of damage.

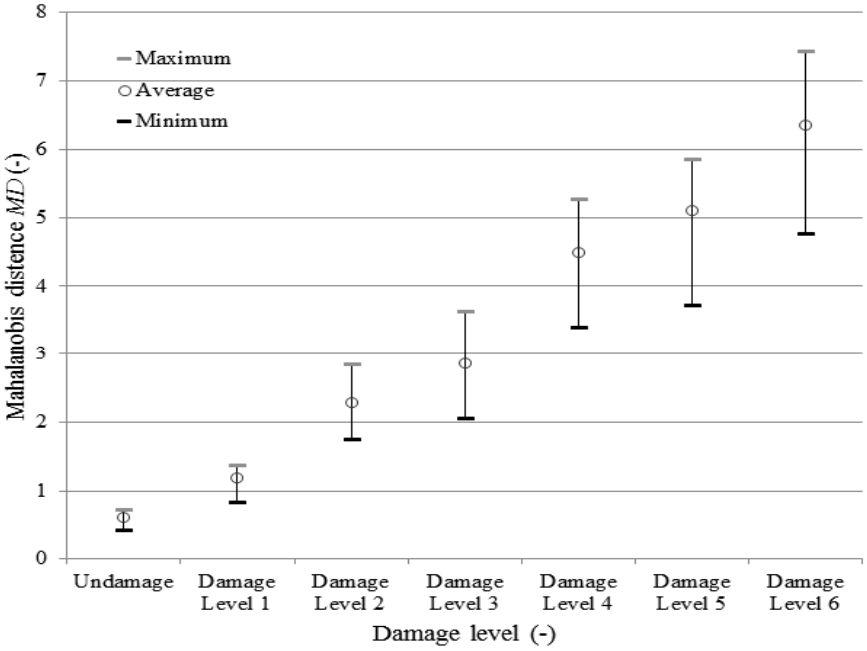

Figure 4.22 Variation diagrams of sensor 3's DSF in damage type II

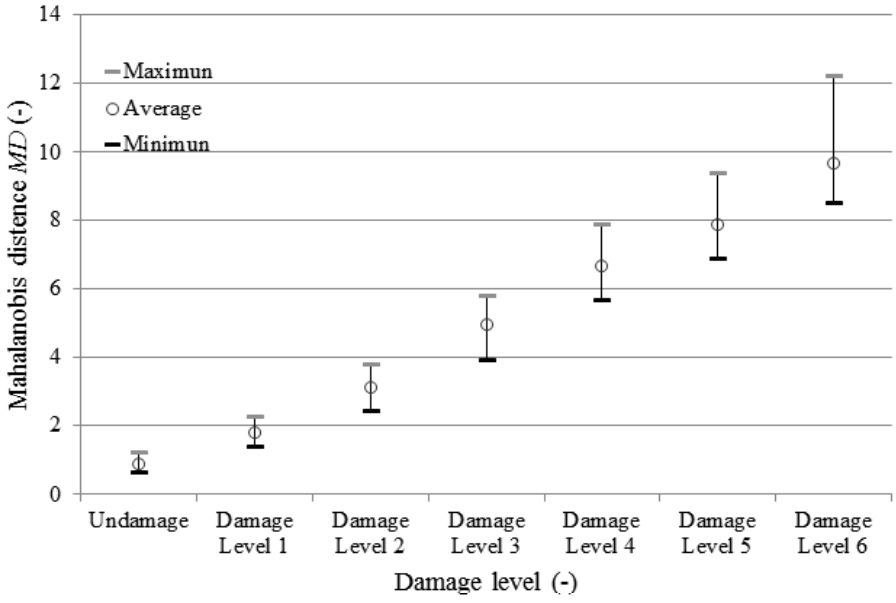

Figure 4.23 Variation diagrams of sensor 1's DSF in damage type III

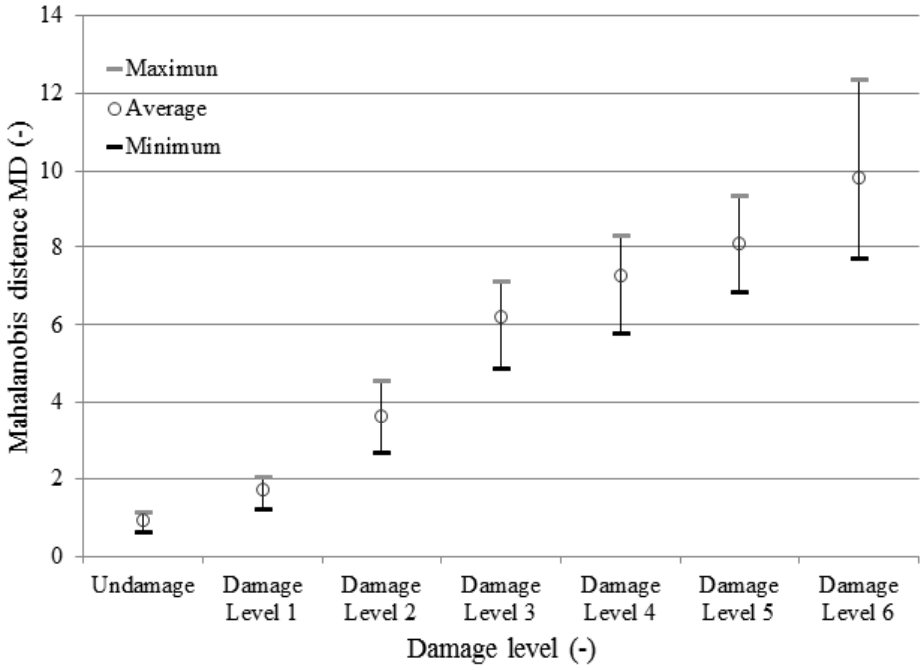

Figure 4.24 Variation diagrams of sensor 2's DSF in damage type III

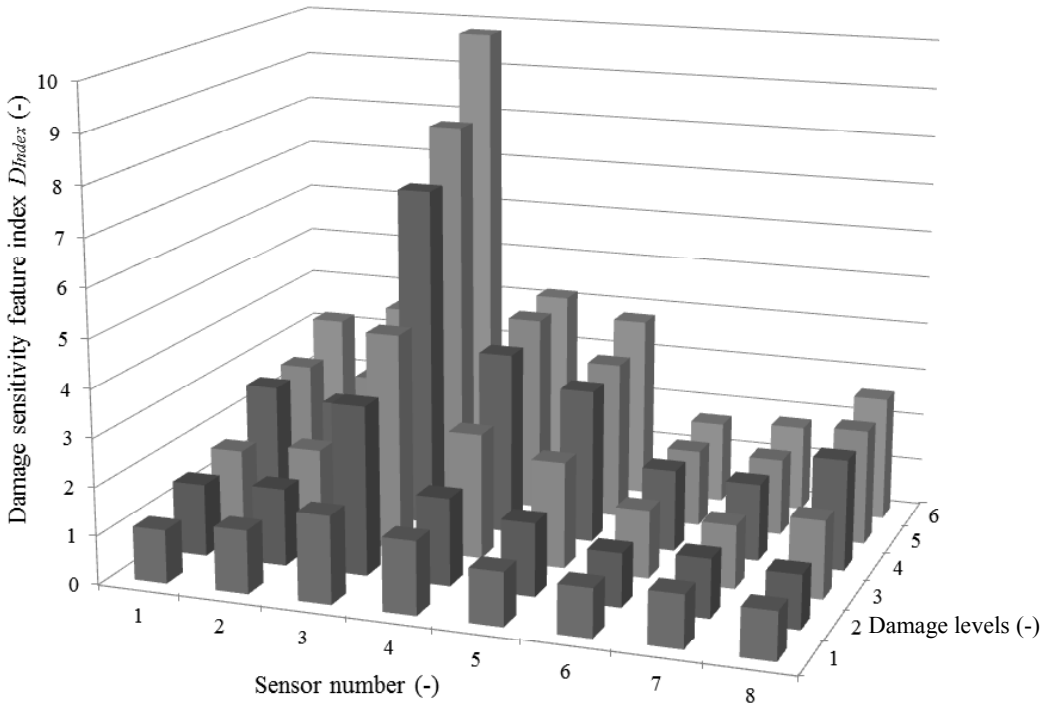

Figure 4.25 D_{index} for damage type II

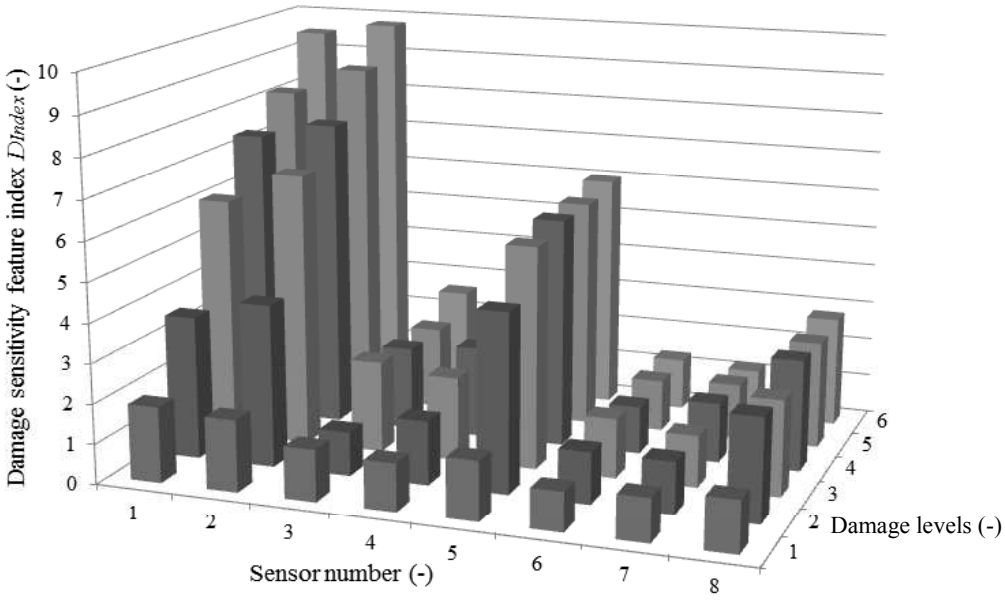

Figure 4.26 D_{index} for damage type III

4.5.3 Performance Comparison

In this experiment, we obtained 57 measurements. Although this paper only shows the results of 18 measurements in detail, all other measurements were analyzed using our proposed algorithm. Here a definition is give as follow:

- **Specificity:** it means the ratio of the number of measurements which classify healthy condition correctly to the total number of measurements in healthy condition, shown as the equation (4.19).

$$R_{specificity} = \frac{N_{cor,health}}{N_{total,health}} \tag{4.19}$$

- **Sensitivity**: it means the ratio of the number of measurements which classify damage condition correctly to the total number of measurement in damage condition, shown as the equation (4.20).

$$R_{sensitivity} = \frac{N_{cor,damage}}{N_{total,damage}} \tag{4.20}$$

The results of the three undamaged time measurements show almost the same patterns. In the results of this experiment, when the vibration is excited by ambient excitation and the data measured at the level 1 of type II and III damage, the D_{index} values are very close to 1. This means our algorithm failed to detect the damage in these two conditions. Thus, in this experiment, the specificity and sensitivity of our algorithm were 100% and 96.3%, respectively. As noted in section 4.5 we monitored the Seiran Bridge for four months. During this period, the bridge was measured by WSN three times per week. Thus, we measured this bridge 48 times. The analysis of these measurements showed that four of the measurements indicated damage on the bridge. The sensitivity of our algorithm was 91.7% in this experiment. Thus, the

results of experiments verify that our diagnosis algorithm not only can detect the damage severity sensitively but it also can locate the damages.

In order to compare other structure diagnosis algorithms (FFT with ICA , SPR with residual [3] [4], Transfer Function [5]) with my algorithm, we use these algorithms to analyze the data measured in 6 bridges (Seiran Bridge, Kando Bridge, Nakajima Bridge, Nishikawa Bridge, Anagigawa Bridge, and Hibikino Bridge). The specificity and sensitivity of these algorithms are shown in Figure 4.27 and Figure 4.28. We must notice: in ever bridge experiment, we measured the bridge many times. The data of each measurement are analyzed by these algorithms. Since we obtain the data of damage condition in Kando Bridge only, Figure 4.28 shows the sensitivity of these algorithms based on the measurement in Kando Bridge. From Figure 4.27 and Figure 4.28, we can get my algorithm is better than others obviously not only in sensitivity but also in specificity. Comparing with SPR with residual method, TF, and FFT with ICA, my method improved 10.3%, 17.1%, and 13.2% in sensitivity, respectively, and improved 9.6%, 13.4%, and 11.8% in specificity.

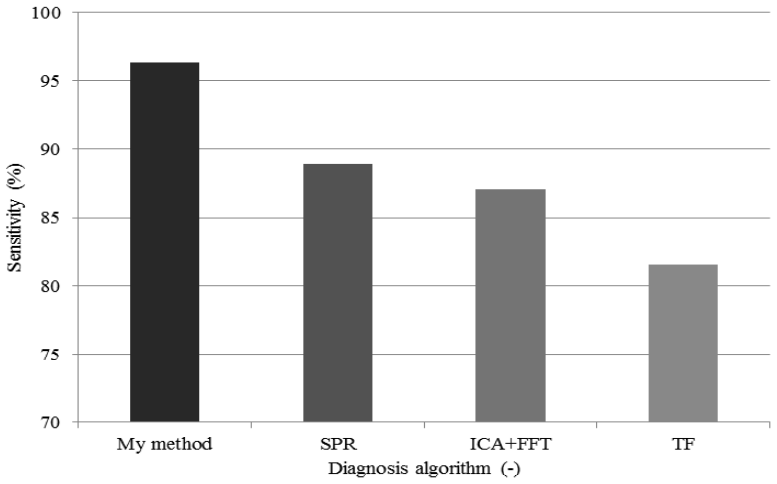

Figure 4.27 Sensitivity of algorithms

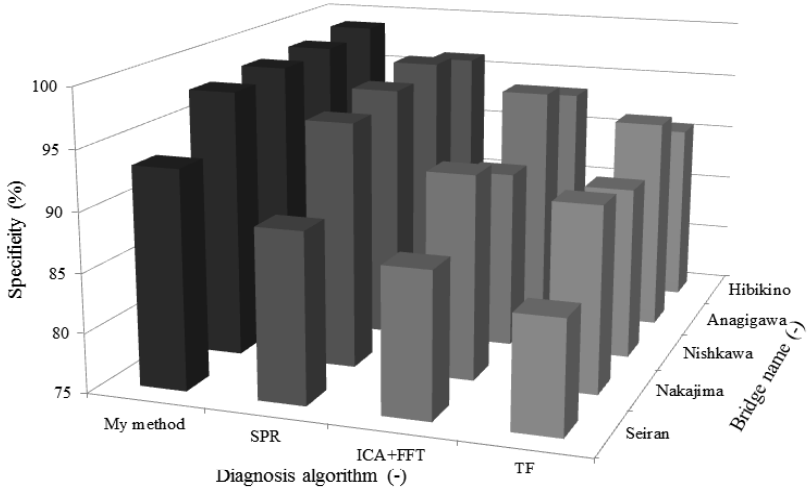

Figure 4.28 Specificity of algorithms

4.6 Summary

In BSHM system, the accuracy and sensitivity of damage diagnosis algorithm directly determines the performance of BSHM system. How to identify damages sensitively and how to accurately detect the damage severity and location become major problems in vibration data based BSHM system. Besides, the effects of noise and varying environment and operation conditions to identification results are also a serious issue. To solve these problems, a two-stage output-only damage diagnosis algorithm is proposed, including a new type of statistical pattern recognition–based structure damage diagnosis algorithm.

In the first stage, after data processing, FFT is used to extract the characteristic frequency of healthy state and unknown state for the structural novelty detection. In the second stage, Based on the first stage a statistical damage identification algorithm, called time-series modeling based Damage Diagnosis Algorithm, is proposed to sensitively detect the severity and location of damage. At first, the normalized data samples are used to establish ARMA model. Based on the model, the pattern vectors perform feature extraction, where PCA is utilized to carry out the effective curtailment of the multi-feature. These features and Mahalanobis distance are used to extract the damage-sensitive-features (DSFs). In DSF extraction, there two cases need to be considered: the First case containing the vibration data in health condition and the second case without that data. In 1^{th} case, the features of the data sample in health condition are chosen as reference to be used for calculating Mahalanobis distance. In 2^{nd} case, the features of any one data sample in unknown condition are chosen as reference. Based on the DSFs, a new sensitive DSF index, D_{index}, is proposed to obtain a diagnosis of structure condition, or identify the severity and location of damages. To summarize, the diagnosis scheme includes global and local structure damage detection.

To verify the performance of this two-stage algorithm, experiments included measurement at the Kando Bridge in Japan. Damage was inflicted at different locations to achieve varying levels of damage severity. The results demonstrate that the severity and position of damage can be detected by utilizing our proposed two-stage diagnosis algorithm. The specificity and sensitivity of this algorithm were 100% and 96.3% respectively in this experiment. Our algorithm is compared with other diagnosis algorithms such as FFT with ICA, SPR with residual, Transfer Function. The results show our algorithm is better than others obviously not only in sensitivity but also in specificity. Comparing with SPR with residual method, TF, and FFT with ICA, my method improved 10.3%, 17.1%, and 13.2% in sensitivity, respectively, and improved 9.6%, 13.4%, and 11.8% in specificity.

Reference

[1] Brockweii P J，Davis R A, “lime series：theory and methods(second edition),” Springer-Verlag (1991)

[2] Gentile A, Messina A, “On the continuous wave let transforms applied to discrete vibrational data for detecting open cracks in damaged beams,” International Journal of Solid and Structures, Vol.40, No.2, PP.295- 315 (2003)

[3] Farrar, C.R., Duffey, T.A., Doebling, S.W., Nix, “A statistical pattern recognition paradigm for vibration-based structural health monitoring”, 2nd International Work shop on Structural Health Monitoring, Stanford, CA, 1999.

[4] K. Roy, H. Ogai, and B.Bhattacharya, “Damage Detection of Bridge using Wireless Sensors”, IFAC workshop on Automation in the Mineral and Metal Industries, pp.107-111, Gifu, Japan, Sep. 10-12, 2012.

[5] C. Shao, H. Ogai, and J. Huang "Verification of Damage Identification Technique Based on Transfer Function and Using on a Real Bridge", SICE Annual Conf. 2010, pp.2146-2150. (2010)

[6] Haitao Xiao, Sheng Luo, Harutoshi Ogai, “A Novel Bridge Structure Damage Diagnosis algorithm based on Post-nonlinear ICA and Statistical Pattern Recognition”, IEEJ Transactions on Electronics and Electronic Engineering, Vol.10, No.3, May, 2015.

Chapter 5

Standing-Wave based Non-destructive Testing System

5.1 Introduction

In chapter 4, a novel damage detection algorithm is designed for the BSHM system, and it can successfully detect the severity and approximate location of various damages on bridges. However, this system records the damages near the sensors only; therefore, the specific location and size of the damage cannot be determined, especially damages inside the concrete block of bridge. Thus, when the vibration based BSHM system, global health diagnosis method, detects serious damages, nondestructive testing (NDT) [1] based local health diagnosis method is needed to pinpoint the exact location and size of the damage for bridge maintenance. Although many complicated and expensive equipment-based nondestructive testing systems can obtain the specific information of damages, the heavy economic and time burden is a serious problem these systems. Therefore, the issue about economically and efficiently detecting the specific information of damages also needs to be solved urgently. Based on the backgrounds, a new standing-wave based structure nondestructive testing system and algorithm is proposed in this chapter. The system sends high-frequency modulated sweeping waves (3.8–5.8 GHz) to an object by the antenna, and the input and reflected waves form a standing wave, which will be recorded by the antenna. Subsequently, the health of the structure is evaluated by checking the amplitude–frequency response $A(f, x)$ of the standing wave.

5.2 Overview of the Standing-wave based Structure NDT System

The basic standing-wave method is used to measure the range and distance from the radar to the object [2] [3]. In order to detect the structure, the basic standing-wave method is improved, and then the standing-wave based structure NDT system is proposed and shown in Figure 5.1. The processes of this system show as follow:

1) The signal source generates a high-frequency sweeping wave (Figure 5.2) and sends the wave to the object to be tested through the waveguide and antenna.

2) The wave is reflected on the front surface of the object (air–object interface). The reflected and incident waves form a standing wave (Figure 5.3), also the reflected waves from the front and back surface of the void (inside in the object) with incident wave form other two standing waves. These are received by the antenna.

3) The amplitude of the standing wave is transformed to volts by the amplitude detector in the radar and then recorded as data in computer.

4) According to the amplitude–frequency response $A(f, x)$, if the distance between two peaks in the $A(f, x)$ curve is known, the distance to the object can be calculated. Since the signal received by the antenna is mixed by the three standing waves, before distance calculation an modified empirical mode decomposition (EMD) is proposed for the data to denoising. And then ICA is used to extract three amplitude–frequency responses to obtain the distances to the object and void.

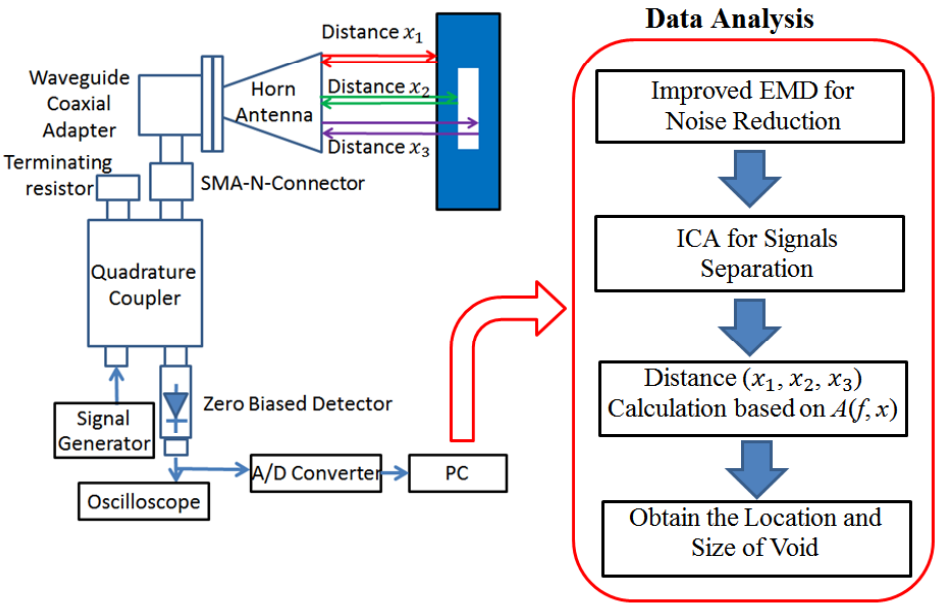

Fiure 5.1 Standing-wave based structure NDT system

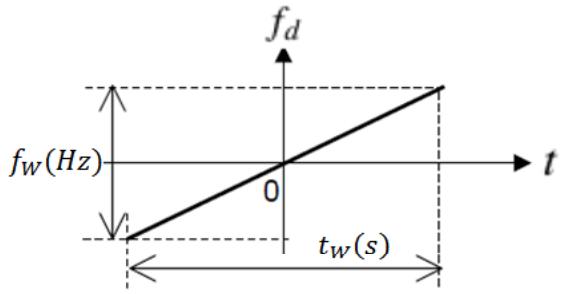

Figure 5.2 Sweeping wave

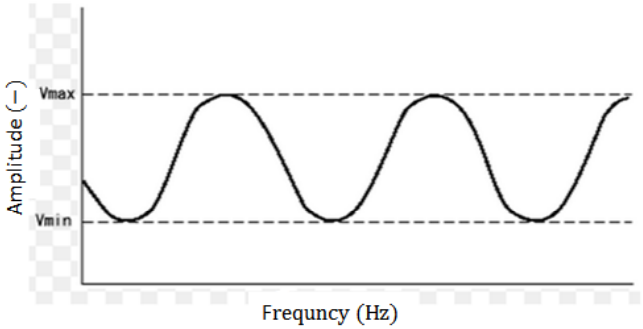

Figure 5.3 Standing wave

5.3 Standing-wave based Structure NDT System

Since the standing-wave based structure NDT system is improved from the basic standing-wave method which was used to measure the range and distance from the radar to the object, in this chapter we recommend the fundamental idea of the basic standing-wave method at first.

5.3.1 Basic Standing-wave Testing System for Distance Detection

5.3.1.1 Basics Algorithm and System

The components of the basic standing-wave testing system are shown in Figure 5.4. The signal source generates a high-frequency sweeping wave and sends the wave to the object to be tested through the waveguide and antenna. The wave is reflected on the surface of the object (air–object interface). The reflected and incident waves form a standing-wave that is received by antenna. The amplitudes of the standing-wave are then transformed to volts by the amplitude detector in the radar. According to the amplitude–frequency response $A(f, x)$, if the distance between two peaks in the $A(f, x)$ curve is known, the distance to the object can be calculated.

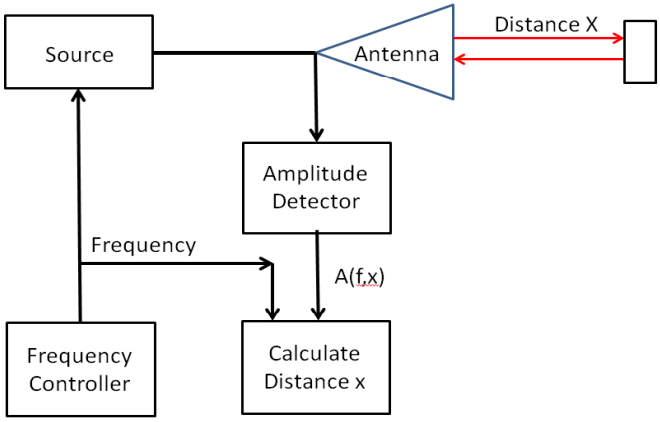

Figure 5.4 Basic components of the standing-wave radar

5.3.1.2 Derivation of Amplitude–frequency Response

If the reflection coefficient on the object surface is Γ, the transmission speed of the electromagnetic wave is c, the amplitude of the incident signal is 1, and the phase of the incident signal is 0, and considering the reflection and time delay Δt, then the received signal $V(f, x)$ on the antenna is

$$\boldsymbol{V(f,x) = 1 + \Gamma e^{-j*w*\Delta t} = 1 + \Gamma e^{-j*w\frac{2x}{c}}} \tag{5.1}$$

The amplitude $A(f, x)$ of the received signal is

$$\boldsymbol{A(f,x) = |V(f,x)| = \left|1 + \Gamma \cos\left(-w\frac{2x}{c}\right) + j * \Gamma \sin\left(-w\frac{2x}{c}\right)\right|} \tag{5.2}$$

$$\boldsymbol{A(f,x) = \sqrt{\left[1 + \Gamma \cos(-w\frac{2x}{c})\right]^2 + \left[\Gamma \sin(-w\frac{2x}{c})\right]^2}} \tag{5.3}$$

Finally, the amplitude $A(f, x)$ is given by

$$\boldsymbol{A(f,x) = \sqrt{1 + |\Gamma|^2 + 2|\Gamma| \cos(\frac{4\pi x f}{c} - \theta)}} \tag{5.4}$$

Where $|\Gamma|$ is the amplitude of the reflection coefficient, and θ is its phase. From equation (5.4), because $|\Gamma|$, θ, and c are constants, the amplitude is only related to distance x and frequency f.

1) If the frequency is fixed, because the amplitude of the wave is only related to position x, the synthesis wave is a standing wave.

2) If the distance x is fixed, the amplitude $A(f, x)$ is maximum when

$$\boldsymbol{\cos\left(\frac{4\pi x f}{c} - \theta\right) = 1} \tag{5.5}$$

From equation (5.5), we obtain

$$\boldsymbol{\frac{4\pi x f}{c} - \theta = 2N\pi} \tag{5.6}$$

If the peak frequency f_N is the frequency at the maximum amplitude point in the $A(f, x)$ curve, then f_N is

$$f_N = (N + \frac{\theta}{2\pi})\frac{c}{2x} \tag{5.7}$$

If the frequency difference between the N^{th} and $(N + 1)^{th}$ peaks is Δf, as shown in Figure 5.5,

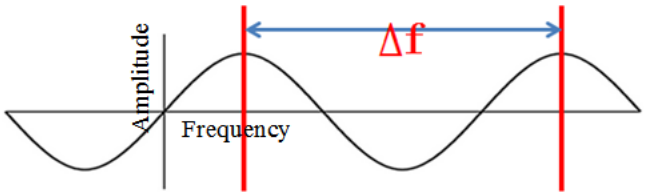

Figure 5.5 Frequency difference Δf between the N^{th} and $(N + 1)^{th}$ peaks

then Δf is

$$\Delta f = f_{N+1} - f_N = \frac{c}{2x} \tag{5.8}$$

Subsequently, the distance x is calculated as

$$x = \frac{c}{2\Delta f} \tag{5.9}$$

Thus, if the steps introduced in section 5.4.1.1 are followed and the frequency difference Δf between two peaks in the amplitude–frequency response $A(f, x)$ curve is obtained, the object distance x can be calculated using equation (5.9).

Many conventional algorithms of pulse waves are used to test objects such as in [4]. However, in the basic algorithm from equations (5.1) (5.2) (5.3), and (5.4), in order to obtain several peaks in the amplitude–frequency response, a specific bandwidth sweeping wave is used for testing, because pulse waves cannot follow the change in the amplitude–frequency response. Thus, the distance x cannot be calculated.

5.3.2 Improvement of Basic Standing-wave Algorithm for Void Testing

The algorithm introduced in section 5.4.1 is used to calculate the distance from the radar to the object surface. For concrete blocks, the object surface is the surface of the concrete block (air–concrete interface) as shown below.

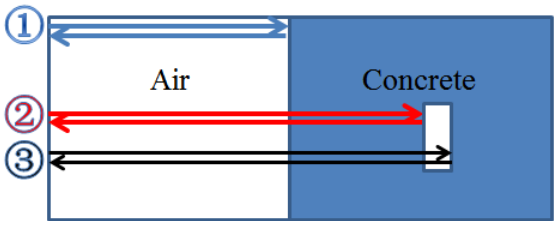

Figure 5.6 Three-interface case

Figure 5.6 shows the case for a subsurface void inside concrete using the basic standing-wave testing system. In this case, only distance *1* (first interface) can be calculated. No additional information regarding voids inside the block can be inferred

(distance *2*–distance *1* and distance 3—distance 2).

To detect voids and their location and size in the object's interior, the algorithm for the basic standing-wave testing system is expanded, as shown in Figure 4.7.

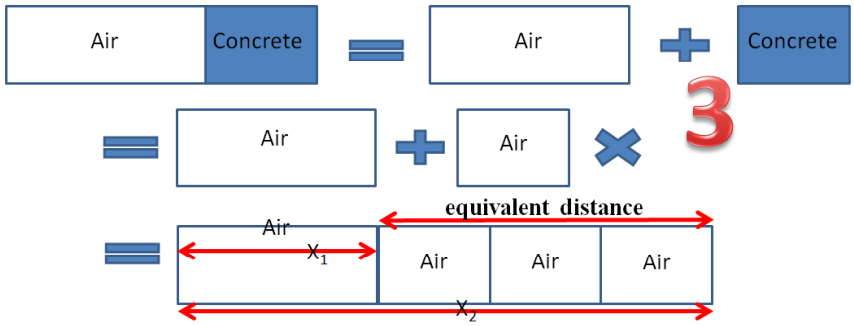

Figure 5.7 Expansion of the basic standing-wave testing system

Figure 5.7 shows how to calculate the distance in the subsurface void case. The white block denotes route 1 in Figure 5.6, where the electromagnetic wave passes through air, and the blue block denotes route 2 in Figure 5.6, where the electromagnetic wave passes through concrete before reaching the air in the concrete–air interface. The wave speed in air is *c* and in concrete is *c/3*; therefore, for the same period, the distance covered by the electromagnetic wave in air is three time that in concrete, shown as the equivalent distance in Figure 5.7.

Considering equation (5.1), because the calculation in the basic standing-wave testing system is based on the time delay of the wave transmission in the medium, the same algorithm is used to calculate the distance of the concrete–air interface. Nonetheless, because the distance of the second interface x_2 contains the equivalent distance, for calculating the location of the air void, the distance in air to that in concrete is converted as follows:

$$L_1 = equivalent\ distance/3 = (x_2 - x_1)/3 \tag{5.10}$$

$$L_2 = x_3 - x_2 \tag{5.11}$$

In equation (5.10) and equation (5.11), L_1 is the location of the subsurface air void (distance from the block surface to the top surface of void) and L_2 is the height of the subsurface air void, x_1 is the distance from the radar to the concrete block surface, and x_2 is the calculated distance from the radar to the top of the air void top, including x_1 and the equivalent distance. x_3 is the calculated distance from the radar to the undersurface of the air void top, including x_2 and the distance between up surface and undersurface. Because the amplitude–frequency response $A(f, x_1)$ is a standing wave, the amplitude–frequency response $A(f, x_2)$ and $A(f, x_3)$ are also standing wave. Because of $x_1 < x_2 < x_3$ and by equation (4.8), the frequency difference between two peaks is $\Delta f_1 > \Delta f_2 > \Delta f_3$.

5.3.3 Modified EMD and ICA based Data Analysis Method

5.3.3.1 Problem of only using ICA to Separate Responses $A(f, x1)$, $A(f, x2)$, and $A(f, x3)$

When we use the standing wave testing system to detect the subsurface air voids in the concrete, as shown in Figure 5.6, the received amplitude–frequency response $A(f, x)$ will be a mixed signal consisting of $A(f, x_1)$, $A(f, x_2)$, $A(f, x_3)$, and noise. As a result, in order to use equation (5.9), (5.10) and (5.11) to calculate the location and size of void, we need to separate the amplitude–frequency responses $A(f, x_1)$, $A(f, x_2)$, and $A(f, x_3)$ in Figure 5.8 from the received response signal and extract the frequency difference between the two peaks Δf_1, Δf_2, and Δf_3. ICA is a famous and common blind source separation technique. In order to obtain good separation results, the total number of observer samples (input of ICA) needs more than or equal to the number of separated signals (output of ICA). However, since the mixed standing-wave response $A(f, x)$ is corresponding to the distance between the sampling antenna and reflecting surface, if we move the sampling antenna to obtain multiple observer samples (mixed standing wave responses) each observer sample's compositions (standing wave response $A(f, x_1)$, $A(f, x_2)$, and $A(f, x_3)$) are different. Therefore, the problem of directly using ICA to separate mixed response signal is there are not enough observer samples as the input of ICA. To solve this problem, an improved empirical mode decomposition (EMD) is proposed to give multiple inputs for ICA and denoising in the standing wave testing system. Then FastICA[17] [3] is applied to obtain the amplitude–frequency response $A(f, x_1)$, $A(f, x_2)$, and $A(f, x_3)$. Based on these three separated responses, equation (5.9), (5.10), (5.11) are used to calculate the location and height of void. Also we move the antenna in parallel to detect the width and length of void, which will be described in section 4.6.

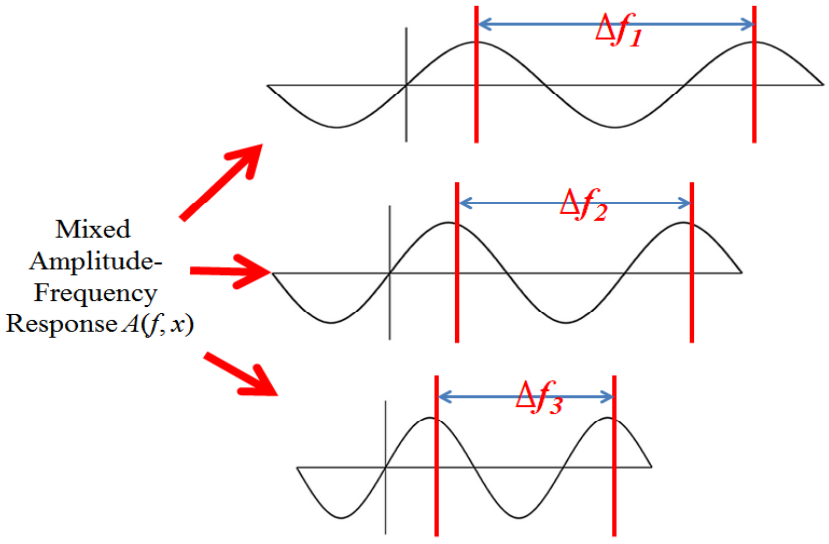

Figure 5.8 Separation of the three amplitude–frequency responses

5.3.3.2 Empirical Mode Decomposition

With the basis which is derived from the data, a signal can be decomposed adaptively into Intrinsic Mode Functions (IMFs) by using the EMD (empirical mode decomposition) [5].

Definition5.1: an IMF must satisfy the two conditions shown as follow.

- The quantity of zero-crossings has to equal or differ to the amount of extrema by at most one in the whole set of numbers.
- At any data point, the average value of the envelope which is defined by using the local-maxima and the envelope which is defined by using the local-minima are equal to zero.

With the above definition of an IMF, Figure 5.9 shows the flow chart of EMD and a signal $x(t)$ can be decomposed using the following EMD algorithm:

(6). Initialize $r_0 = x(t)$, $i = 1$, $h_{i,(k-1)} = r_{i-1}$, $k = 1$.

(7). Confirm all the local maximum and minimum of the signal $h_{i,(k-1)}$, which is $x(t)$ when $i = 1$ and $k = 1$, and then insert between each set of the extrema using cubic curves to develop an upper envelope $e_{max}(t)$ and a lower envelope $e_{min}(t)$.

(8). Give the two envelopes' mean $m_{i,(k-1)}(t) = (e_{max}(t) + e_{min}(t))/2$.

(9). The signal $x(t)$ and $m_1(t)$ should be defined the difference to be the first component, that is, $h_{i,k}(t) = h_{i,(k-1)}(t) - m_{i,(k-1)}(t)$.

(10). If $h_{i,k}(t)$ satisfies definition 5.1, let $c_i(t) = h_{i,k}(t)$ to be the first IMF; rest let $k = k + 1$ and return to step (2).

(6) Compute the residue $r_i(t) = r_{i-1}(t) - c_i(t)$.

(7) if $r_i(t)$ still is not monotonic or has least 2 extema, let $i = i + 1$ and return to steps (1); else $r_i(t)$ is monotonic or has a sole extremum from which none IMF can be extracted, the decomposition process is finished.

If the decomposition process of EMD ends up at $i = n$, we can get n IMFs, c_n(i = 1, 2, …, n), and a surplus r_n, which shown as equation (5.12). Therefore, the signal $x(t)$ can be shown as equation (5.13), where $r_n(t)$ represents the potential trend and the modes c_n(i = 1, 2, …, n) are zero-mean waveforms of frequency modulation and amplitude modulation.

$$\begin{aligned} r_2(t) &= r_1(t) - c_2(t) \\ &\vdots \\ r_n(t) &= r_{n-1}(t) - c_n(t) \end{aligned} \tag{5.12}$$

$$x(t) = \sum_{i=1}^{n} c_i(t) + r_n(t) \tag{5.13}$$

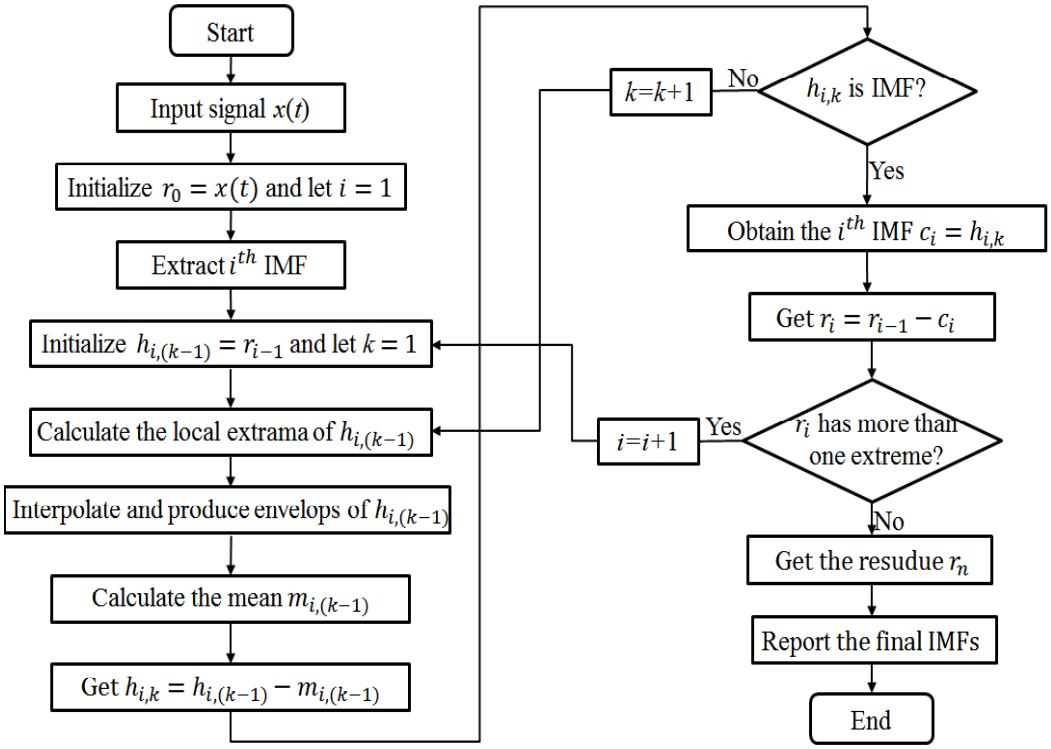

Figure 5.9 Flow chart of EMD

5.3.3.3 Untrue IMF Components Problem of EMD

EMD has been proven that it can be used in widely applications because it can extract signals from the data produced in non-stationary processes and noisy nonlinear. Although EMD is very useful, there are still difficulties need to be solved.

When do EMD to signal, in some cases, there are some IMFs, which are not the components of original signal and called as untrue IMF components. This caused by insufficient sampling rate and spline interpolation. In order to describe the untrue IMF components problem, an example using EMD to decompose the signal, including two sine signals and shown as equation (5.14), is presented. Figure 5.10 shows the results of EMD. Obviously, the IFM 3 and IFM 4 are new set of IMFs, which may contain parts of original signal or maybe untrue IMF components. Generally, in order to reduce the untrue IMF components, the signal needs to take oversampling. In ideal station, the sampling rate needs to big than four times Nyqvist frequency. However, when the frequency of signal is very high, oversampling is bound to cause a great amount of calculation.

To solve this problem, a modified EMD, called MEMD, is proposed and described in the next sub section.

$$s(t) = 2\sin(2\pi 10t) + 5\sin(2\pi 100t) \tag{5.14}$$

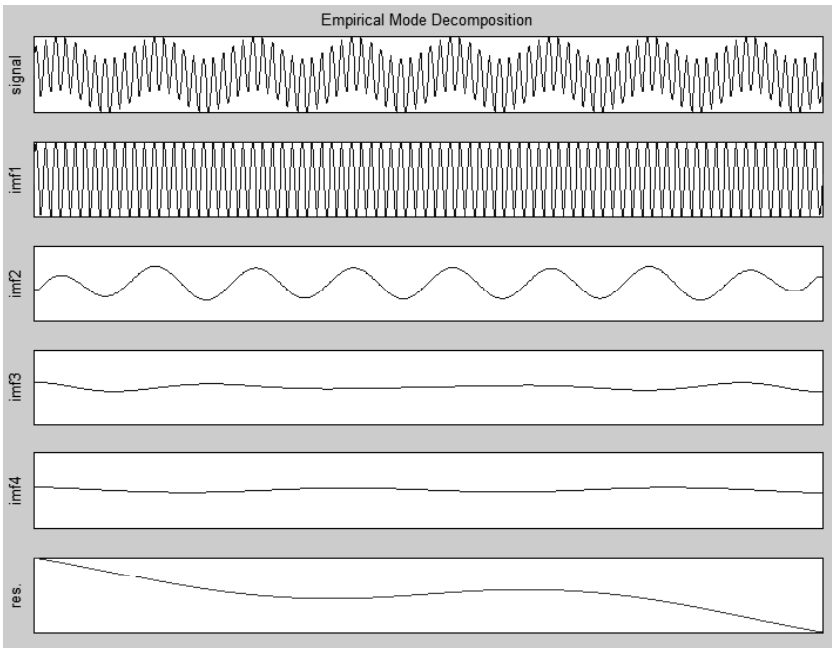

Figure 5.10 IMFs of EMD

5.3.3.4 Modified Empirical Mode Decomposition

In order to solve the untrue IMF components problem, a modified MED is proposed. In this scheme, the correlation between IMFs and the original signal is used as the standard to judge which IMFs belong to the signals' real components, and which are untrue IMFs. The untrue IMFs will be combined to residual. The Modified EMD is as follows:

(1) Do EMD for the signal $x(k)$ to get the IMF components $\{c_i(t), i = 1,..., n\}$.

(2) Calculate the correlation coefficient $\{cor_i, i = 1,..., n\}$ between the IMF components $\{c_i(t), i = 1,..., n\}$and the original signal by using equation 5.15, where $x(k)$ is the original signal.

$$cor_i = \frac{\sum_{k=0}^{\infty} c_i(k)x(k)}{\sqrt{\sum_{k=0}^{\infty} {c_i}^2(k) \sum_{k=0}^{\infty} x(k)}} \tag{5.15}$$

(3) If $cor_i \geq \mu$, keep the IMF component $c_i(t)$, otherwise combine this IMF component into the residual. Usually, the threshold μ is set as one tenth of the maximum value of correlation coefficients.

The result of using modified EMD to decompose the signal of equation (5.14) is shown in Figure 5.11. From this result, the untrue IMF components problem is solved.

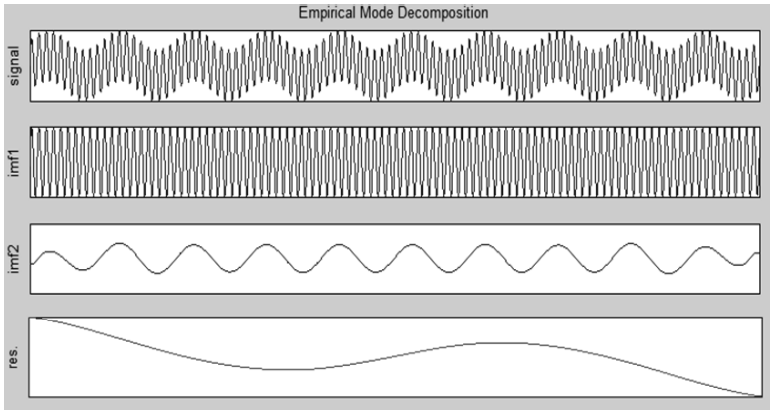

Figure 5.11 IMFs of Modified EMD

5.3.3.5 New Data analysis method based on Modified EMD and ICA

To solve the problem of no enough observer samples as the input of ICA to separate mixed response signal, the modified empirical mode decomposition (EMD) is proposed to denoise and give multiple inputs for ICA. Thus, a new data analysis method based on Modified EMD and ICA is designed to extract the amplitude–frequency response $A(f, x1)$, $A(f, x2)$, and $A(f, x3)$. The new method is shown as Figure 5.12.

(1) Do modified EMD for the mixed amplitude–frequency response $A(f, x)$, and obtain IMFs. Since the first IMF is the component of noise in usual, the IMFs are used as the input of ICA except the first IMF and residue.

(2) Fast-ICA [17] is applied to obtain the amplitude–frequency response $A(f, x_1)$, $A(f, x_2)$, and $A(f, x_3)$ by using these IMFs.

(3) After extracting these there standing-waves, all the peak points of these standing-waves are found out by using $data[i-1] < data[i] > data[i+1]$, and all the zero points are found out. Between two zero points, the maximum peak point is selected as the final peak point. In this way all the final peak points of standing waves are obtained automatically.

(4) Based on the final peak points, the frequency differences Δf between two peaks are calculated. Then this new method calculate the error between these frequency differences Δf. If the error is greater than threshold, the Δf will be give up. Others will be used to calculate the mean value. And then, this mean value is used to calculate distance by equation (5.9).

(5) Based on these three separated responses, equation (5.9), (5.10), (5.11) are used to calculate the location and height of void. Also we move the antenna in parallel to detect the width and length of void, which will be described in section 5.6.

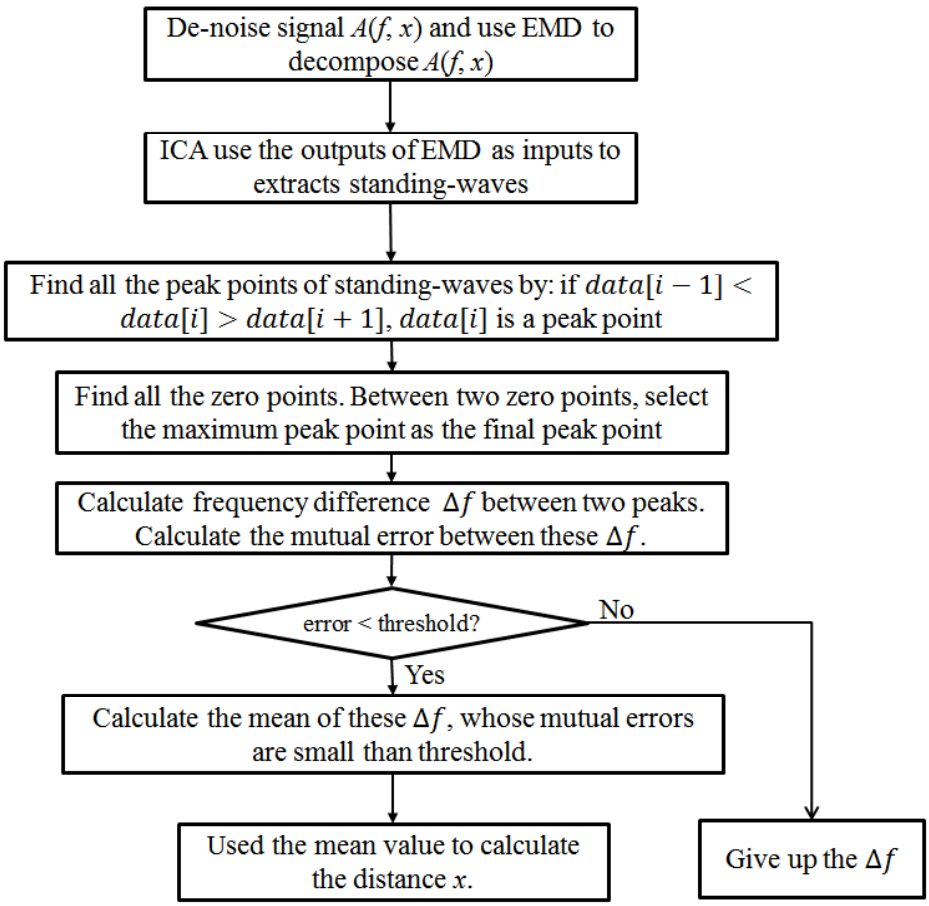

Figure 5.12 Processes of new data analysis method

5.4 Simulation by Numerical Analysis

Simple numerical analysis was performed to verify the proposed system. The reflection and refraction rate, and the attenuation constant and phase factor were used to calculate each reflection, refraction, and attenuation. The following coefficients are necessary.

1) Reflection rate

$$\boldsymbol{\Gamma} = \frac{\sqrt{\varepsilon_1}-\sqrt{\ }}{\sqrt{\ }+\sqrt{\varepsilon_2}} \tag{5.16}$$

2) Refractive rate

$$\mathbf{T} = \mathbf{1} + \boldsymbol{\Gamma} \tag{5.17}$$

3) Attenuation constant

$$\alpha \approx \frac{\sigma}{2}\sqrt{\frac{\mu}{\varepsilon}} \tag{5.18}$$

4) Phase factor

$$\beta \approx \omega\sqrt{\mu\varepsilon} \tag{5.19}$$

ε_1 and ε_2 are the dielectric constants of air and concrete, respectively, σ is the electric conductivity of concrete, and μ is the permeability.

The framework of the calculations is shown in Figure 5.13. The probe is placed on the surface of the concrete block. The thickness of the concrete block is 6.6 cm, and the air void is located 2.2 cm inside the concrete. The size of the air void is 2.2 cm.

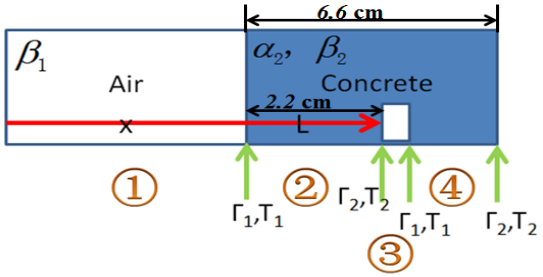

Figure 5.13 Numerical calculation

For the wave propagation calculation, the route shown with the red arrow in Figure 5.12 is chosen. If the incident signal is E_0, then the wave signal for this route is

$$\boldsymbol{E_0 * e^{-j\beta_1 x} * T_1 e^{-j(\beta_2 - j\alpha_2)L}} \tag{5.20}$$

where $e^{-j\beta 1x}$ denotes the phase lag, which is related to time delay of the wave propagation in air; T_1 denotes the air–concrete interface where refraction takes place, and the amplitude is reduced to T_1 if the incident amplitude is 1; $e^{-j(\beta - \ )L}$ denotes the phase lag and the attenuation in concrete and depends on the distance L of the wave propagation in concrete. In concrete, the attenuation constant is not zero because the electric conductivity σ of the concrete is not zero.

Although the number of repeated reflections inside the concrete is infinite, only the

first three reflections between any of the four interfaces are considered since the higher order reflections are weak (< 0.4%). The repeated reflections between the second and third interface are shown in Figure 5.13.

In the calculations, the total area is divided into four parts (shown as ①②③④ in Figure 5.13), and then the interior repeat reflection routes are divided into two classes.

1) The first class comprises the repeat reflection routes in areas ②, ③, and ④. The repeat reflection route in area ② contains four signals, which contribute to the total reflection. The signals are shown as blue arrows in Figure 512, where the first time is the reflection and the next is the refraction.

2) The second class comprises the repeat reflection routes in areas ②③, ②③④, and ③④. The repeat reflection route in area ②③ is shown in Figure 5.13.

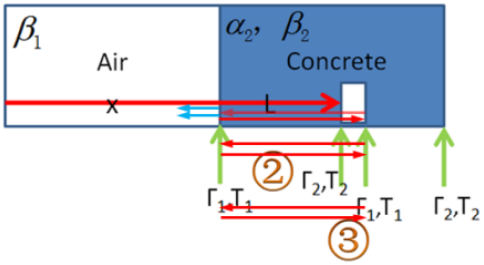

Figure 5.14 Repeat reflections in area ②③

For sweeping frequencies between 3.8 GHz and 5.8 GHz, the computations are shown in Figure 5.15.

From Figure 5.15, the following are inferred:

1) The amplitude–frequency response $A(f, x)$ shows periodicity that satisfies equation (5.4) and resembles Figure 5.3.

2) In the case of no void, the peaks correspond to the frequency difference Δf between two peaks and the distance of the concrete surface x satisfies equation (5.12).

3) If a void exists, the amplitude–frequency response $A(f, x)$ curve changes. Several signals with different periodicities are included in the new amplitude–frequency response $A(f, x)$ curve.

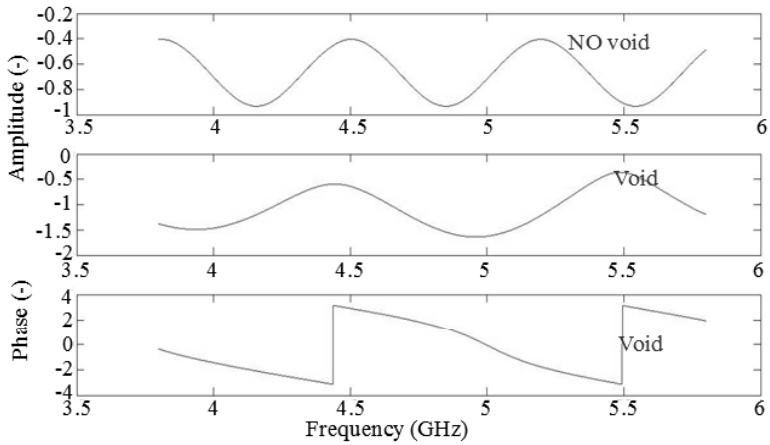

Figure 5.15 Computations for 3.8 GHz – 5.8 GHz

5.5 Experiment and Analysis

5.5.1 Implementation of the Standing-wave based Structure NDT System

In this section, the prototype system according to the improved standing-wave testing algorithm is described. The system consists of the four parts shown in Figure 5.16. The standing-wave radar prototype system is shown in Figure 5.16. The system consists of the signal generator, the standing-wave radar, the A/D converter, and a signal processor.

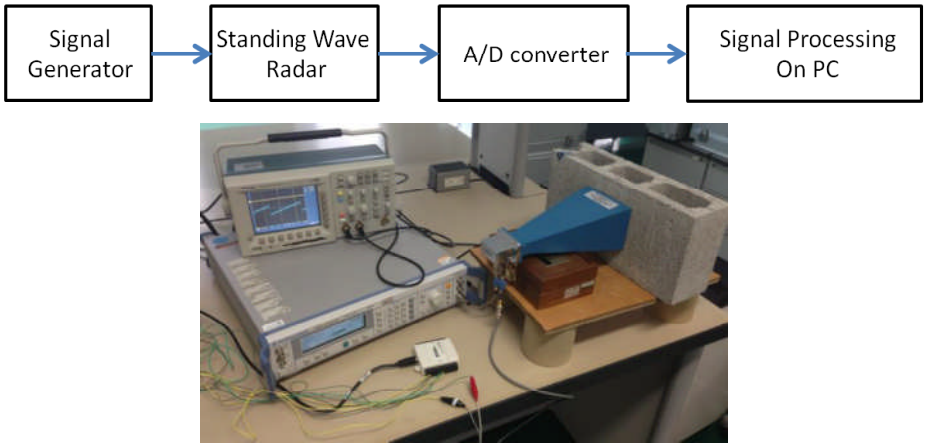

Figure 5.16 Standing-wave testing prototype system

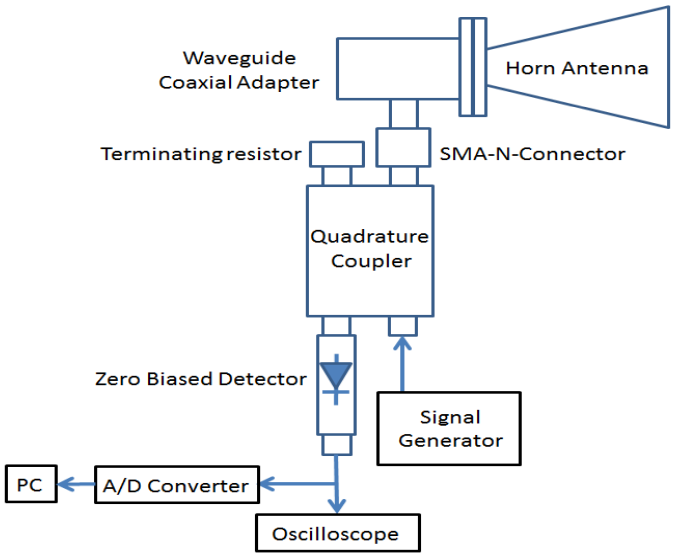

Figure 5.17 Schematic of the standing-wave radar

The signal generator generates sweeping waves (sweep mode), and it has a start frequency of 3.8 GHz, a stop frequency of 5.8 GHz, a center frequency of 4.8 GHz, and a frequency span of 2 GHz. The linear sweep mode is used in the spacing setup.

The step size is 1 MHz (step line = 1 MHz), and the dwell time is 10 ms. The total sweeping time from 3.8 GHz to 5.8 GHz is 23.6 s.

The standing-wave radar sends the sweeping waves to the object, combines the incident and reflected waves, and then transforms the wave amplitude to voltage. The standing-wave radar is the core of the prototype system shown in Figure 5. 17. The analog voltage signal is transformed to digital signal by A/D converter. Then the digital signal is sent to the PC. The signal processor on the PC analyzes the received amplitude–frequency response *A(f, x)* and is used to detect whether there are voids inside the object.

5.5.2 Experiments and Data Analysis

Concrete, and clay and marble blocks were used to test the prototype system. As described in section 5.4, the algorithm obtains the location of voids by using the frequency difference Δf and the speed of the electromagnetic wave in the materials. There are two methods to obtain the wave speed in different materials. The first calculates the approximate speed using Equation (5.21), where c is the speed of the electromagnetic wave in air, and ε_v is the dielectric constant of the material.

$$v = c/\sqrt{\varepsilon_v} \tag{5.21}$$

The second method measures the speed in the material. In this case, an algorithm similar to that in [4] is used to measure the speed in concrete without voids, and clay and marble blocks. In [4], the time delay between the first and the second-surface reflected wave is used to calculate the distance using Equation (5.22),

$$H = c \cdot \Delta t_1/\sqrt{\varepsilon_v} \tag{5.22}$$

where H is the thickness of the block, c is the speed of the radar wave in air and is constant, and Δt_1 is the time delay between the first and the second-surface reflected wave. In the experiments, the thickness of the block is known. The data in Table 5.1 show individual measurements and averages. Because the bridge diagnosis system in chapter 3 and 4 can distinguish the approximate area of damage, a nondamaged area is selected to measure the wave speed in the field.

Table 5.1 Wave speed in the tested materials

Times / Speed (*mm/ns*) / Material	1th	2th	3th	4th	5th	average
Concrete	100.25	101.38	100.04	99.69	100.51	100.374
Clay	118.44	121.17	119.08	119.26	120.31	119.652
Marble	199.76	198.39	201.87	200.15	199.07	199.848

5.5.2.1 Case 1

Three types of concrete blocks (wave speed = c/3) were used (Figure 5.18):

1) A 5-cm-thick concrete block with no air voids.

2) A 2.2-cm-thick concrete block with 2.2-cm-thick voids.

3) A 2.2-cm-thick concrete block with 5.8-cm-thick voids.

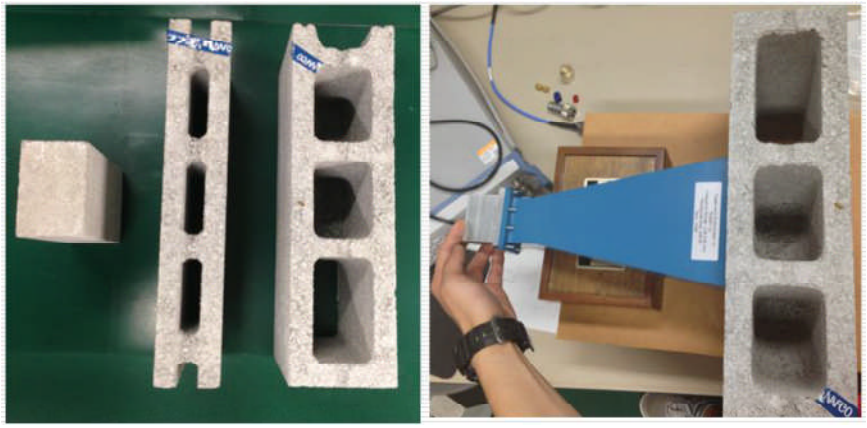

Figure 5.18 Three types of concrete blocks

Then, the antenna is positioned at the surface of the sample, and the signal generator is turned on. The amplitude–frequency response $A(f, x)$ observed in the oscilloscope for each concrete block is shown in Figure 5.19.

The blue line in Figure 5.19 denotes the sweeping frequency in the range 3.8–5.8 GHz. The yellow waves show the amplitude of the response detected by the wave detector. When the signal generator is turned on, two or more periods of data are collected by the A/D converter. Because of the large interference in the first-period data, these data are discarded in the subsequent analysis. The starting point of the second-period data is the start of the second period of the blue line in Figure 5.19, which is the lowest frequency point in the second period.

From the results, it is inferred that in the nonvoid concrete case, the $A(f, x)$ curve shows periodicity, whereas in the case of concrete with air voids, the periodicity of amplitude–frequency response $A(f, x)$ is somewhat lost, as shown in Figure 5.19 and Figure 20.

The proposed data analysis mothed is used to extract the amplitude–frequency response $A(f, x1)$, $A(f, x2)$, and $A(f, x3)$, which represent the first reflection(top of the block), second reflection interface (top of the air voids), and third reflection respectively. These responses are used to identify the location and size of the air voids.

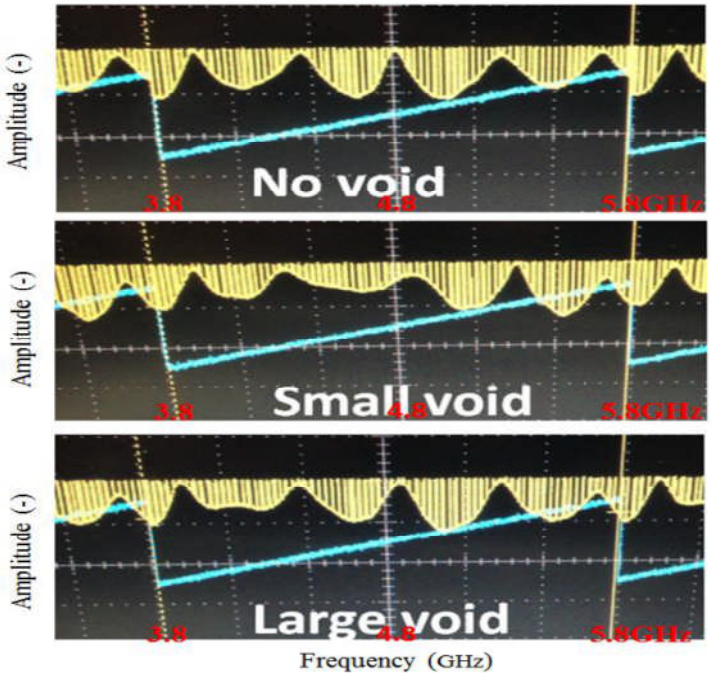

Figure 5.19 Observed oscilloscope signals for case 1

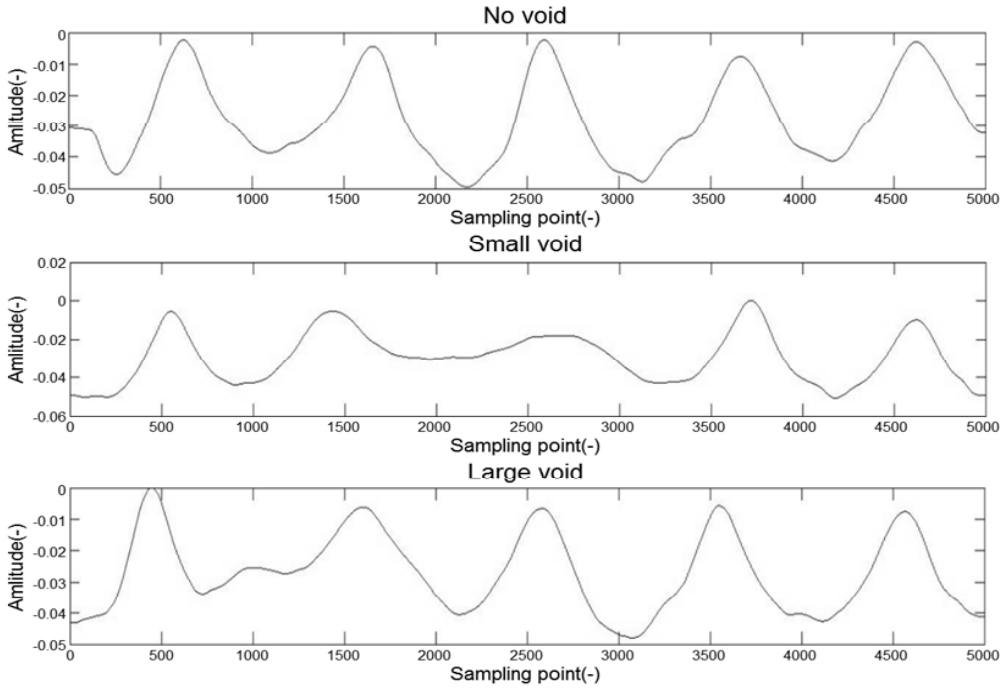

Figure 5.20 Sampling data for case 1

In case 1, all sampling data contain the $A(f, x_1)$ that represents the reflection on the concrete surface, whereas the data for the small void contains the $A(f, x_2)$ that represents the reflection on the top of the air void and the $A(f, x_2)$ that represents the reflection on the bottom of the air void.

The independent analysis of the data for the small voids gives the three main independent components in Figure 5.21. The frequency differences are shown in table

5.2. The errors between these frequency differences are shown in the Table 5.3 (the threshold is 5%). From Table 5.3, we can find the frequency difference Δf_3 of $A(f, x_1)$, Δf_1 of $A(f, x_2)$, and Δf_4 of $A(f, x_3)$ are greater than threshold and will not be used to calculate the mean value of frequency difference. Other errors are very small. Thus, the average sampling points between two peaks of the standing-wave formed by the concrete surface is 1021; the average sampling points between two peaks of the top of the air void is 867, the average sampling points between two peaks of the bottom of the air void is 821.

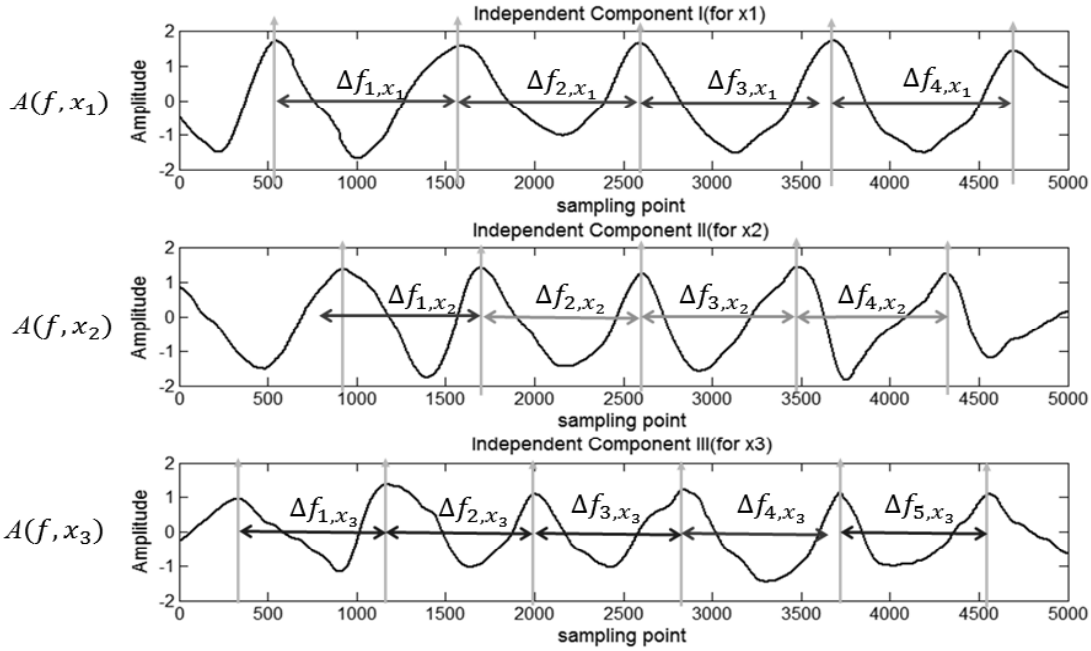

Figure 5.21 Independent components for case 1

Table 5.2 Frequency difference of standing-waves

signal	Δf_1	Δf_2	Δf_3	Δf_4	Δf_5
$A(f, x_1)$	1026	1018	1088	1021	-
$A(f, x_2)$	784	875	860	866	-
$A(f, x_3)$	820	823	831	890	810

Table 5.3 Errors between frequency differences

signal	Error of Δf_1, Δf_2	Error of Δf_1, Δf_3	Error of Δf_1, Δf_4	Error of Δf_1, Δf_5	Error of Δf_2, Δf_3	Error of Δf_2, Δf_4	Error of Δf_2, Δf_5	Error of Δf_3, Δf_4	Error of Δf_3, Δf_5	Error of Δf_4, Δf_5	No used Δf
$A(f, x_1)$	0.8%	6.5%	0.5%	-	6.8%	1.6%	-	6.2%	-	-	Δf_3
$A(f, x_2)$	11.6%	9.7%	10.5%	-	1.4%	1%	-	0.6%	-	-	Δf_1
$A(f, x_3)$	0.4%	1.3%	8.5%	1.2%	0.9%	8.1%	1.5%	7.1%	1.9%	8.9%	Δf_4

There are also other $A(f, x)$ curves for reflections on other surfaces; however, considering the propagation of electromagnetic waves, these three amplitude–frequency responses are the strongest. And can be used to calculate the distance to the two surfaces.

For the concrete surface, because the sampling frequency is 200 Hz and the average sampling points between the two peaks is 1045, the time between the two peaks is 5.225 s. For the sweeping wave, the frequency is proportional to time, and the total sweeping time from 3.8G Hz to 5.8 GHz is 23.6 s; thus, Δf_1 = 432.6MHz. Based on Equation (5.9), x_1 is 34.67 cm and is shown in Figure 5.22.

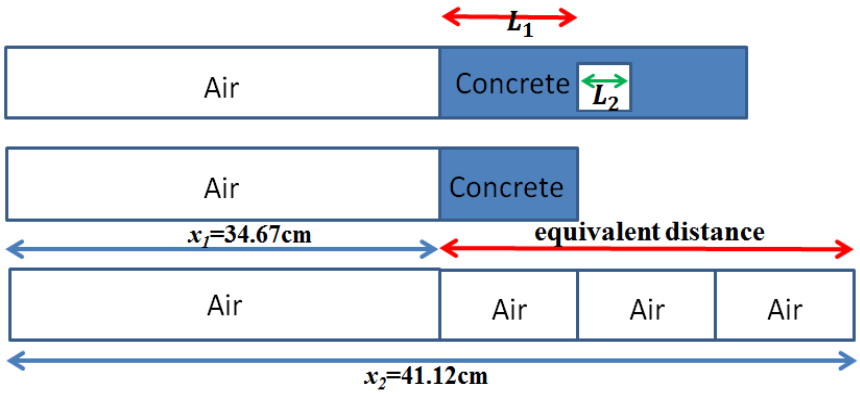

Figure 5.22 Equivalent distance for case 1

For the top of the air void, the calculation is the same as that in the concrete case. x_2 is 41.12 cm. For the bottom of the air void, the x_3 is 43.41.

According to Figure 5.22, the equivalent distance between the concrete surface and the top of the air void is 6.45 cm. Then, for the small void, the distance from top of air void to the top of concrete is

$$L_{1,small} = 6.45cm/3 = 2.15\text{cm} \tag{5.23}$$

The distance from top of air void to the bottom of air void is

$$L_{2,small} = 43.41 - 41.12 = 2.29\text{cm} \tag{5.24}$$

Table 5.4 shows the results of small void and large void blocks. From Table 5.4, we can find the two detected values are very close to the real distance L_1 and L_2 in small void and large void blocks. The maximum error is about 4%, which are very small.

Table 5.4 Results of case 1 experiment

Test condition	Real location: L_1	Detected location	Error	Real void size: L_2	Detected void size	Error
Small void condition	2.2cm	2.15cm	**2.3%** (0.05cm)	2.2cm	2.29cm	**4.1%** (0.09cm)
Large void condition	2.2cm	2.23cm	**1.4%** (0.03cm)	5.8cm	5.73cm	**1.2%** (0.07cm)

5.5.2.2 Case 2

The testing samples are two 3.3-cm-thick clay bricks (wave speed = c/2.5). The cases considered are shown in Figure 5.23 and are 1) one clay brick, 2) two clay bricks with in-between distance x = 0, and 3) two clay bricks with in-between distances of x = 1 cm, x = 3 cm, and x = 6 cm.

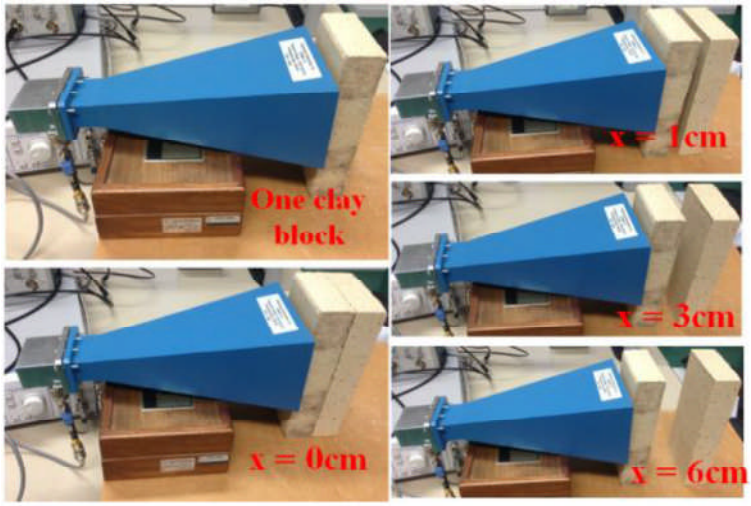

Figure 5.23 Case 2 setup

The amplitude–frequency responses $A(f, x)$ are shown in Figure 5.24. The blue line denotes the sweeping frequency range of 3.8–5.8GHz. The yellow waves represent the detected amplitude responses detected by the wave detector.

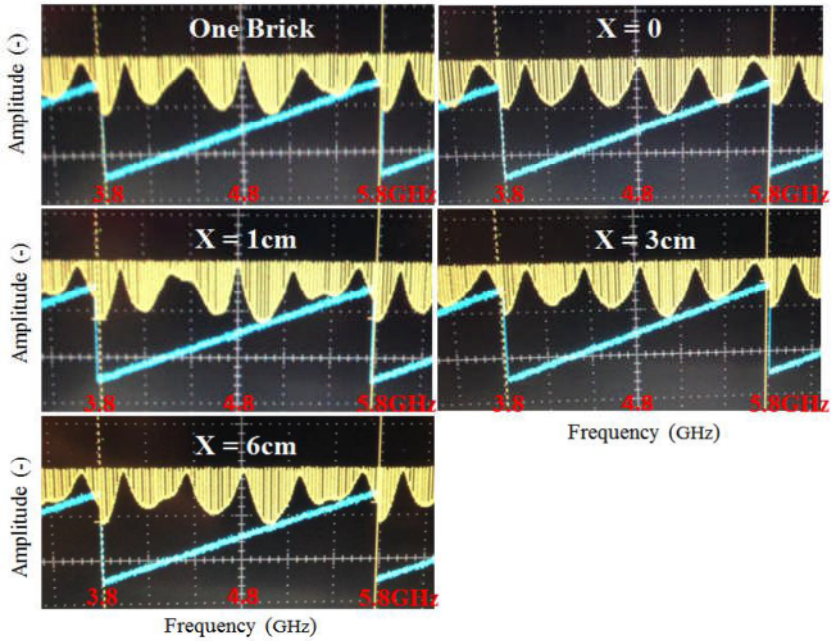

Figure 5.24 Observed signals for case 2

When the thickness of the clay bricks changes, the amplitude–frequency response also changes. In the case of no voids, the $A(f, x)$ curve shows good periodicity, which

is lost in the case of air void and when the size of the voids changes.

Application of Fast-ICA to the data returns the independent components in Figure 5.25. Three components are the standing-wave $A(f, x_1)$, $A(f, x_2)$, and $A(f, x_3)$, respectively. The same processes of case 1 are used in case 2 to calculate the detected location and size of void. In the clay blocks, the wave speed is c/2.5; therefore, for the same period, the distance in air covered by the electromagnetic wave is 2.5 times that in clay. The results of case 2 are shown in Table 5.5. From Table 5.5, the detected values of location and size are very close to the real distance L_1 and L_2. The maximum error of case 2 is 3%, which is very small.

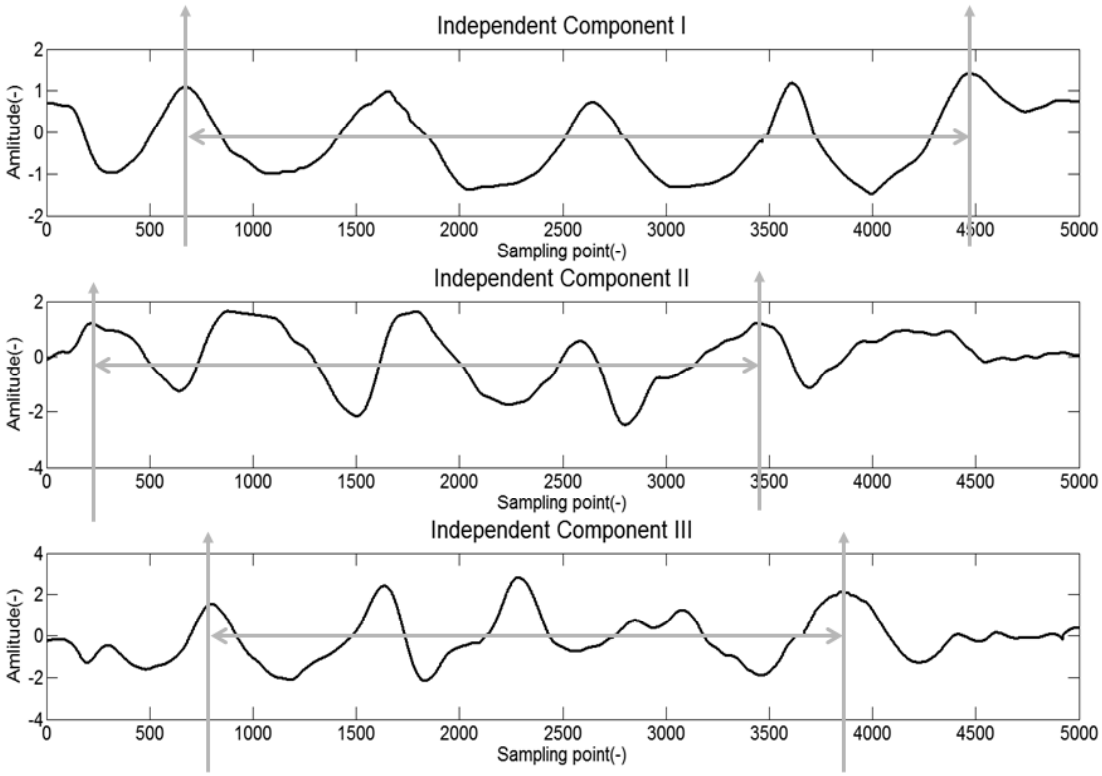

Figure 5.25 Three independent components for 1cm void in case 2

Table 5.5 Results of case 2 experiment

Test condition	Real location: L_1	Detected location	Error	Real void size: L_2	Detected void size	Error
1cm void condition	3.3cm	3.36cm	**1.8%** (0.06cm)	1cm	1.03cm	**3%** (0.03cm)
3cm void condition	3.3cm	3.38cm	**2.4%** (0.08cm)	3cm	3.07cm	**2.3%** (0.07cm)
6cm void condition	3.3cm	3.33cm	**0.9%** (0.05cm)	6cm	6.07cm	**1.2%** (0.07cm)

5.5.2.3 Case 3

The testing samples are two concrete bricks and one 1.8cm thick marble brick (wave speed = c/1.5). The distance between the marble brick and concrete bricks is 1cm (Figure 5.26). First, the antenna is placed on one place on the marble surface, and then the antenna is repositioned.

Figure 5.26 Case 3 setup

The sampling data collected by the A/D converter are shown in Figure 5.27. Data analysis with the new data analysis method gives the independent components in Figure 5.28. Three components are the standing-wave $A(f, x_1)$, $A(f, x_2)$, and $A(f, x_3)$, respectively. In the marble block, the wave speed is c/1.5; therefore, in the same period, the distance in air covered by the electromagnetic wave is 1.5 times that in the marble. The same processes of case 1 are used in case 3 to calculate the detected location and size of void. The results of case 3 are shown in Table 5.6. From Table 5.6, the detected values of location and size are very close to the real distance L_1 and L_2. The maximum error of case 3 is 4%, which is very small.

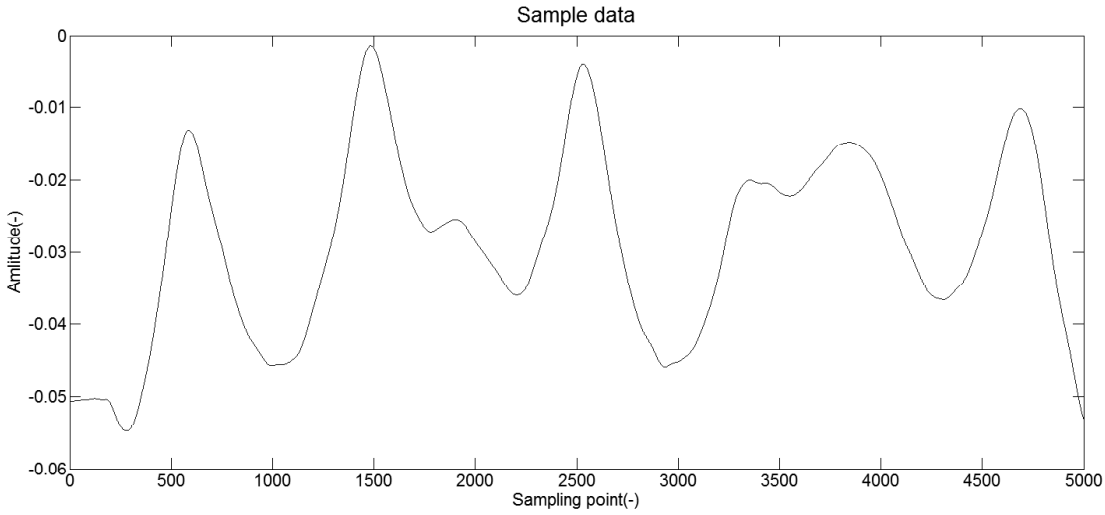

Figure 5.27 Sampling data for case 3

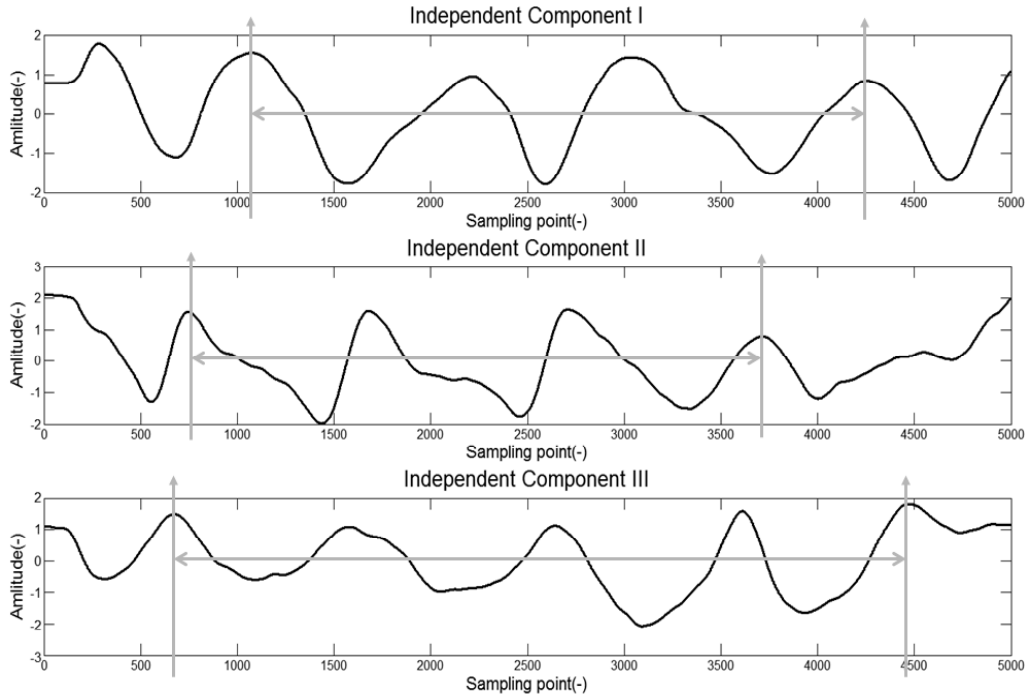

Figure 5.28 Independent components for case 3

Table 5.6 Results of case 3 experiment

Test condition	Real location: L_1	Detected location	Error	Real void size: L_2	Detected void size	Error
Marble brick	1.8cm	1.79cm	**0.7%** (0.01cm)	1cm	0.96cm	**4%** (0.04cm)

From Figure 5.20, 5.24, and 5.27, it is observed that the interval of the amplitude peaks differs in the same figure. Noise and the application of Fast-ICA contribute to the error. To solve this problem, the errors between frequency differences Δf are calculated. If the error is greater than threshold, the Δf will be give up. Others will be used to calculate the mean value. And then, this mean value is used to calculate distance. In this way, the differences in the intervals of the amplitude peaks do not affect the results significantly. Otherwise, since we adopt several peaks to obtain the average interval, we also can easily calculate the average interval when two peaks are close each other. From these 3 cases, we can find the errors in the data in the 3 experiments are less than 5%, the precision (millimeter) is enough for actual case, since several millimeters thickness (distance L) usually will not appear in actual structure diagnosis. Therefore, in practice, it is suitable for bridge local health diagnosis. Otherwise, the space between the horn antenna and the top surface of the block should be separated to avoid scuffing of antenna. The distances between the receiver antenna and the top surfaces of the blocks depend on the material under investigation.

5.5.3 Comparison

As described in chapter 2, many NDT techniques and systems are developed to obtain the specific information of damages, such as X-ray based system, radiography based system, Ultrasonic inspection based system, Ground-penetrating radar based system, and etc. However, the limitations of harmful to humans and difficultly deploying the receiver part on the bottom of bridge deck let the X-ray based system and radiography based system to be difficulty applied for bridge. Therefore, in order to show the advantages of my system, I compare my system with ground penetrating radar system (GPR) and ultrasonic NDT system.

5.5.3.1 Ultrasonic Inspection based NDT System

Figure 5.29 shows the principle of NDT method by using ultrasonic inspection techniques to detect bridge. The ultrasonic based NDT system consists of an ultrasonic transducer, receiver, and a data processing equipment. At first, transducer transmits ultrasonic waves into object. Then the receiver records the returning waves. At last the data processing equipment analyzed the received waves to obtain the location of damages. If there is a void, crack or impurity, the sound will rebound and the data processing equipment will show the returned waves. Based on the time delay between the returned waves, the location of them will be obtained and shown by the data processing equipment.

An ultrasonic based NDT method is presented by Shah in [10] to detect the concrete. The main lack of using ultrasonic inspection for bridge structural detection is it is difficultly to effectively obtain ultrasonic coupling between the surface of bridge and transducer. Another defect of ultrasonic inspection in bridge structural NDT is the small size of probe limit system to detect the deck of bridge.

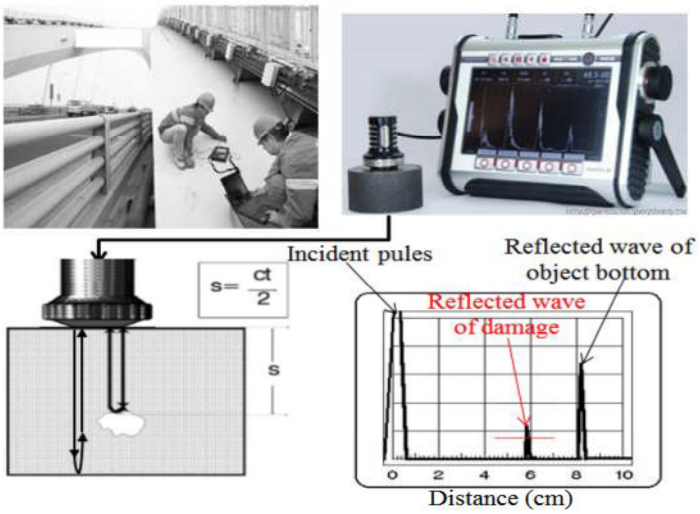

Figure 5.29 Ultrasonic based NDT system

5.5.3.2 Ground Penetrating Radar System

Microwave inspection techniques are based on the propagation characteristic of electromagnetic-waves. Ground penetrating radar (GPR) is typical microwave inspection technique. The principle of GPR system is shown as Figure 5.30. It uses an antenna intergrade transmitter and receiver to send wave and receive the reflected wave. Then based on the reflected wave techniques can obtain the time difference of two or three difference surfaces. The time difference can be used to detect the location and size of damages or defects. Yehia et al. [11] studied many different type NDT techniques, such as ground penetrating radar with 800MHz antenna, designed to detect the health conditions of concrete deck in bridges. Field data complexities and difficulties in data interpretation limit the application of the abovementioned techniques. However, considering the frequency limitations of the oscilloscope and A/D converter, it might be difficult to clearly capture the waveform at high frequencies (higher than 1 GHz). Otherwise, using time delay to calculate the location and the depth of damage size will limit the detection precision.

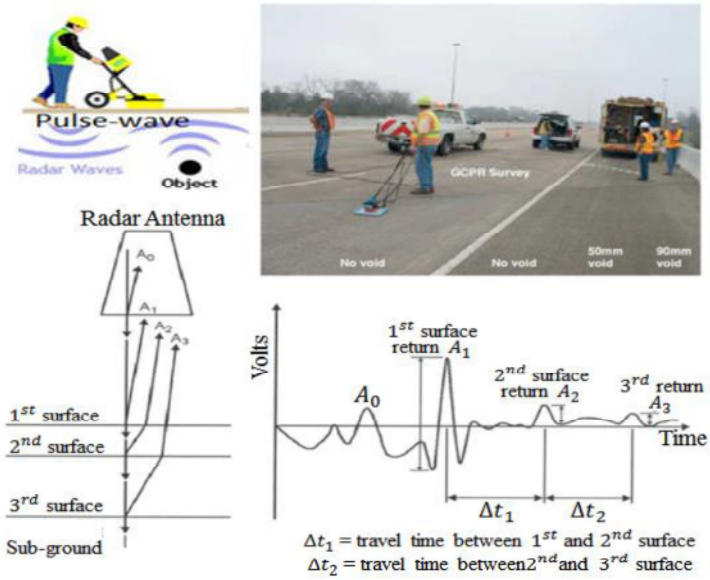

Figure 5.30 Ground penetrating radar system [11]

5.5.3.3 Comparison of three NDT Systems

Table 5.7 shows the comparison results of my system, ultrasonic based NDT system, and GPR system. From table 5.7, we can find my system no need a special medium for receiver, such as the coupling medium of ultrasonic system, to record the reflected wave. It means my system no need to consider the difficult of ultrasonic based NDT system, which is difficultly to effectively obtain ultrasonic coupling between the surface of bridge and transducer. The resolution of my system is far better than the GPR system, which means my system can detect the small size damage which cannot be detected by GPR system. Comparing with the ultrasonic based NDT

system and GPR system, the detection precision of my system improves 44.4% and 67.7% respectively. This is because my system uses frequency difference to calculate the location and size of damages, but other two systems use time delay. In my system, the waveform also changes for voids smaller than one-fourth of the wave length. Since the frequency of wave in my system is higher than other two systems, the detection precision of my system is far better than others. Although, the detection depth limitation of my system is lower than other two systems, the detection depth of my system is enough for bridge and other builds structure detection. Otherwise the detection depth can be extended by reducing the frequency of my system.

Since my system and GPR system are based on electromagnetic wave, I compare my system with GPR system by using the same hardware to take the 3 case experiments described in section 5.5.2 to show the advantage of my system in detection precision. The detection error of two systems shows as Figure 5.31. The detection error is defended by equation (5.25), where $L_{calculate}$ is the detected value and L_{actual} is the actual value. Figure 5.30 shows the detection error of my system is far lower than GPR system. This means the detection precision of my system is far better than GPR system, and my system improves 67.7% averagely.

$$\Delta_{error} = \frac{L_{calculate} - L_{actual}}{L_{actual}} \tag{5.25}$$

Fig.5.7 The comparison of my system, GPR, and ultrasonic NDT

System	Coupling medium	Detect small size cracks and void	Depth limitation	Resolution	Detection Error	For bridge diagnosis
Standing wave NDT	No required	Very Easy	1.6m (3.8-5.8GHz)	0.01cm	0.1cm	Very useful
GPR system	No required	Difficult	4.2m (800MHz)	1.6cm	0.31cm	Difficult for cracks
Ultrasonic NDT	Required	Easy	2.5m (5MHz)	0.01cm	0.18cm	Difficult for large size bridge

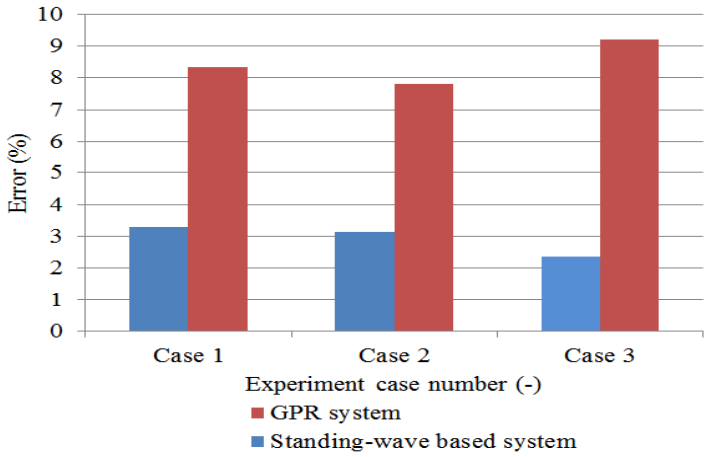

Figure 5.31 Detection error of my system and GPR system

5.6 Summary

In this chapter, in order to pinpoint the exact location and severity of damages, a standing-wave structure DNT system was successfully built. In this system, the signal generator generates a 3.8 GHz–5.8 GHz sweeping wave to the radar. The radar sends the sweeping wave to the object, and the incident and reflection waves from the object form a standing wave whose amplitude $A(f, x)$ is related to the input wave frequency f and object distance x. The amplitude signal is detected and converted to volts with a zero-biased detector. Finally, the amplitude–frequency response $A(f, x)$ was analyzed by the proposed data analysis method based on modified EMD and ICA, and the object state including the existence, exact location and size of subsurface damages such as voids was identified.

To verify the performance of this system, Simulations and experiments using different samples were performed. The data analysis suggests the following. First, for the case of no air voids, the $A(f, x)$ curve always has good periodicity. Second, in the presence of air voids and when the size of the voids changes, the $A(f, x)$ curve changes. Third, the voids are detected by generating sweeping waves and storing the amplitude–frequency response data. Then, the modified EMD and ICA based data analysis mothed is proposed to extract the responses from $A(f, x)$ to estimate the distances. Finally, by calculating the frequency difference between two peaks on the extracted amplitude–frequency responses, the void location and size can be determined. The errors in the data in the experiments are less than 5%. It means the precision (millimeter) is enough for actual case, since several millimeters thickness (distance L) usually will not appear in actual structure diagnosis. Therefore, in practice, it is suitable for bridge diagnosis.

Compared with other NDT systems, the proposed system offers the following advantages. First, compared with other BSHM system, it offers higher sensitivity and can detect the specific location and senverity of the damage. Second, compared with the conventional ultrasonic wave method and other electromagnetic wave methods (GPR system), it has higher resolution owing to its higher frequency and more accurate owing to the algorithm because for voids smaller than one-fourth of the wave length, the waveform also changes. Comparing with the ultrasonic based NDT system and GPR system, the detection precision of my system improves 44.4% and 67.7% respectively. Finally, compared with commercial systems, it is more compact and less expensive.

Reference

[1] Ch. Hellier: “Handbook of Nondestructive Evaluation”, McGraw-Hill. p. 1.1. ISBN 0-07-028121-1 (2003).

[2] T. Uebo T. Kitagawa T. Iritani: “Short Range Radar Utilizing Standing Wave of Microwave or Millimeter Wave”, Proceedings of the IEEE Intelligent Vehicles Symposium (2001)

[3] T. Uebo: “Measurement of Distance down to Zero Meters by Standing Wave Radar”, SAIKA Technological Institute Foundation

[4] H. Chen and T. Scullion: “Detecting Subsurface Voids Using Ground-Coupled Penetrating Radar”, Geotechnical Testing Journal, Vol.31, No.3 (2008)

[5] N. Huang, S. R. Long, “The empirical mode decomposition and the Hilbert spectrum for nonlinear and non-stationary time series analysis”, the Royal Society of London A, Vol. 454, No.1971, pp.903-995.(1998)

[6] Z. Wei, L. Jin, and Y. Jin: “Independent Component Analysis”, Department of Statistics, Stanford University (2002)

[7] K. Yee: “Numerical solution of initial boundary value problems involving Maxwell's equations in isotropic media”, IEEE Transactions on Antennas and Propagation, Vol.14, No.3, pp.302–307

[8] A. Taflove: “Application of the finite-difference time-domain method to sinusoidal steady state electromagnetic penetration problems”, IEEE Transactions on Electromagnetic Compatibility, Vol.22, No.3, pp.191–202

[9] Haitao Xiao, Jianan Qin, Harutoshi Ogai, Xiuchen Jiang, “A New Standing Wave Testing System for Bridge Structure Non-destructive Damage Detection using Electromagnetic Wave”, IEEJ Transactions on Electronics and Electronic Engineering, Vol.10, No.2, March, 2015.

[10] A. A. Shah and S. Hirose: “Nonlinear ultrasonic investigation of concrete damaged under uniaxial compression step loading,” Journal of Materials in Civil Engineering, Vol.22, No.5, pp.476–483 (2010)

[11] S. Yehia, O. Abudayyeh, S. Nabulsi, and I. Abdelqader: “Detection of common defects in concrete bridge decks using nondestructive evaluation techniques,” Journal of Bridge Engineering, Vol.12, No.2, pp.215–224 (2007)

Chapter 6

Conclusion

6.1 Conclusion

In order to comply with increasing requirements of bridge structure health diagnosis, including accuracy and sensitive of damage detection and locating, SHM method should be improved further. In this research, data process method is proposed to reduce the impact of noises and varying environment on damage diagnosis performance and improve the accuracy and sensitive of damage detection. In addition, betterment of damage diagnosis performance was also applied to pursue higher accuracy and sensitive in detecting damage location and severity. Improvement in damage diagnosis performance is achieved by an advance time-series modeling based damage diagnosis method, including applying ARMA and Mahalarobis distance to extract damage features. Also it involves, designing a new damage sensitive feature index to obtain highly accurate and sensitive location and severity of damage. Detailed location and severity information of local damages is indispensable to bridge maintenance or reparation. As a result, locate the detailed location and severity of local damages (especially inside) is crucial for bridge structure monitoring and maintenance system.

The research can be summarized as three aspects,

(1) Design of high-performance data process method to reduce the impact of noise and varying environment
(2) Design of advanced damage diagnosis method for damage detection and locating
(3) Design of effective NDT system to acquire the detailed location and severity information of damages

In chapter 3, from the viewpoint of increasing accuracy and sensitivity of damage detection and reducing the impact of noises and varying environment, a data process method based on improved post-nonlinear ICA and similarity matching is proposed. To achieve efficiency in de-noising, an improved post-nonlinear

geometric-linearization ICA algorithm (pcgICA) is designed. In this improved ICA algorithm, compensation based scheme is processed to reduce the geometric-linearization error of post-nonlinear geometric ICA (pgICA). It is revealed that improved pgICA is superior to conventional pgICA,

- Convergence performance, at least 1.5 times faster than conventional pgICA
- Better de-noising of non-linear system

The improved ICA is used for de-noising of vibration data measured on bridge. To verify the advantage of improved method (pcgICA), it is compared with Fast-ICA and pgICA by correlation-coefficient and signal-noise-ratio (SNR) in simulation. Comparing with Fast-ICA and pgICA, the average correlation-coefficient of my method is improved by 62.1%, and 16.7% respectively, the SNR is improved by 51.8% and 16.3% respectively. In the Nakajima bridge experiment, results show pcgICA is better than Fast-ICA and pgICA.

In order to reduce the impact of varying operating and environment condition on data analysis, a novel environment impact reduction method based on AR model and similarity matching is proposed. Vibration data are divided into two sets, undamaged condition data set S^U and unknown condition data set S^D. AR model is used to extract the features of each data in the two sets. Using these features, a matching scheme based on Euclidean distance is designed to obtain the data sample pair, one of S^U and one of S^D, which are measured in a similar operation and environment condition. In this way, change of structure caused by varying environment is eliminated. It is revealed that my method is superior to the conventional method in two aspects,

- ☐ No need to measure environment, such as temperature, humidity, loading, etc.
- ☐ Better accuracy and not only consider the factors that can be measured (temperature), also consider that can't be measured (traffic loading, etc.).

To verify effectiveness of the proposed algorithm, data of Nakajima bridge experiment is used. Results show our method can effectively eliminate false damage detection caused by varying environment and operation condition, which means our proposed method is efficient.

In chapter 4, in addition to improve the accuracy and sensitive of damage detection by data process method, an advance damage diagnosis method is designed to directly detect location and severity of damage, accurately and sensitively. In this chapter, a two-stage damage diagnosis method based on statistic pattern recognition is proposed for detecting and locating damages accurately. In the first stage, after data process, FFT is used to obtain characteristic frequency of bridges. By comparing the frequency

in a healthy state with an unknown state, we detect the structural novelty (damage identifying).

In second stage, to detect severity and location of damage, a time-series modeling based damage diagnosis algorithm is proposed. At first, data samples are used to establish ARMA model. Based on the model, pattern vectors form damage feature, where PCA is utilized to reduce the amount of features. These features and Mahalanobis distance are used to extract the damage-sensitive-features (DSFs). Based on the DSFs, a new sensitive DSF index, D_{index}, is proposed to take statistically diagnose structure condition, and identify severity and location of damages. It is revealed that my method is superior to the conventional method,

- Highly accuracy and sensitive, statistical reduce error and D_{SPR} magnify the difference between damage and health.
- Better locating, at least locate all kinds of damages (close to sensor).

To verify performance of this two-stage algorithm, experiments were conducted at the Kando Bridge in Japan. Damages were inflicted at different locations to achieve varying levels of damage severity. The results demonstrate that location and severity of damage can be identified using our proposed two-stage diagnosis algorithm. Sensitivity of my method is 96.3% in this experiment. Our algorithm is compared with other diagnosis algorithms such as FFT with ICA, SPR with residual method, and Transfer Function based method. The results show our algorithm is better not only in sensitivity but also in specificity.

- ☐ Comparing with SPR with residual method, TF, and FFT with ICA, my method improved by 10.3%, 17.1%, and 13.2% in sensitivity, respectively.
- ☐ My method improved by 9.6%, 13.4%, and 11.8% in specificity, respectively.

In chapter 5, as described in chapter 4, a two-stage damage diagnosis algorithm is proposed for BSHM system. This method can successfully detect severity and approximate locations of various damages on bridges. With the viewpoint of locating detailed location and severity information of local damages for bridge maintenance or repair, a nondestructive testing (NDT) system based on stand-wave is developed to pinpoint exact location and severity of the damage by using the approximate location information of chapter 4. This system consists of two parts:

- ☐ **Stand-wave detection**

  1). the sender antenna sends 3.8 GHz–5.8 GHz sweeping wave to the object, and the incident and reflection waves from the top-surface of object form

a standing wave whose amplitude $A(f, x)$ is related to the input wave frequency f and object distance x.

2). The amplitude signal is recoded by receiver antenna, shows on the oscilloscope and store in PC. When there are no damages (void or crack) in object, $A(f, x)$ is a perfect stand-wave.

3). Else, $A(f, x)$ is a mixture wave mixed by the $A(f, x_1)$ (formed by reflected wave of object's top-surface), $A(f, x_2)$ (formed by reflected wave of Void's top-surface), and $A(f, x_3)$ (formed by reflected wave of Void's lower-surface).

4). Thus, by reading changes in waves on oscilloscope, horizontal position can be located. Also, by horizontal moving the antenna and checking wave on oscilloscope, the width of void is obtained.

☐ **Data analysis for detecting the damage's depth**

To detect depth and size of damage accurately, a new data analysis method based on modified EMD and ICA is proposed to calculate two values. In this way location and size of inside damages such as voids was identified.

- To improve decompensation accuracy of EMD, a modified EMD based a correlation coefficient is proposed. The mixture stand-wave $A(f, x)$ is decompensated by modified EMD to give multiple inputs for ICA.
- ICA extract the three separated stand-waves $A(f, x_1)$, $A(f, x_2)$, and $A(f, x_3)$. Based on these stand-waves get the x_1, x_2, and x_3.
- Then based on x_1, x_2, and x_3, the two values are calculated.

It is revealed that this system is superior to other NDT systems in two aspects,

- Better accuracy, high frequency sweep wave and using frequency difference to calculate distance make better accuracy then using time.
- Simple, easy to carry, inexpensive, and safety to human health.

To verify the performance of this system, Simulations and experiments were performed. The data analysis suggests the following. By reading the frequency difference between two peaks on the extracted stand-waves, void location and size can be determined. Detection error in the experiments is less than 5%. It means precision (millimeter) is enough for actual case. Comparing with ground penetrating radar system and ultrasonic based NDT system, the detection error of my system reduces by 67.7% and 44.4%, respectively. Also, my system has higher resolution, higher accuracy, and less expensive. Therefore, in practice, it is suitable for bridge diagnosis than other NDT systems.

6.2 Future Research

The proposed methods and systems for bridge health diagnosis can be validated in the future research by Appling in real bridge health diagnosis and maintenance system. The illustration of future researches is shown in Figure 6.1

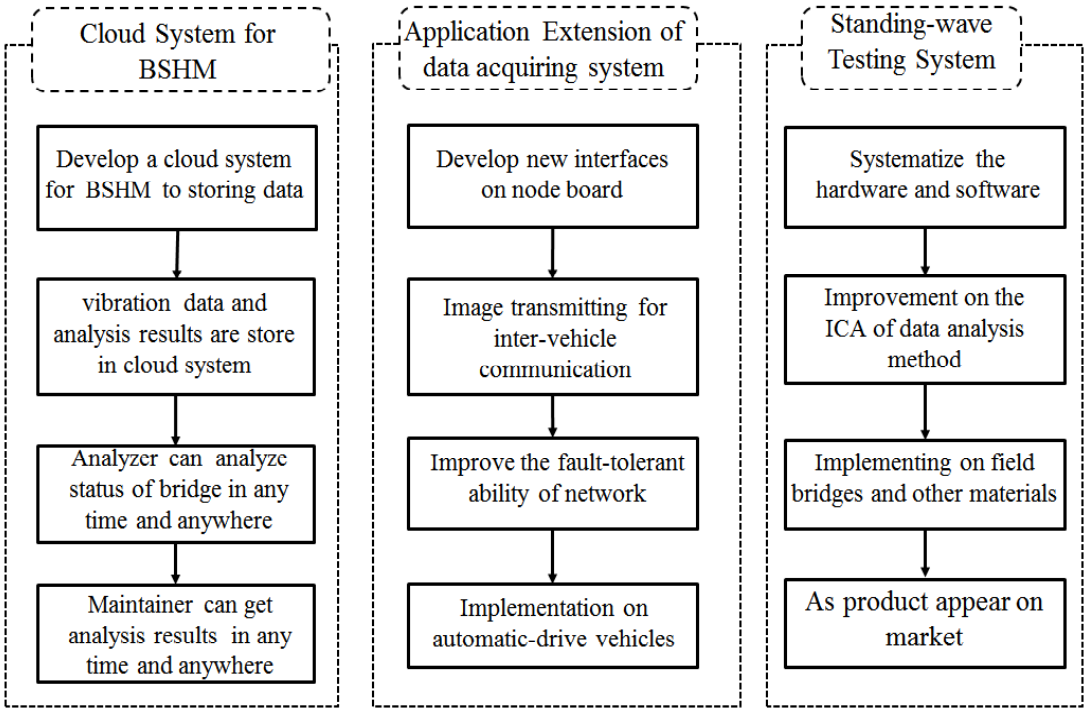

Figure 6.1 Future research

6.2.1 Cloud system for BSHM

Although a bridge structural health monitor and maintenance system is built based on the proposed methods and system in the research, there are still some parts needed to be improved.

- First, the data storage and analysis results sharing needs to be improved. In this BSHM system, acquired vibration data of bridges are stored in data sever and data analysis center. Researchers need to get data from data analysis center to do analysis and send the analysis reports to bridge maintenance relevant departments. This not only costs time but also increases expenditure. In the future, a cloud system needs to be developed for storing vibration data of bridges and analysis results of analyzers. In this system, data acquiring system directly transmit measured vibration data in cloud system. Also, the analyzers directly take these data to perform analysis and store these results in cloud system. In this way, analyzers can analyze status of bridges at anytime and anywhere. Also the maintainers can get the analysis results at anytime and anywhere.

- Second, the data analysis software needs to be improved. In this BSHM system, although a data analysis software is developed, it is difficult and complex for general users. Thus, in future, an integrated and easy-to-use software should be developed for any user based on the proposed methods in this thesis.

6.2.2 Application Extension of Data Acquiring System

In our built BSHM system, a data acquiring system based on low-power wireless sensor network (WSN) is developed for acquiring vibration data. In this data acquiring system, a new node board with low-power and low-power protocols are designed. In the future, this data acquired system would be extended to use in other applications. For example, this system can be extender for inter-vehicle communication in automatic drive application.

- In this application, a camera interface is needs to be added in node board to exchange images and control information. Also information process software is needed to add in the nodes. Otherwise, in BSHM system, the routing method is a static routing method. Thus, when the WSN is used in inter-vehicle communication, routing method is needed to be improved, because topology of network changes dynamically and quickly. In future, we need to develop some techniques, such as routing, to improve fault-tolerant ability of topology and effective of data transmitting.
- Also, this BSHM system can be applied in other status monitoring and diagnosis field. By improve small parts such as sensors, the BSHM system is easily extended to apply in monitoring status of builds, machine or towers, etc. Also, the data acquiring system can be applied in many application of daily life, such as automatic meter reading system.

6.2.3 Standing-wave based structure NDT system

In this research performance analysis of standing-wave based structure NDT system is perform by using concrete bricks and granite bricks in laboratory. In further, this system needs to be test in different materials used in bridge, road, and builds etc.

- Do more experiment on more materials and if possible, change the shape of subsurface void to verify our system. Add steel bar to the concrete and check its influence. Try to use radar to detect subsurface void in material of high dielectric constant such as metal bars.
- Try to improved separation processing of data analysis method. In proposed method, after modified EMD, Fast-ICA is applied to separate stand-waves of surfaces. Some peaks of separated signals are not obvious. Thus, in future, improvement on ICA is needed to improve the effect of separation.

- The NDT system is built, but it is a prototype system. In the future, we need to systemize these hardware equipment to make system for easy to use and reduce cost of the system. Also, the software needs to be systemized to extract the location and size of void, directly. In this way, users can easily use this system.

And then, after systemizing, this system should be developed as a product to appear on the market with the BSHM system.

Acknowledgements

Firstly, I would like to express heartfelt gratitude and appreciation to my dedicated advisor, Professor Harutoshi Ogai, who has offered me valuable suggestions in the academic studies, for giving me the opportunity to continue my doctoral degree. Without his professional guidance, kindly understanding, outstanding teaching, patience, and encouragement, this research would not have been possible. I would also like to thank Dr. Dongmei Wu, Dr. Masatoshi Ogawa, and Dr. Yichun Yeh for their willingness to give me insightful suggestions to my research and manuscripts, and also appreciate for their patiently answering my questions. In addition, I will express my appreciation to Professor Hiroshi Inujima, Professor Shigeyuki Tateno, and professor Hee-Hyol Lee, for their patiently reviewing my dissertation and giving me lot of suggestions.

I will never forget people in the Ogai Lab. Research fellows, and graduate students created a pleasant research environment. Their friendship and helps during my studying in Japan would be remembered for ever. Here, I also want to give many thanks to all the members of bridge diagnosis group, especially Tansheng Li, Zhehan Ding, Jianan Qing, Xue Zhao, and Nayanjyoti Baishya, for supporting me in every endeavor and always giving me a helping hand. I also thank Cheng LU, Zhenyuan XU, Nan Wang, Yunfeng Lou, and Di Ai for helping me not feel lonely and being sincere friends.

Finally, I would like to dedicate the dissertation to my loving wife, Yun Ren, without hers understanding and supports, I would not have been able to continue my education life. Also I need to say thanks to my loving parents, sister, brother, and wife's parents, for their understanding and supports.

Publication List

International Journals

1. ○ Haitao Xiao, Sheng Luo, Harutoshi Ogai, “A Novel Bridge Structure Damage Diagnosis algorithm based on Post-nonlinear ICA and Statistical Pattern Recognition”, IEEJ Transactions on Electronics and Electronic Engineering, Vol.10, No.3, pp.287-300, May, 2015.
2. ○ Haitao Xiao, Jianan Qin, Harutoshi Ogai, Xiuchen Jiang, “A New Standing Wave Testing System for Bridge Structure Non-destructive Damage Detection using Electromagnetic Wave”, IEEJ Transactions on Electronics and Electronic Engineering, Vol.10, No.2, pp.157-165, March, 2015.
3. Haitao Xiao, Xue Zhao, and Harutoshi Ogai, “A New Clustering Routing Algorithm for WSN based on Brief Artificial Fish-School Optimization and Ant Colony Optimization”, IEEJ Transactions on Electronics, Information and Systems, Vol.133, No.7, pp.1339-1349, May, 2013.
4. Haitao Xiao, Xue Zhao, and Harutoshi Ogai, “A Clustering Routing and Coverage Algorithm for WSN Based on Brief Artificial Fish-School Optimization”, Sensor Letters, Vol.11, No.4, pp.697-703, April, 2013.
5. Haitao Xiao, Harutoshi Ogai, and Noriyoshi Yamauchi, “An energy efficient clustering time synch algorithm for WSN in bridge health diagnosis system”, IEICE Communications Express, Vol.2, No.2, pp.049-054, February, 2013.
6. Haitao Xiao, Harutoshi Ogai, and Zhehan Ding, “A Distributed Multi-hop Low Cost Time Synchronization Algorithm in Wireless Sensor Network developed for Bridge Diagnosis System”, IEEJ Transactions on Electronics, Information and Systems, Vol.132, No.5, pp.656-665, May, 2012.
7. Haitao Xiao, and Harutoshi Ogai, “A Self-Health Monitoring System for a Wireless Sensor Network Used in Bridge Diagnosis”, SICE Journal of Control, Measurement, and System Integration, Vol.5, No.1, pp.048-054, January 2012.

8. Tansheng Li, Haitao Xiao, Harutoshi Ogai and Noriyoshi Yamauchi, “A Multi-hop Wireless Sensor System for Bridge Health Monitoring”, IEEJ Transactions on Electronics, Information and Systems, Vol.131, No.10, PP.1760-1766, October, 2011.

International Conferences

1. Haitao Xiao, Cheng Lu, and Harutoshi Ogai, “A Novel Bridge Structure Damage Diagnosis algorithm based on Statistical Pattern Recognition”, SICE2014 Annual Conference, pp.775-780, September 9-12, 2014.
2. Haitao Xiao, Cheng Lu, and Harutoshi Ogai, “A Multi-hop Low Cost Time Synchronization Algorithm for Wireless Sensor Network in Bridge Health Diagnosis System”, 2012 IEEE 18th International Conference on Embedded and Real-Time Computing Systems and Applications (RTCSA), pp.392-395, August 19-22, 2012.
3. Haitao Xiao, Harutoshi Ogai, Yixuan Gong, Xiaohong Zou, Takenari Otawa, Shinya Umeda, Takunori Tsuji and Jie Zhang, “A Data Collection System in Wireless Network combined WSN and ZIGBEE for Bridge Diagnosis”, SICE2011(SICE Annual Conference), pp.2024-2028, September 13-18, 2011.
4. Haitao Xiao and Ogai Harutoshi, “A Distributed Localized Decision Self-Health Monitoring System in WSN developed for Bridge Diagnosis”, 2011 3rd IEEE International Conference on Communication Software and Networks (ICCSN 2011), pp.23-28, May 27-29, 2011.
5. Haitao Xiao, Tansheng Li and Ogai Harutoshi, “The Health Monitoring System based on Distributed Data Aggregation for WSN used in Bridge Diagnosis”，SICE Annual Conference 2010, pp.2134-2138, August 18 - 21, 2010.

Domestic Conference

1. Haitao Xiao, Tansheng Li and Ogai Harutoshi, “A health monitoring system for wireless sensor network in bridge diagnosis”, SICE 10th Annual Conference on Control Systems, Kumamoto, March 16-18, 2010.
2. Haitao Xiao, Tansheng Li, Ogai Harutoshi, Zou Xiaohong, Takenari Otawa, Shinya Umeda and Takunori Tsuji, “A health monitoring system for wireless sensor network in bridge diagnosis”, The 62nd Joint Conference of Electrical and Electronics Engineers, Kyushu Institute of Technology (Iizuka Campus), 28-29, September 2009.
3. 李　譚生，肖 海涛，大貝晴俊，大多和丈成，梅田慎也，鄒　暁紅，辻　卓則, “A Multi-hop Wireless Sensor System of Bridge Health Monitoring”, 平成 22 年 電気学会電子・情報・システム部門大会, Kumamoto, September 2, 2010.